

**Anhydrous Proton Conducting Polymer  
Electrolytes Based on Polymeric  
Ionic Liquids**

**Dissertation**

zur Erlangung des Grades

“Doktor der Naturwissenschaften”

am Fachbereich Chemie und Pharmazie der

Johannes-Gutenberg-Universität

in Mainz

**Hamit Erdemi**

born in Siirt, Turkey

Mainz 2008

## ABSTRACT

Imidazolium types of ionic liquids were immobilized by tethering it to acrylate backbone. These imidazolium salt containing acrylate monomers were polymerized at 70°C by free radical polymerization to give polymers poly(AcIm-n) with n being the side chain length. The chemical structure of the polymer electrolytes obtained by the described synthetic routes was investigated by NMR-spectroscopy. The polymers were doped with various amounts of H<sub>3</sub>PO<sub>4</sub> and LiN(SO<sub>2</sub>CF<sub>3</sub>)<sub>2</sub>, to obtain poly(AcIm-n) x H<sub>3</sub>PO<sub>4</sub> and poly(AcIm-2-Li) x LiN(SO<sub>2</sub>CF<sub>3</sub>)<sub>2</sub>. The TG curves show that the polymer electrolytes are thermally stable up to about 200°C. DSC results indicate the softening effect of the length of the spacers (n) as well as phosphoric acid.

The proton conductivity of the samples increases with x and reaches to 10<sup>-2</sup> S cm<sup>-1</sup> at 120°C for both poly(AcIm-2)2H<sub>3</sub>PO<sub>4</sub> and poly(AcIm-6)2H<sub>3</sub>PO<sub>4</sub>. It was observed that the lithium ion conductivity of the poly(AcIm-2-Li) x LiN(SO<sub>2</sub>CF<sub>3</sub>)<sub>2</sub> increases with blends (x) up to certain composition and then leveled off independently from blend content. The conductivity reaches to about 10<sup>-5</sup> S cm<sup>-1</sup> at 30°C and 10<sup>-3</sup> at 100°C for poly(AcIm-2-Li) x LiN(SO<sub>2</sub>CF<sub>3</sub>)<sub>2</sub> where x is 10. The phosphate and phosphoric acid functionality in the resulting polymers, poly(AcIm-n) x H<sub>3</sub>PO<sub>4</sub>, undergoes condensation leading to the formation of cross-linked materials at elevated temperature which may improve the mechanical properties to be used as membrane materials in fuel cells. High resolution nuclear magnetic resonance (NMR) spectroscopy was used to obtain information about hydrogen bonding in solids. The low T<sub>g</sub> enhances molecular mobility and this leads to better resolved resonances in both the backbone region and side chain region. The mobile and immobile protons can be distinguished by comparing <sup>1</sup>H MAS and <sup>1</sup>H-DQF NMR spectra. The interaction of the protons which may contribute to the conductivity is observed from the 2D double quantum correlation (DQC) spectra.

# Contents

<b>1. Introduction.....</b>	<b>1</b>
<b>2. Polymer Electrolyte Systems.....</b>	<b>3</b>
2.1 Hydrated Membranes.....	3
2.1.1 Perfluorinated Ionomer Membranes.....	3
2.1.2 Other Sulfonated Hydrocarbon Polymer Systems.....	5
2.2 Anhydrous Proton-Conducting Polymers.....	5
2.2.1 Phosphoric Acid-Based Membranes.....	5
2.2.2 Other Anhydrous Materials.....	8
2.3 Ionic Liquids.....	10
2.4 Proton Conduction Mechanisms.....	12
2.5 Applications.....	13
2.5.1 Fuel Cells.....	13
2.5.1.1 Solid Polymer Electrolyte Membrane (PEM) Fuel Cells.....	14
2.5.2 Batteries.....	15
2.5.2.1 Lithium-Ion Batteries.....	17
<b>3. Synthesis.....</b>	<b>20</b>
3.1 Motivation for Synthesis.....	20
3.1.1 The Synthesis of Ionic Liquids.....	22
3.1.2 Immobilization of Ionic Liquids.....	24
3.2 Synthesis of Monomers.....	27
3.2.1 Imidazolium Salt Containing Acrylate Monomers.....	27
3.3 Synthesis of Polymers.....	31
3.3.1 Polymerizable Ionic Liquids.....	31
3.3.2 Synthesis of Ionenenes.....	35

<b>4. Thermal Analysis.....</b>	<b>38</b>
4.1 Thermogravimetric Analysis (TGA) Results.....	39
4.1.1 TGA of the Poly(AcIm-n) x H <sub>3</sub> PO <sub>4</sub> .....	39
4.1.2 TGA of the Poly(AcIm-Li) x LiN(SO <sub>2</sub> CF <sub>3</sub> ) <sub>2</sub> .....	41
4.1.3 TGA of the Ionenes.....	41
4.2 Differential Scanning Calorimetry (DSC) Results.....	42
4.2.1 DSC Results of Poly(AcIm-n) x H <sub>3</sub> PO <sub>4</sub> .....	42
4.2.2 DSC Results of Poly(AcIm-2-Li) x LiN(SO <sub>2</sub> CF <sub>3</sub> ) <sub>2</sub> .....	45
4.2.3 DSC Results of Ionenes.....	45
<b>5. Dynamic Mechanical Analysis.....</b>	<b>47</b>
5.1 Mechanical Properties of Poly(AcIm-n) .....	50
<b>6. Dielectric Spectroscopy.....</b>	<b>55</b>
6.1 Theoretical Treatment of Ion Conduction in Solid Electrolytes.....	63
6.1.1 Ion Conduction in Solid Electrolytes.....	63
6.1.2 Ion Conduction in Amorphous Polyelectrolytes.....	64
6.2 Proton Conduction in Polymer-Phosphoric Acid Systems.....	66
6.3 Dielectric Relaxation of Polymeric Ionic Liquids.....	68
6.3.1 Conductivities of Poly(AcIm-n) x H <sub>3</sub> PO <sub>4</sub> .....	68
6.3.2 Conductivities of Poly(AcIm-2-Li) x LiN(SO <sub>2</sub> CF <sub>3</sub> ) <sub>2</sub> .....	76
6.4 Conductivity of Poly(Im-6-6) .....	83
<b>7. Solid State Nuclear Magnetic Resonance (NMR) .....</b>	<b>86</b>
7.1 Nuclear Spin Interactions in The Solid Phase.....	86
7.1.1 Chemical Shielding.....	86
7.1.2 J-Coupling (Scalar Coupling).....	87
7.1.3 Dipolar Coupling.....	87
7.2 Modern Solid-State NMR spectroscopy.....	88
7.2.1 <sup>1</sup> H NMR.....	88

7.2.2	Cross Polarization MAS NMR.....	89
7.3	Results of NMR Spectroscopy.....	90
7.3.1	Results of $^1\text{H}$ -MAS and $^1\text{H}$ -DQF NMR Spectroscopy.....	90
7.3.2	$^1\text{H}$ -MAS Variable Temperature Studies and Correlation to Conductivity.....	94
7.3.3	2D $^1\text{H}$ - $^1\text{H}$ Double Quantum MAS Results.....	96
7.3.4	$^{31}\text{P}$ MAS NMR Results.....	99
<b>8.</b>	<b>Conclusion.....</b>	<b>101</b>
<b>9.</b>	<b>References.....</b>	<b>104</b>
<b>10.</b>	<b>Experimental Part.....</b>	<b>115</b>
	Chemicals.....	115
	Instrumentation and Procedures.....	115
	Synthesis.....	117

## 1. Introduction

The development of high energy density batteries with good performance, safety, and reliability has been an active area of research for many years [Fenton 73, Armand 78, Dell 00]. Advances in electronics, especially portable electronics (i.e. mobile phones, portable computers, etc.), have created a demand for smaller, lighter, yet more powerful energy sources.

Polymer electrolytes may generally be defined as polymers that possess ion transport properties comparable with that of common liquid ionic solutions. The development of polymer electrolytes has drawn the attention of many researchers in for their applications not only in fuel cells and lithium batteries but also, in other electrochemical devices such as super capacitors and electrochromic devices, etc. These polymer electrolytes have several advantages over their liquid counter parts such as no internal shorting, no leakage [Gray 91-97, Scrosati 93, MacCallum 87<sup>1</sup>-87<sup>2</sup>]. The very first example of a “dry solid” polymer electrolyte was a poly(ethylene oxide) (PEO) based blends with sodium and potassium thiocyanates salts showed very low ambient temperature conductivities of the order of  $10^{-8}$  S/cm [Fenton 73, Wright 75]. The blends with inorganic salts such as LiI, LiPF<sub>6</sub>, LiBF<sub>4</sub>, LiClO<sub>4</sub> etc., or more complex organic salts, for instance, LiN(SO<sub>2</sub>CF<sub>3</sub>)<sub>2</sub>, LiCF<sub>3</sub>SO<sub>3</sub>, among others has also been studied [Costa 2007]. Since this system does not possess any organic liquid, the polymer host acts as solid solvent. However, the cycling performance of this dry solid polymer electrolyte with lithium metal electrodes was not satisfactory and was restricted to as low as 200–300 cycles. The poor performance of the cells was attributed to poor ionic conductivity. Armand's subsequent suggestion to use solid polymer electrolytes in lightweight and powerful solid state batteries opened an intensive research for better conducting materials [Armand 78].

A significant amount of research has been focused on the development of materials for the electrolyte layer which transports lithium ions between the anode and the cathode [Dias 00, Vincent 00]. Polar aprotic liquid electrolytes provide good media for the transport of lithium ions [Vincent 00]. However, organic liquid electrolytes require bulky and sometimes heavy enclosures [Gray 97]. Thus, attempts have been made to develop solid polymer electrolytes that allow the use of complex shapes, greater ease of

fabrication, reduced weight containment, lower flammability, and a lower toxicity of the battery components [Gray 97]. So far no solid polymer electrolyte is known that efficiently transports lithium ions at commercially viable levels (conductivities  $10^{-3}$  S/cm at 25°C).

Several research groups have been actively searching for anhydrous proton conducting polymers for their use in high temperature fuel cells. The material design concept is primary based on acid-base interactions. It was shown that the addition of  $H_3PO_4$  to polybenzimidazole (PBI) delivered appreciable proton conductivity at elevated temperature under anhydrous conditions [Wang 96]. Also proton-conducting polymer electrolytes based on phosphoric acid was reported by Bozkurt et. al. [Bozkurt 99]. In this approach cationic polyelectrolyte poly(diallyldimethylammonium-dihydrogenphosphate),  $PAMA^+H_2PO_4^-$  was used as the polymer matrix. The conductivity of this material increased with phosphoric acid content, reaching  $10^{-2}$  S/cm at 100°C.

Kreuer et. al showed that the use of imidazole as the base component in place of water has delivered not only higher proton conductivity, but also displayed better temperature stability due to the fact that imidazole is a stronger Brønsted base compared to water [Kreuer 98]. More recent development has been carried out on acid/base oligomer systems by Honma et. al [Honma 99], and on polymer blend systems bearing acid base functional groups by Kerres et. al. [Kerres 01].

## 2. Polymer Electrolyte Systems

### 2.1 Hydrated Membranes

#### 2.1.1 Perfluorinated Ionomer Membranes

Perfluorinated Ionomer Membranes are well-established low temperature materials, which have a Teflon-like backbone structure with sulfonated side chains attached by ether bonds (Figure 2.1). Within this family of ionomers, Nafion<sup>®</sup> is the best known and commercially available material.

These polymers are available in a large range of equivalent weights (EW is the mass of polymer per mole of sulfonic acid group). The development of perfluorinated membranes by DuPont in the 1960s has played a significant role in electrochemical applications (chlor/alkali electrolysis, fuel cells, etc). These materials are particularly suitable for fuel cell applications.

The unique feature of Nafion<sup>®</sup>-type ionomers is their superacidity, which is based on a very high degree of proton dissociation from the sulfonic acid group attached to the perfluorinated spacer group.

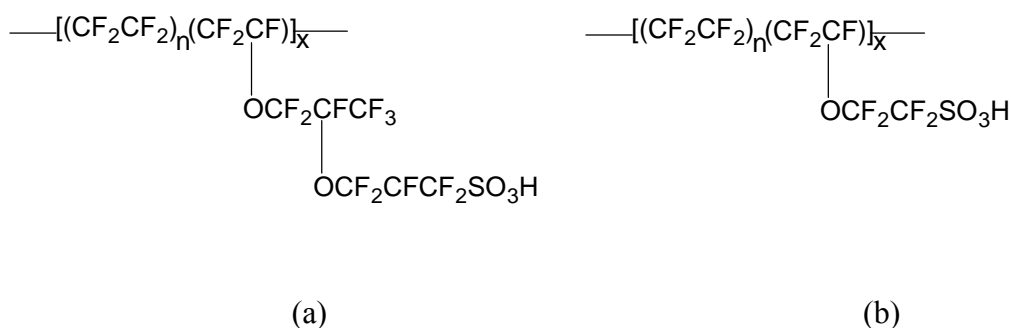


**Figure 2.1** Structures of perfluorinated ionomers (Nafion<sup>®</sup>) from DuPont (a) and Dow Chemical (b). The values of  $n$  and  $x$  can be varied to produce materials with different equivalent weights (EW).

The structural model of an ionomer membrane which comprises ionic hydrophilic clusters, and an amorphous hydrophobic region has been suggested previously by [Schlick 96] and revised by [Kreuer 01] (Figure 2.2).



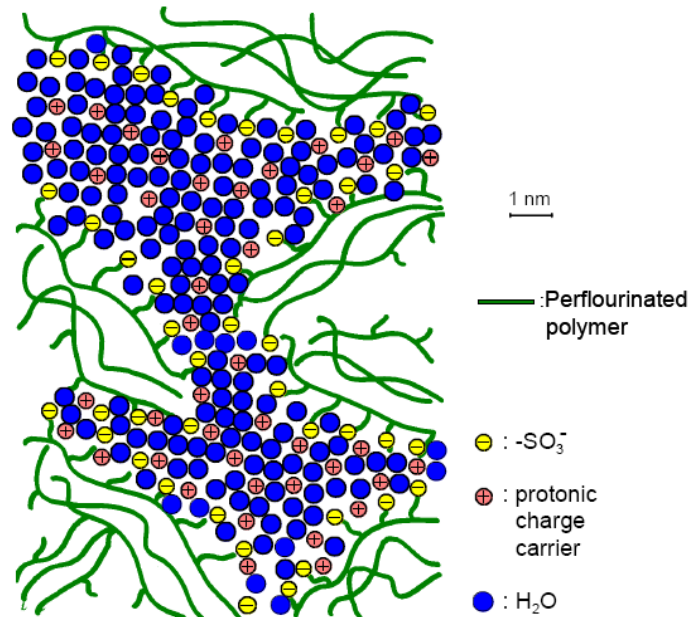


**Figure 2.2** Model for Perfluorosulfonic Polymer, Nafion [Kreuer 01].

The transport properties of perfluorosulfonic membranes are largely influenced by the water content. Nafion combines the extreme hydrophobicity of the polymer backbone with the extreme hydrophilicity of the sulfonic acid function, which leads to a hydrophilic/hydrophobic nano-separation (Figure 2.2) when the material comes in contact with water. The hydrophilic domains spontaneously take up water and swell to form nanochannels. These nanochannels are formed by the aggregation of sulfonic acid functional groups. They are responsible for the transport of water and protons. In the nanochannels, charge carriers are formed by dissociation of the acidic functional groups in the presence of water, and proton conduction takes place through the hydrophilic channels. On the other hand, hydrophobic domains provide the polymer with morphological stability and prevent its dissolution in water [Kreuer 01].

The conductivity of Nafion<sup>®</sup> is around 0.1 S/cm at room temperature when swollen with 100 % of water [Ren 96]. In the dry state the membrane behaves like an insulator but, when hydrated, it becomes a conductor [Pourcelly 90]. The proton conductivity reaches a maximum in the temperature range of 55-70°C. Outside of this temperature range, the conductivity decreases perhaps a change of the hopping distance between cluster zones [Rieke 87], but especially because of dehydration at temperature above 100°C.

### 2.1.2 Other Sulfonated Hydrocarbon Polymer Systems

These polymers include aromatic polyesters, polyphenylene sulphides, polysulfones, polyethersulfones, various polyketones, polyphenylquinoxalines, polybenzimidazoles and polyimides, which all exhibit exceptional thermal and chemical stability. In the hydrated state, the proton conducting properties of these sulfonated aromatic polymers are improved. The main representatives of sulfonated polymers and their conductivities are given in Table 2.1.

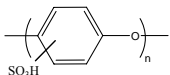
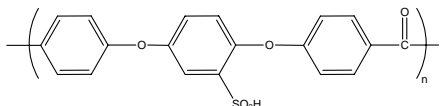
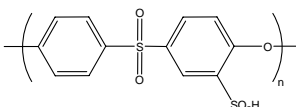
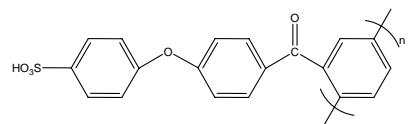
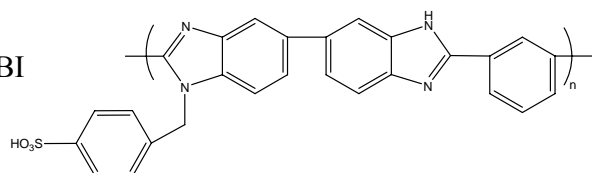
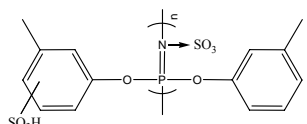
## 2.2 Anhydrous Proton-Conducting Polymers

### 2.2.1 Phosphoric Acid-Based Membranes

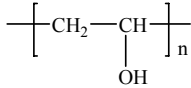
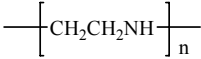
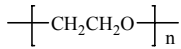
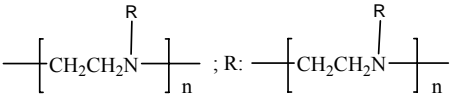
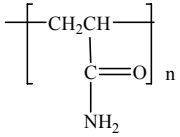
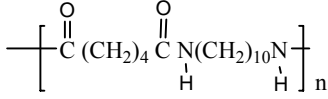
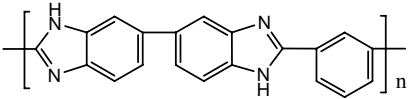
The requirement of these membranes for fuel cells, hydrogen sensors and high temperature batteries has led many researchers to focus on the development of new materials to serve as an electrolyte [Kerres 01, Kreuer 01, 02, Schuster 04, Pu 01, Li 03]. During the last decade, investigations on anhydrous polymer electrolyte systems with high proton conductivity at intermediate temperatures (100–200°C) have been carried out. The proton conduction does not depend on the presence of an aqueous phase in anhydrous proton conducting polymer electrolytes. This requires the replacement of water by a suitable proton solvent which would provide proton conduction similar to water but at higher temperatures. In this context, phosphoric acid is used as proton solvent. Various blends of Polymer-H<sub>3</sub>PO<sub>4</sub> were studied and they are summarized in Table 2.2.

One of the most promising new membranes for operation above the boiling point of water is PBI doped with phosphoric acid for proton conductivity. PBI has attracted the interest of scientists and engineers because of its good thermal and chemical stability. These properties make phosphoric acid doped PBI useful for PEMFC at temperatures up to 200°C [Wainright 95]. PBI is an amorphous basic polymer with high thermal stability. However, in the pure state the conductivity is very low, about 10<sup>-12</sup> S/cm [Aharoni 79, Pohl 64]. The conductivity of phosphoric acid doped PBI increases with increasing doping level, temperature and humidification. The conductivity of the PBI- H<sub>3</sub>PO<sub>4</sub> is about 10<sup>-3</sup> S/cm at 110°C for x=1.45 [Pu 02].

**Table 2.1. Sulfonated Polymer Electrolyte Membranes for Fuel Cell Applications**

Sulfonated Electrolyte	Abbreviation	Structure	Conductivity (S.cm <sup>-1</sup> ) (°C)	Ref.
Poly(phenylene oxide)	S-PPO		-	[Walker 99]
Poly(ether-ether ketone)	S-PEEK		6x10 <sup>-2</sup> (RT)	[Soczka-Guth 99]
Poly(arylether sulfone)	S-PAES		-	[Kerres 96]
Poly(4-phenoxybenzoyl-1,4-phenylene)	S-PPBP		9x10 <sup>-2</sup> (80)	[Hogarth 01]
Polybenzimidazole	S-PBI		1x10 <sup>-1</sup> (RT)	[Gieselman 92]
Polyphosphazene	S-PP		7x10 <sup>-2</sup> (RT)	[Guo 99]

**Table 2.2. Anhydrous proton conducting polymer electrolytes based on blending with H<sub>3</sub>PO<sub>4</sub>**

Type of Electrolyte	Polymer Structure	Doping Ratio	Maximum RT Conductivity (S/cm)	Application	Ref.
PVA-H <sub>3</sub> PO <sub>4</sub>			~ 10 <sup>-5</sup>	hydrogen sensor	Petty-Week 88]
IPEI-H <sub>3</sub> PO <sub>4</sub>		0<x<1	~ 10 <sup>-5</sup>		[Tanaka 00]
PEO-H <sub>3</sub> PO <sub>4</sub>		0<x<2	~ 10 <sup>-5</sup>		[Donoso 88]
PVA-H <sub>3</sub> PO <sub>4</sub> -IPN			10 <sup>-4</sup> -10 <sup>-5</sup>	hydrogen sensor	[Polak 86]
PEO-PMMA-H <sub>3</sub> PO <sub>4</sub>			> 10 <sup>-3</sup>	fuel cell	[Przyluski 93]
bPEI-H <sub>3</sub> PO <sub>4</sub>		0<x<3	1 0 <sup>-4</sup>	electrochromic display	[Tanaka 00]
PAAM-H <sub>3</sub> PO <sub>4</sub>		0.6<x<2	10 <sup>-3</sup>	electrochromic display	[Rodriguez 93]
PAAM-H <sub>3</sub> PO <sub>4</sub> -MBA			~ 10 <sup>-3</sup>		[Wieczorec 95]
Nylon 610-H <sub>3</sub> PO <sub>4</sub>		0<x<3	~ 10 <sup>-3</sup>		[Grondin 95]
PBI-H <sub>3</sub> PO <sub>4</sub>		0<x<3	~ 10 <sup>-6</sup>		[Pu 02, Wainright 95]

### 2.2.2 Other Anhydrous Materials

The proton-conducting properties of nitrogen-containing aromatic heterocycles such as imidazole and benzimidazole were studied [Kreuer 98, 99]. The pure materials showed reasonable conductivities in the liquid state [Kreuer 99], which was assigned to some degree of self-dissociation. The behavior of imidazole toward protons is very similar to that of water: The heterocycles are amphoteric molecules; they exhibit extensive hydrogen bond interactions that result in a fluctuating network, and to some extent undergo self-dissociation (Figure 2.3).

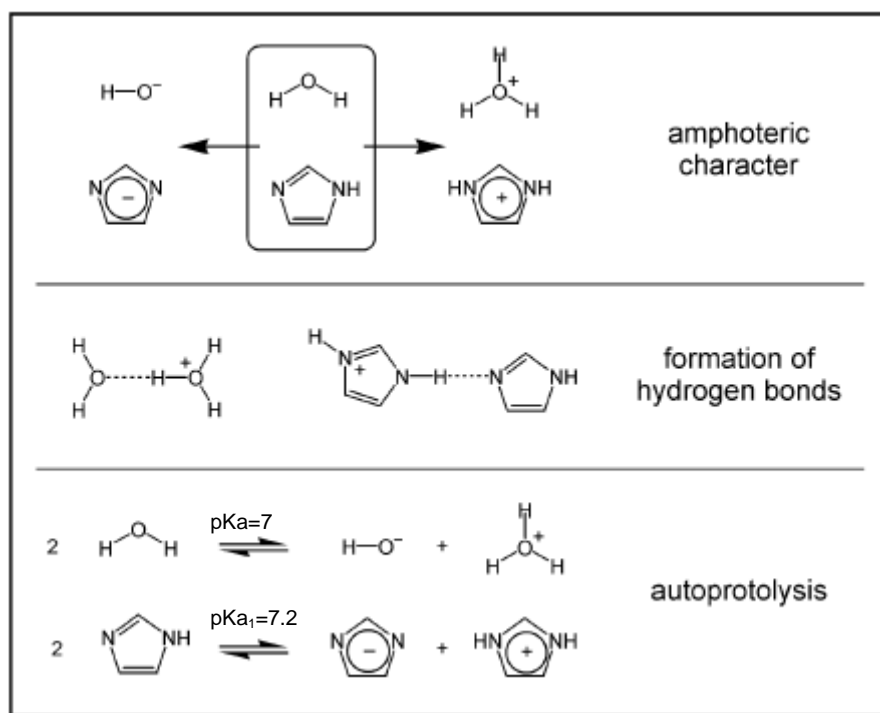


**Figure 2.3** Imidazole and water exhibit similar behavior toward protons [Schuster 02, Acheson 76].

The substitution of water by heterocycles such as imidazole or benzimidazole as alternative proton solvents was also studied. The proton transport under anhydrous or low humidity conditions might be based on a non-vehicular mechanism, in which only protons are mobile from site to site without an assistance of mobile vehicle molecules. Imidazole has better thermal and/or chemical stability compared to water [Gelus 68,

Kirsche 94]. Specific conductivities of Nafion swollen with different proton solvents are displayed in Figure 2.4. PAA/Imidazole blends reach a conductivity of  $10^{-3}$  S/cm at  $120^{\circ}\text{C}$  [Bozkurt 03]. Another interesting material is the PAMPSA/Imidazole based blend which showed a maximum conductivity of  $1.5 \times 10^{-3}$  S/cm at  $100^{\circ}\text{C}$  [Erdemi 03].

Another interesting approach for obtaining high proton conductivity in polymers based on proton solvating heterocycles covalently bound via flexible spacers (EO units) was also presented [Schuster 01]. Intermolecular proton transfer and structural reorganization by hydrogen bond breaking and forming processes are to be the dominant conduction processes, which gave rise to proton conductivities of up to  $5 \times 10^{-3}$  S/cm at  $120^{\circ}\text{C}$  in completely water-free imidazole terminated oligomers.

Additionally, the preparation and characterisation of fully polymer-bound heterocycles as proton solvents was also presented [Herz 03]. Two different types of polymers were reported: Polystyrene with imidazole terminated flexible side chains and benzimidazole covalently linked to an inorganic  $\text{SiO}_2$  network by a flexible spacer. High proton conductivities of up to  $7 \times 10^{-4}$  S/cm at  $200^{\circ}\text{C}$  were obtained for these polymers in the anhydrous state.

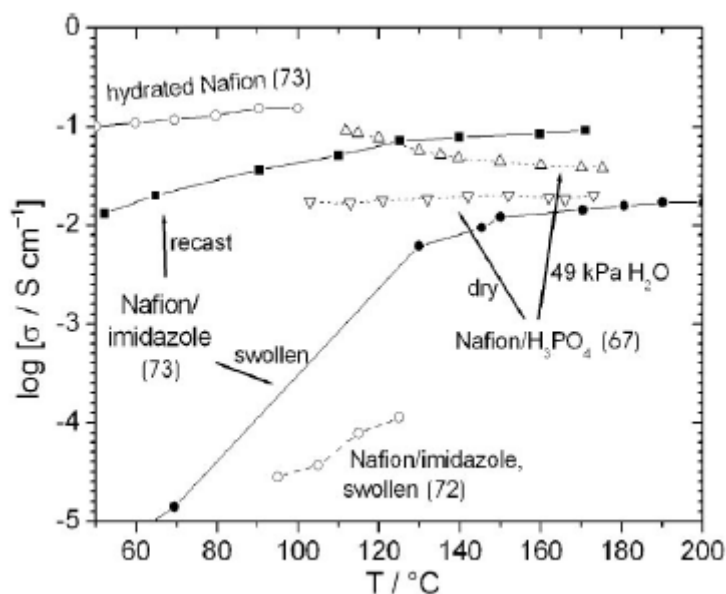


**Figure 2.4** Conductivities of Nafion swollen with water, phosphoric acid, and imidazole, respectively, and those of a recast Nafion/imidazole blend [Schuster 03].

### 2.3 Ionic Liquids

Ionic liquids (ILs) are liquids at ambient usually below 100°C. These are comprised entirely of ions and are receiving an upsurge of interest for their unique physicochemical properties such as high thermal stability, negligible vapor pressure, relatively high ionic conductivity, and good electrochemical stability.

The commonly used imidazolium based ionic liquid structures are shown in Figure 2.5.

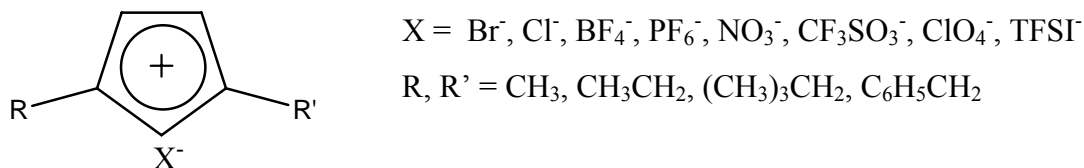


**Figure 2.5** Imidazolium-based ionic liquids with different counter ion.

The realization that the constraints, associated with the use of water at temperatures higher than 100°C, place a uncertain block on the widespread use of proton exchange membrane fuel cells [Kreuer 02, Yang 01] which can result in an upsurge of interest in the option of ubiquitous ionic liquids. Ionic liquids are very promising due to low vapor pressure, high ionic conductivity and greater thermal and electrochemical stability, but need to act as proton solvents or themselves be capable of conducting protons for their true use in proton conductors [Fuller 99, Doyle 00]. With the aim towards innovating proton conducting ionic liquids for anhydrous proton conductors at elevated temperatures, several research groups studied ILs as protic solvent and electrochemically provide insight into the proton conduction [Sun 01, Susan 03<sup>1</sup>, Noda 03, Ohno 02, Hirao 00, Souza 03]. Ionic liquids [Welton 99, Wasserscheid 00, Dupont 02, Noda 01, Tokuda 04], due to their unique physicochemical properties mentioned above, have received significant attention for their use in multidisciplinary areas. These significant properties make the ionic liquids ideal as electrolytes for electrochemical devices. In present case,

lithium-ion conductivity can be molecularly designed for the ionic liquids, the scope and utility of the ionic liquids will expand to lithium rechargeable batteries [Shobukawa 04]. Studies showed that ILs as electrolyte in Li-ion batteries is promising [Shobukawa 05, Hayamizu 04].

The ionicity of ionic liquids is determined by using the classification diagram shown in Figure 2.6 which is based on the classical Walden rule. The Walden rule relates the ionic mobilities (represented by the equivalent conductivity  $\Lambda$  ( $\Lambda = F \sum \mu_i z_i$ ) to the fluidity  $\phi$  ( $\phi = \eta^{-1}$ ) of the medium through which the ions move (where  $F$  is Faraday's constant,  $\mu$  is the mobility of  $i$ ,  $z$  is charge of  $i$  and fluidity is the inverse of viscosity,  $\eta$ ). In ideal condition which means in the absence of any ion-ion interactions, the slope should be unity. The position of the ideal line is established using aqueous KCl solutions at high dilution [Yoshizawa 03].

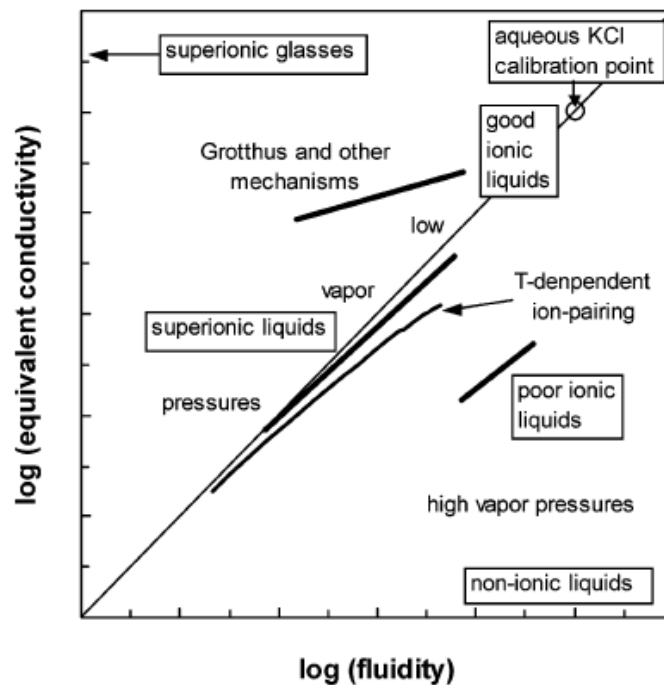


**Figure 2.6** Classification diagram for ionic liquids, based on the classical Walden rule, and deviations therefrom [Yoshizawa 03].



## 2.4 Proton Conduction Mechanisms

Besides the electrode reactions, the proton transport through the separator membrane is of high importance for the function of a fuel cell. The proton is unique in that it is the only ion which does not possess an electronic shell. It therefore strongly interacts with the electronegative species of its environment. Proton transfer phenomena follow two principal mechanisms. The most trivial case of proton migration requires the translational dynamics of bigger species: this is the **vehicle mechanism** [Kreuer 82]. In this mechanism, the proton diffuses through the medium together with a “vehicle” (for example, with  $\text{H}_2\text{O}$  as  $\text{H}_3\text{O}^+$ ). The counter diffusion of unprotonated vehicles ( $\text{H}_2\text{O}$ ) allows the net transport of protons. The observed conductivity, therefore, is directly dependent on the rate of vehicle diffusion (Figure 2.7a). In the other principal mechanism, the vehicles show pronounced local dynamics but reside on their sites. The protons are transferred from one vehicle to the other via hydrogen bonds (proton hopping). Simultaneous reorganization of the proton environment, consisting of reorientation of individual species or even more extended ensembles, then leads in the formation of an uninterrupted path for proton migration. This mechanism is known as the **Grotthuss mechanism**. This reorganization usually involves the reorientation of solvent dipoles (for example  $\text{H}_2\text{O}$ ), which is an inherent part of establishing the proton diffusion pathway. The rates of proton transfer and reorganization of its environment affect directly this mechanism. Those basic transport mechanisms are illustrated in Figure 2.7b.

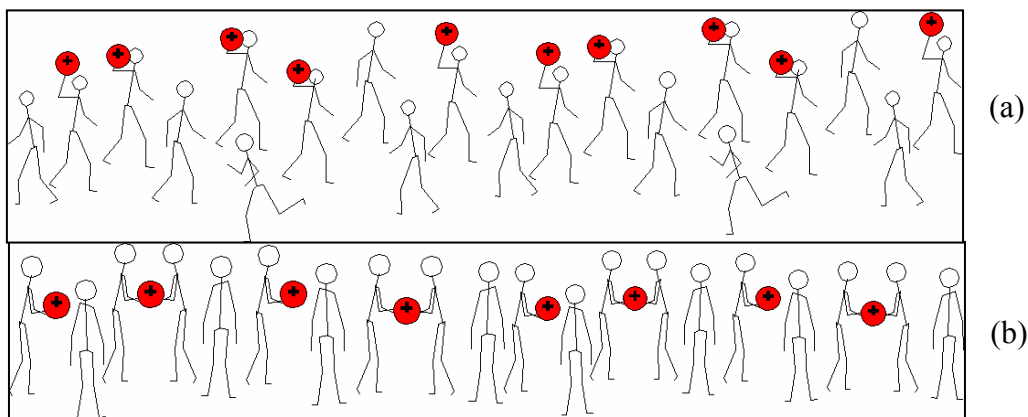


**Figure 2.7** Schematic representation of phenomena involved in proton conduction mechanisms: (a) Vehicle Mechanism (b) Grotthuss Mechanism [Kreuer 82].

## 2.5 Applications

### 2.5.1 Fuel Cells

Fuel cells are electrochemical devices which convert the energy of a chemical reaction directly into electricity and heat. They are similar in principle to primary batteries except that the fuel and oxidant are stored externally, enabling them to continue operating as long as reactants are supplied. For instance, when hydrogen is generated from such fuels as gasoline, methanol, or natural gas, a fuel-reformer device must be added to the system. In addition, if pure hydrogen or methanol is to be used instead of gasoline, then the necessary infrastructure must be in place; for example some kind of facility for hydrogen or methanol refueling must be provided along with or instead of existing gas stations. No matter which fuel-based system will ultimately become the mainstream, hydrogen is a main fuel. Each cell consists of an electrolyte sandwiched between two electrodes. Fuel is oxidized at the anode, liberating electrons which flow via an external circuit to the cathode. The circuit is completed by a flow of ions (protons) across the electrolyte that separates the fuel and oxidant streams (Figure 2.8).

Among them, solid polymer electrolyte membrane fuel cells “PEMFC” are our interest due to the electrolyte used in this type.

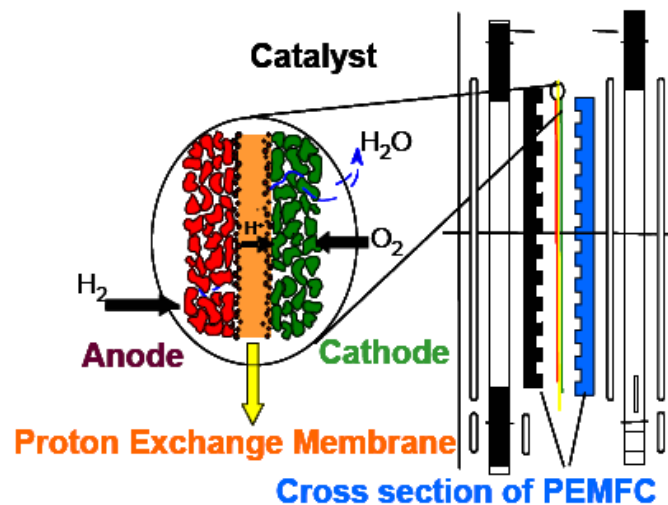


**Figure 2.8** The cross-section of a polymer electrolyte membrane fuel cell (PEMFC)

[Petterson 06].

### 2.5.1.1 Solid Polymer Electrolyte Membrane (PEM) Fuel Cells

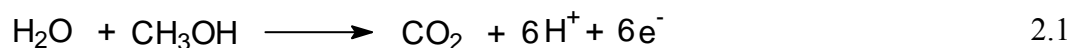
The schematic representation of the principle of a  $\text{H}_2\text{-O}_2$  fuel cell is shown in Figure 2.8. Hydrogen supported from the fuel gas stream is consumed at the anode, where it yields electrons to the cathode. Hydrogen ions enter the electrolyte and diffuse to the cathode by electro-osmotic flux. At the cathode, oxygen combines with the electrons and protons from the electrolyte to produce water which is expelled from the electrolyte [Scherer 90]. Unlike internal combustion engines (ICE), fuel cells offer the potential to convert energy very efficiently. The most advanced fuel cell systems are fuelled with hydrogen and are based on perfluorinated sulfonic acid ionomers. These solid electrolytes offer numerous advantages over classical liquid electrolytes, such as sulphuric acid, including higher power densities, reduced fuel crossover and more obviously, improved handling.

The state of the art PEM fuel cell uses an aqueous sulphonic acid electrolyte which is incorporated into a polymer membrane so that the separator is effectively a solid (ionomers). A bipolar plate provides the electrical connection between cells and acts as an impermeable barrier between the fuel and oxidant flows; it also supports the electrodes. A platinum-based catalyst is used at both, cathode and anode.

The conventional electrolyte must be kept hydrated at all times, effectively limiting the operating temperature of the cell. At atmospheric pressure the operating temperature is about  $80^\circ\text{C}$ , but over  $100^\circ\text{C}$  has been achieved under pressure. The cell can be run directly on hydrogen or on reformed hydrocarbon fuels such as methanol or natural gas, but as platinum is poisoned by carbon monoxide (CO) this must be removed during fuel processing, or the catalyst tolerance versus CO need to be improved. PEM fuel cells are now being demonstrated in a range of commercial applications including buses and cars, as a result of a massive global effort to develop this technology for automotive markets, and combined heat and power (CHP) systems.

Another important variant of the PEM fuel cells is the direct methanol fuel cell (DMFC). DMFC directly oxidises methanol at its anode, thereby removing the need for fuel-reforming systems. In the long term, the DMFC is likely to be an attractive option, though much fundamental research is still required to improve the kinetics of the methanol oxidation reaction and to reduce methanol diffusion through the electrolyte. Methanol is either provided as gas or as aqueous solution.

In methanol fuel cells [Hampson 79] the total anodic reaction is (2.1)



This type of fuel cell systems is suitable for automotive application since  $\text{CH}_3\text{OH}$  as a liquid can be safely stored and efficiently oxidized to give energy. Methanol fuel cells operate with proton conducting polymers as the membrane in a wide temperature range [Kordesch 96].

### 2.5.2 Batteries

The importance of energy storage in the optimal utilization of our energy resources arises. A battery is a device that stores chemical energy and makes it available in an electrical form when it is needed. Batteries consist of electrochemical devices such as one or more galvanic cells or fuel cells.

Two or more electrochemical cells, are electrically interconnected, each of which contains two electrodes and an electrolyte. The redox (oxidation-reduction) reactions that occur at these electrodes convert chemical energy into electrical energy. In everyday usage, 'battery' is also used to refer to a single cell.

Batteries can be generally divided into two main types: primary and secondary batteries [Castellan 83]. Primary cells, also called disposable batteries, are intended to be used once, until the chemical changes that induce the electrical current supply are complete. The cell reaction is not reversible, and when the materials are consumed the device must be discarded. These are most commonly used in smaller, portable devices with either low current drain, only used intermittently, or used well away from an alternative power source. Commonly used chemical systems for primary batteries are zinc-carbon, zinc chloride, silver oxide, mercuric oxide, alkaline/manganese oxide, and lithium.

In contrast to primary cells, secondary cells or rechargeable batteries can be re-charged after they have been drained. This is done by applying externally supplied electrical

current, which reverses the chemical reactions that occur in use. Some examples for commonly used secondary batteries are lead-acid battery especially used in vehicles, nickel metal hydride, nickel-cadmium, used in many domestic applications, nickel-zinc, lithium ion batteries.

The performance of the batteries is evaluated according to some parameters:

The **energy density** of a battery is a measure of how much energy the battery can supply relative to its weight ( $\frac{W.h}{kg}$ ) or volume ( $\frac{W.h}{l}$ ). The energy density of a battery is mainly

dependent on the composition of its active components. This definition is purely theoretical as it does not take into account the mass or volume of inactive materials, or the variation in chemical reactions [Tarascon 01].

**Memory Effects** - As a rechargeable battery is used, recharged, and used again, it loses a small amount of its overall capacity, energy density. This loss is to be expected in all secondary batteries as a certain fraction of the active components become irreversibly consumed in each cycle.

**Self-Discharge Rates** - All charged batteries (except some) will slowly lose their charge over time, even if they are not connected to a device. Moisture in the air and the slight conductivity of the battery housing will serve as a path for electrons to travel to the cathode, discharging the battery. The rate at which a battery loses power in this way is called the self-discharge rate.

The **cycle life** of a battery is the number of discharge/recharge cycles the battery can sustain, with normal care and usage patterns, before it can no longer hold a useful amount of charge.

**Operating Temperatures** - As a general rule, battery performance, which is defined with some parameters discussed above, deteriorates gradually with a rise in temperature. At very low temperatures (-20- 0°C), battery performance decreases as well. At low temperatures, the loss of energy density is due to the reduced discharge rate and the increased internal resistance of the electrolyte. At high temperatures, the loss of energy density is due to the increase of unwanted, parasitic chemical reactions in the electrolyte. Common types of commercial batteries and some of their properties are summarized in Table 2.3 [Frankfurter 03].

**Table 2.3 Properties of some common types of commercial batteries**

Battery Type	Cell Voltage (V)	Gravimetric Energy Density (W.h/kg)	Volume Energy Density (W.h/l)	Cycle Life	Toxicity
Nickel-Cd	1,25	45-80	100-130	1500 <sup>1</sup>	Highly toxic harmful to environment
Nickel-Metal Hydride	1,25	60-120	170-190	300-500 <sup>1,2</sup>	Relatively low toxicity should be recycled
Lead-Acid	2	30-50	40-65	200-300 <sup>2</sup>	Toxic lead and acid, harmful to environment
Reusable Alkaline	1,5	80 (initial)		50 <sup>2</sup>	Low toxicity, may contain mercury
Lithium-Ion <sup>3</sup>	3,6	110-160	250-270	300-500 <sup>2</sup>	Low toxicity, can be disposed in small quantities
Lithium-Ion-Polymer <sup>4</sup>	3,6	100-130	200-240	300-500	Low toxicity, can be disposed in small quantities

<sup>1</sup>Cycle life is based on battery receiving regular maintenance; <sup>2</sup>Cycle life is based on the depth of discharge  
<sup>3</sup>liquid organic electrolyte, <sup>4</sup>polymer as electrolyte

### 2.5.2.1 Lithium Ion Batteries

There has been enormous activity in the development of lithium batteries for portable electronic devices. Lithium is the lightest metal and has one of the highest standard reduction potentials. The combination of these two characteristics gives the element particularly favourable energy content, with a theoretical specific capacity of 3860 Ah/kg in comparison with 820 Ah/kg for zinc and 260 Ah/kg for lead. Since the standard reduction potential of lithium is -3.045 V [Fischer 58], the metal is thermodynamically unstable in protic solvents such as water, and the realization of practical lithium cells had to await the development of suitable non-aqueous electrolyte systems. Primary cells normally employ lithium metal foil as anode, whereas secondary lithium cells are not usually based on lithium metal since experience has shown that repeated recharging of lithium metal anodes can be dangerous due to its flammable property which can lead to fires and explosions. The presence of liquids requires special battery pack sealing to prevent leakage and volatiles can lead to explosions. Reactions of liquid solvents with Li

metal also result in poor battery performance. It is therefore desirable to have all-solid-state batteries in which the anode, electrolyte and cathode are flexible films, e.g., Lithium-Metal-Polymer batteries, for ease in assembly, versatility in battery shape/design, safety and improved performance. Thus,  $\text{Li}^+$  ions are intercalated into a carbon to be used as anode in the charged state and into a metal-oxide cathode in the discharged state. Therefore, the most promising approach is that of the “rocking chair” cell, in which the lithium metal is replaced by a lithium-carbon ion source [Scrosati 93]. During charging and discharging of such batteries, lithium ions are “rocked” between lithium-carbon and lithium-metal oxide intercalation compounds, which act as the electrode couple (Figure 2.9).

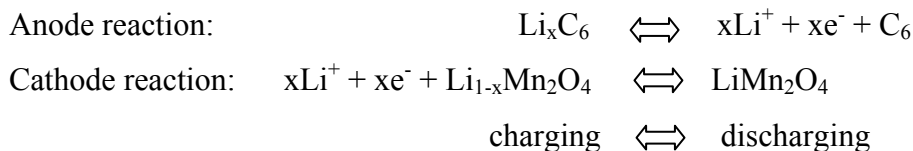
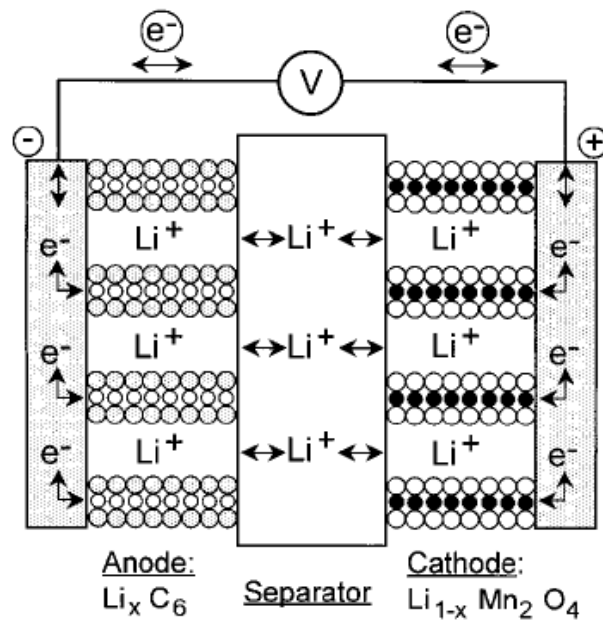


**Figure 2.9** Schematic illustration of a lithium rocking chair battery with graphite and spinel as intercalation electrodes and its electrode reactions [Meyer 98].

Portable electronic devices often operate at or near ambient temperature of  $\sim 25^{\circ}\text{C}$ , however, producing battery which can be used at high temperature is difficult to meet this requirement [Tarascon 01]. As pointed out before, poly(ethylene oxide) (PEO) was the first polymer used as a polymer solvent for lithium salts [Armand 79]. In recent years, ionic liquids with organic cations have been suggested for electrolyte applications [Fung 93, MacFarlane 99, Bonhote 96]. Unlike conventional solvents, ionic liquids have negligible vapor pressures. The absence of volatiles greatly improves the safety characteristics of a battery. Some ionic liquids have conductivities of  $10^{-2}$  S/cm or higher at  $25^{\circ}\text{C}$ . A lithium battery, however, requires  $\text{Li}^{+}$  cations to be transported between the anode and cathode. The ionic liquids must therefore be doped with a suitable LiX salt [Fung 93, MacFarlane 99]. The doped ionic liquids may then be incorporated into a flexible, thin membrane to form a battery electrolyte.



### 3. Synthesis

#### 3.1 Motivation for Synthesis

Traditional ion-conducting polymers such as poly(ethylene oxide)-based polymer electrolytes, are solid solutions of salts in polymers [Armand 86, Vincent 87, Watanabe 88, Ratner 88]. Ionic motion in these polymer electrolytes is coupled with the local segmental motion of the polymer. In this type of electrolytes an increase of carrier-ion density and mobility are difficult to achieve because both, depend on the interaction of polymer segments with the ions. These facts are reflected by the appearance of a maximum in ionic conductivity in polyethers with increasing salt concentration. On the other hand, in certain salt–polymer systems, in the range of high salt concentrations, the ionic conductivity increases and  $T_g$  decreases again.

These electrolyte salts are characterized by low  $T_g$  and  $T_m$ , and they form supercooled liquids with high conductivity at room temperature. In the salt–polymer systems, the number of carrier ions and their mobility increase with increasing the electrolyte concentration [Watanabe 93, Angell 93]. As a result, a high ionic conductivity that is not coupled with the segmental motion of the polymers can be expected.

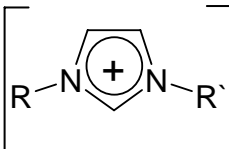
Based on this concept, the use of ionic liquids (ILs) appears to be promising with respect to high ion conductivity in polymers. They are known for many years, for instance [EtNH<sub>3</sub>]-[NO<sub>3</sub>], which has a melting point of 12°C, was first described in 1914 [Walden 14, Sugden 29]. However, their importance was understood only in the last two decades. ILs are being investigated for many applications including electroplating, batteries, electrochemical capacitors and photochemical (PEC) cells. Ionic liquids can be utilized as the electrolyte solvent in batteries and fuel cells. The physical properties which make the systems attractive in such a role are the following [Hussey 88, Papageorgiou 96]:

- excellent thermal and chemical stability
- negligible vapor pressure at elevated temperature
- miscibility in a diverse range of solvents

- they are often composed of poorly coordinating ions, so they have the potential to be highly polar yet noncoordinating solvents.

The comparison of melting points of different chlorides shown in Table 3.1 illustrates the influence of the cation on the thermal properties clearly.

**Table 3.1. Melting points of various chloride salts**

Salt	m. p. (°C)
NaCl	803
KCl	772
 $\left[ \text{R}-\text{N}^+\text{C}_2\text{N}-\text{R}' \right] \text{Cl}^-$	R=R`=methyl ([MMIm]Cl) 125 R=methyl, R`=ethyl ([EMIm]Cl) 87 R=methyl, R`=n-butyl ([BMIm]Cl) 65

a : MMIm = 1,3-dimethylimidazolium

For cations of low-melting salts the following requirements should be fulfilled [Mehnert 02, DeCastro 00, Ogawa 01]:

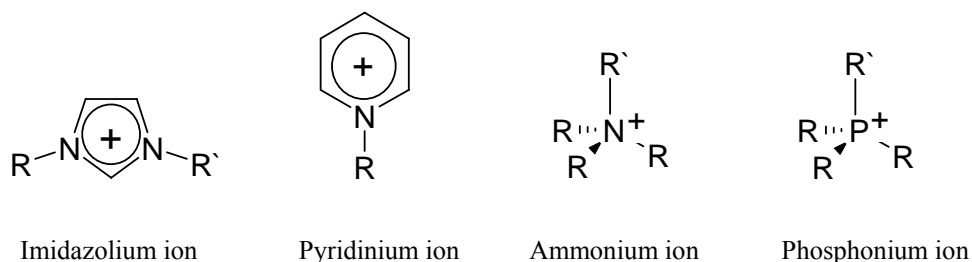
- low symmetry
- weak intermolecular interactions
- good distribution of charge in the cation

In addition to the cation, the anion influences the melting point, too. In most cases, an increasing size of the anion with the same charge leads to a further decrease in the melting point as shown in Table 3.2.

**Table 3.2. Influence of different anions on the melting point of ILs**

Imidazolium salt	M. p. (°C)
[EMIm]Cl	87
[EMIm]NO <sub>2</sub>	55
[EMIm]BF <sub>4</sub>	8
[EMIm]CF <sub>3</sub> SO <sub>3</sub>	-9

The initial step in the synthesis of ILs is the quaternization of alkyimidazole, pyridine etc. to form the desired cation such as imidazolium, pyridinium, ammonium [Hussey 88, Wilkes 82]. The most important, reported cation types are shown in Figure 3.1.

**Figure 3.1** Some types of cations in ionic liquids.

### 3.1.1 The Synthesis of Ionic Liquids

It is readily apparent from Table 3.4 that the series of room temperature ionic liquids (RTILs) was studied. The synthesis of RTILs was described in previous works [Holbrey 99, Bonhôte 99, Wasserscheid 00].

Up to present, 1,3-dialkylimidazolium salts appear to be among the most stable and highly conducting ionic liquids [Bonhôte 96]. The thermal decomposition temperatures are similar for the different cations but appear to decrease as the anion hydrophilicity increases. The effect of water on the thermal stability of ILs is not clear yet. Relative

anion stabilities have been suggested as  $\text{PF}_6^- > \text{BF}_4^- > \text{halides}$ . Increasing the cation size dramatically increased thermal stability. The main factors that influence the melting point are the charge distribution on the ions, H-bonding ability, the symmetry of the ions and the van der Waals interactions [Ngo 00]. It is clearly seen that in our systems the melting points increased with the symmetry of the cations. However, the melting point of some ionic liquids is uncertain because they undergo substantial supercooling [Ngo 00]. It was displayed that the temperature of the phase change can differ considerably depending on whether the sample is heated or cooled. The materials showed supercooling when the temperature is about  $100^\circ\text{C}$  below their melting temperatures,  $T_m$ . Phase change from liquid to glassy state was observed at very low temperatures. The influence of alkyl chains on the melting points was reported by other research groups [Holbrey 99, Visser 01, Dzyuba 01]. They also showed that the melting point decreases from the methyl substitution to the butyl to hexyl compound and then increases.

The water content of these ILs was determined by the Karl-Fischer titration method. All the salts were dried under high vacuum ( $\sim 10^{-5}$  mbar) for 3 days before titration.

The identity of the anion greatly influences the water miscibility and hence water content which decreases as the hydrophobicity of the ILs increases. The transitions ( $T_g$ ,  $T_m$ ,  $T_c$ ) and decompositions of the ILs ( $T_d$ ) are summarized in Table 3.4.

**Table 3.4. Thermal properties of imidazolium salts synthesized in this work**

Ionic Liquid	T <sub>g</sub> (°C)	T <sub>c</sub> (°C)	T <sub>m</sub> (°C)	T <sub>d</sub> (°C)	Water Content (ppm)
EEImBF <sub>4</sub>				215	47,3
EEImPF <sub>6</sub>			69,73	175	92,7
EEImH <sub>2</sub> PO <sub>4</sub>				200	40,1
EEImCF <sub>3</sub> SO <sub>3</sub>	-91,21	-53,33	19,35	200	65,7
BMImBF <sub>4</sub>	-85,9			310	21,0
(BMIm) <sub>2</sub> ZnCl <sub>4</sub>	-46,38		46,9	295	35,6
(BMIm) <sub>2</sub> ZnCl <sub>2</sub> Br <sub>2</sub>	-46,63		44,76	295	92,6
BMImH <sub>2</sub> PO <sub>4</sub>	-44,23			200	62,3
BMImCF <sub>3</sub> SO <sub>3</sub>	-89,88	-53,54	10,65	340	25,4
BEImBF <sub>4</sub>	-87,35			265	59,8
BEImCF <sub>3</sub> SO <sub>3</sub>	-89,28			160	30,7
EMImH <sub>2</sub> PO <sub>4</sub>	-60,5			170	30,3
EMImPF <sub>6</sub>		-19,49	58,92	300	23,8
EMImBF <sub>4</sub>	-97,78	-61,71	8,06	260	63,6
EMImTos	-55,49			135	13,1
(EMIm) <sub>2</sub> ZnBr <sub>4</sub>			87,62	280	32,0
EEImTos	-52,58			150	70,2
BMImTos	-52,12	2,44	47,68	240	67,7

T<sub>g</sub> : glass transition temperatureT<sub>m</sub> : melting temperature

Tos : Tosylate

T<sub>c</sub> : crystallization temperatureT<sub>d</sub> : decomposition temperature

### 3.1.2 Immobilization of Ionic Liquids

Polymer supported ILs received much attention as media to conduct various chemical processes. Table 3.5 shows some monomers for the synthesis of these types of polymers. ILs, as mentioned before, do the most concentrated electrolytic fluids possess a high number of charge carriers per unit volume. When these charge carriers are mobile, very high conductivities are possible. In addition to this, they exhibit a wide electrochemical

stability window. Recent works by various groups has extended the excellent performance of ILs to electrochemical devices such as solar cells [Wang 03], lithium batteries [Garcia 04], fuel cells [Susan 03<sup>2</sup>] and supercapacitors [Stenger-Smith 02].

Liquid electrolytes do present some drawbacks difficult to overcome, such as leakage through the battery. On the other hand, an all solid state polymer electrolyte has important advantages including mechanical stability, safety and simple processing. However, their conductivity is still insufficient for practical use. A strategy to translate the benefits of ILs to polymer electrolytes is to design functional polymers presenting some of the characteristics of ionic liquids but in a solid electrolyte. Ohno and coworkers [Yoshizawa 01, Hirao 00, Ohno 04] reported the preparation of different types of polymeric ionic liquids (PILs), as a way of developing high performance polymer electrolytes. However, they are still far from the desired results. Some polymerizable ionic liquids are shown in Table 3.5.

Table 3.5. Polymerizable ionic liquids

	n	X	Ref.
	4	BF <sub>4</sub> , OTf	[Kim 04]
		BF <sub>4</sub> , PF <sub>6</sub>	[Tang 05]
	1,7	Cl, TFSI	[Yoshizawa 01]
		Tos	[Hirao 00]
	2,3,6,9	TFSI	[Washiro 04]
		Cl	[Marcilla 04]
		BF <sub>4</sub>	[Hirao 00]

## 3.2 Synthesis of Monomers

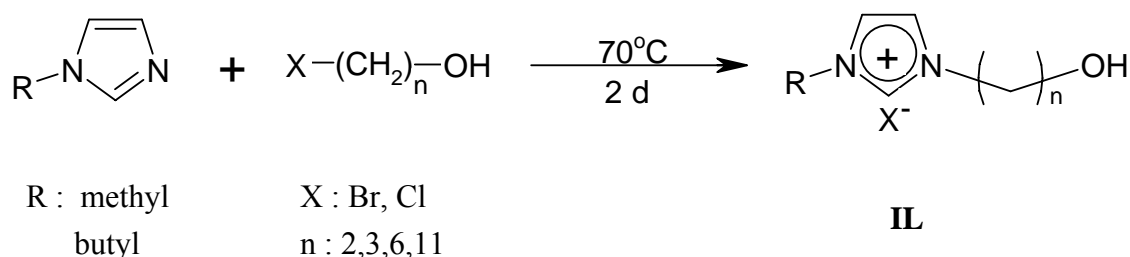
### 3.2.1 Imidazolium Salt Containing Acrylate Monomers

All the acrylic monomers which may also be considered as ionic liquid and have been synthesized in this work have the structure **1** (Scheme 1). The  $-\text{CH}_2-$  groups are used as linkers with  $n$  being 2, 4 and 6. The monomers were synthesized by two different approaches and they are named as method 1 and 2.

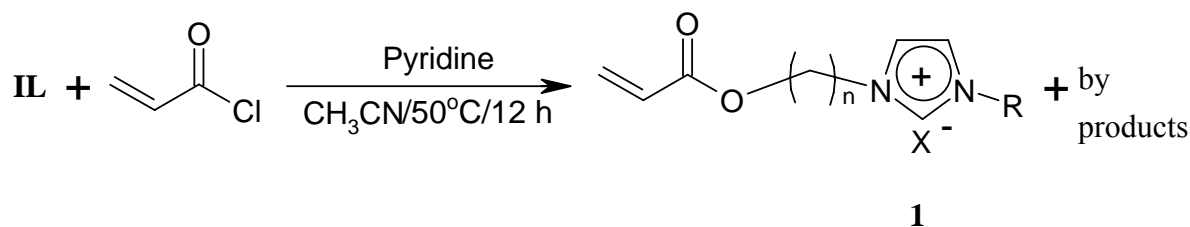
#### *Method 1*

The synthesis of the imidazolium salt part is straightforward as described in the literature [Hussey 88, Wilkes 82]. Bromo or chloro alcohol was successfully reacted with N-methyl or butyl imidazole to give the respective N-(methyl or butyl)imidazolium cations. After that, these salts must be linked to the acrylate units (Scheme 1). It was carried out according to the Schotten-Baumann method using pyridine as base. However, it was not possible to isolate the desired monomers. There were the following difficulties:

- Since the solubility of by products such as pyridinium chloride, unreacted starting compounds and monomers are similar to each other, it was not possible to retrieve the monomers from the product solution by using common methods (recrystallization, precipitation, etc.)
- It turned out that column chromatography is not a suitable way to purify ionic liquids, because they adsorb to the silica gel, and could not be removed from the column. In this work the silica gel 60 with 0.040-0.063 mm size was used for purification.



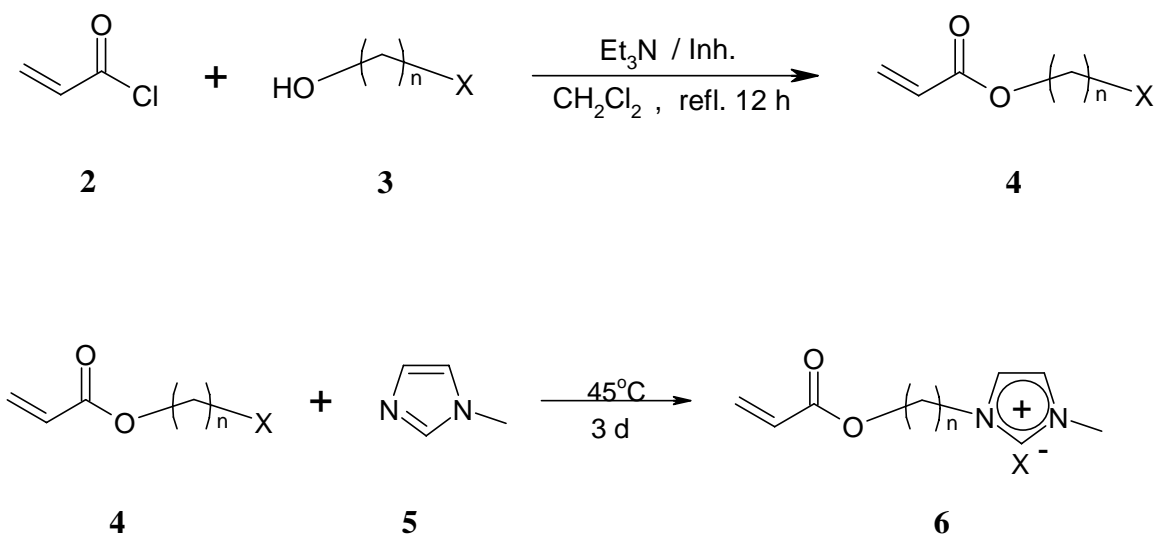




**Scheme 1.** The synthesis route of polymerizable ionic liquids.

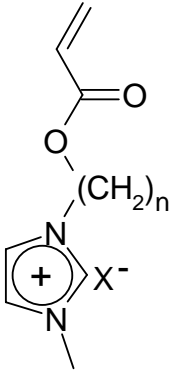
### Method 2

In this method, firstly the acrylic ester (**4**) was synthesized by the Schotten-Baumann reaction. 1-bromo or chloro alcohol (**3**) was reacted with acryloylchloride (**2**) in the presence of triethylamine which was used as HCl scavenger. Then, the ester was coupled with N-methyl imidazole (**5**) in the usual way to obtain polymerizable ionic liquids (**6**) (Scheme 2) [Hussey 88, Wilkes 82]. The synthesis of the monomers with this method was successful



**Scheme 2.** The synthesis route of polymerizable ionic liquids.

**Table 3.6. Acrylic monomers synthesized after method 2 (Scheme 2)**

Monomer	Sample	n	X	Yield (%)	Amount (g)
	AcIm-2-Br	2	Br	72	20.91
	AcIm-4-Cl	4	Cl	75	16.22
	AcIm-6-Cl	6	Cl	61	15.67
	AcIm-2- PF <sub>6</sub>	2	PF <sub>6</sub>	70	8.71
	AcIm-6- PF <sub>6</sub>	6	PF <sub>6</sub>	67	2.95
	AcIm-2- BF <sub>4</sub>	2	BF <sub>4</sub>	63	5.23
	AcIm-2	2	H <sub>2</sub> PO <sub>4</sub>	86	8.8
	AcIm-4	4	H <sub>2</sub> PO <sub>4</sub>	50	5.21
	AcIm-6	6	H <sub>2</sub> PO <sub>4</sub>	91	14.41

The structure of the monomers was verified by <sup>1</sup>H-NMR spectroscopy (Figure 3.2). It can be seen that the chemical shifts of the imidazolium ring protons change with anion type. H-bonding causes the proton chemical shift to move to lower field depending on the electronegativity of the anions. Lower chemical shift is observed with more electronegative anions. The sharp singlet signal higher than 9 ppm is attributed to the N-CH-N protons in the imidazolium ring. Other aromatic protons give two singlets at 7.4 and 7.5 ppm. Typical acrylic double bond signals (CH<sub>2</sub>=CH) can be seen as triplets of doublet at 6 ppm. The two separate triplet peaks are assigned to O-CH<sub>2</sub> and N-CH<sub>2</sub> hydrogens.

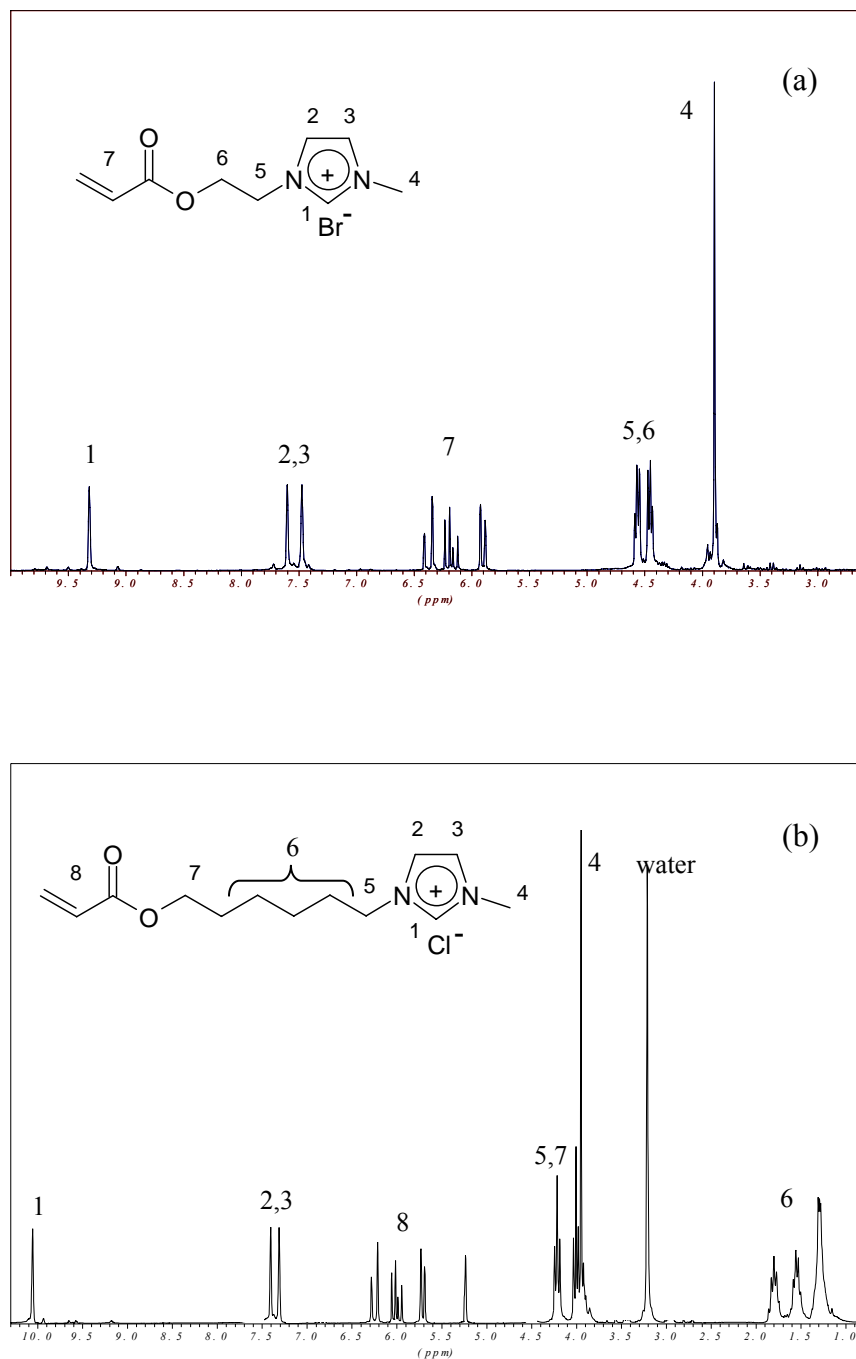


**Figure 3.2**  $^1\text{H}$ -NMR spectra of (a) AcIm-2-Br in  $\text{CD}_3\text{CN}$  (b) AcIm-6-Cl in  $\text{CD}_2\text{Cl}_2$ .

### 3.3 Synthesis of Polymers

#### 3.3.1 Polymerizable Ionic Liquids

Free-radical polymerizations of different monomers which were carried out at different conditions are summarized in Table 3.7.

**Table 3.7. Conditions and results of the polymerization reactions**

Monomer	Solvent	Initiator	T (°C)	Reaction time (h)	% Yield
AcIm-2-Br	Acetonitrile	AIBN	75	2 - 24 - 48	NP <sup>2</sup>
	THF			2 - 24 - 48	
	DMF			2 - 24 - 48	
	Ethanol			2 - 24 - 48	
	Water	AIBA <sup>1</sup>	70	0,5	82
AcIm-4-Cl	Water	AIBA	70	0,5	78
AcIm-6-Cl	Acetonitrile	AIBN	75	2 - 24 - 48	NP
	THF			2 - 24 - 48	
	DMF			2 - 24 - 48	
	Ethanol			2 - 24 - 48	
	Water	AIBA	70	0,5	80
AcIm-2- PF <sub>6</sub>	Acetonitrile	AIBN	75	2 - 24 - 48	NP
	THF			2	72
	DMF			2	61
AcIm-6- PF <sub>6</sub>	Acetonitrile	AIBN	75	2 - 24 - 48	NP
	THF			2	75
	DMF			2 - 24 - 48	NP
AcIm-2- BF <sub>4</sub>	Methanol	AIBN	70	2 - 24 - 48	NP
	Ethanol	AIBN	80	2 - 24 - 48	
	DMF	AIBN	80	2	
AcIm-2	Water	AIBA	70	0,5	65
AcIm-4	Water	AIBA	70	0,5	62
AcIm-6	Water	AIBA	70	0,5	70

<sup>1</sup> 2,2'Azo(isobutyroic acid amidine)dihydrochloride

<sup>2</sup> No Polymerization

The success of the polymerizations is strongly solvent and counter ion dependent. Attempts to polymerize were not successful when the initiator was AIBN and the counter ions were halides. On the contrary, polymerizations were achieved when  $\text{PF}_6^-$  was used as counter ion. However, the polymerizations were successful when water was used as solvent in combination with the water soluble initiator (AIBA). It can be concluded that for the acidic anion an acidic initiator is needed. Firstly, the kinetics of the polymerization was investigated at  $70^\circ\text{C}$  (Figure 3.3). Conversions of the monomers were calculated from the decrease of intensity of the double bond NMR signals. According to the results, the polymerizations were finished with 1 mol % of initiator after 30 min. After polymerization, the products were purified by dialysis with a 2000 MWCO (molecular weight cut-off) membrane.

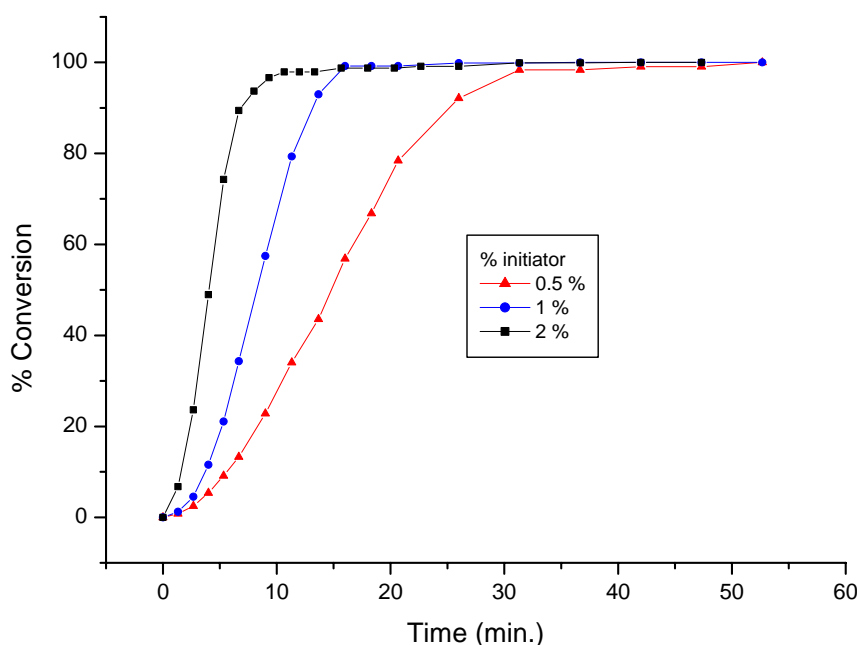
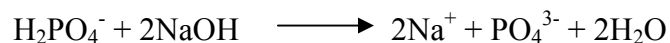


**Figure 3.3** Time-conversion curves for the polymerization of AcIm-6-Cl with various initiator concentrations (mol %) in water at  $70^\circ\text{C}$ .

The counter anions of the monomers of AcIm-*n*-X were exchanged with  $\text{H}_2\text{PO}_4^-$  in methylenchloride to obtain AcIm-*n* monomers and polymerized in water at  $70^\circ\text{C}$  (the

processes were explained in experimental part). After purification of the polymers by dialysis, the titration of the polymers ( $4 \times 10^{-5}$  M) with NaOH (0.01 M) was performed in water to determine ion-exchange of  $\text{H}_2\text{PO}_4^-$  with halides ( $\text{Br}^-$ ,  $\text{Cl}^-$ ). Figure 3.4 verifies the presence of  $\text{H}_2\text{PO}_4^-$  ions since two end points are observed clearly according to the following reaction:



The presence of  $\text{H}_2\text{PO}_4^-$  ion couldn't be proved with solution NMR because these samples were not soluble in common NMR-solvents. Polymers with  $\text{H}_2\text{PO}_4^-$  counter anions are only soluble in water and methanol. Since these solvents have also an -OH group their signals overlap with ones from  $\text{H}_2\text{PO}_4^-$  ions in the NMR spectra. However, it is possible to determine the presence of the  $\text{H}_2\text{PO}_4^-$  with solid-state NMR (shown in section 7.3, solid state NMR part) since it gives separated signals of the different -OH groups.

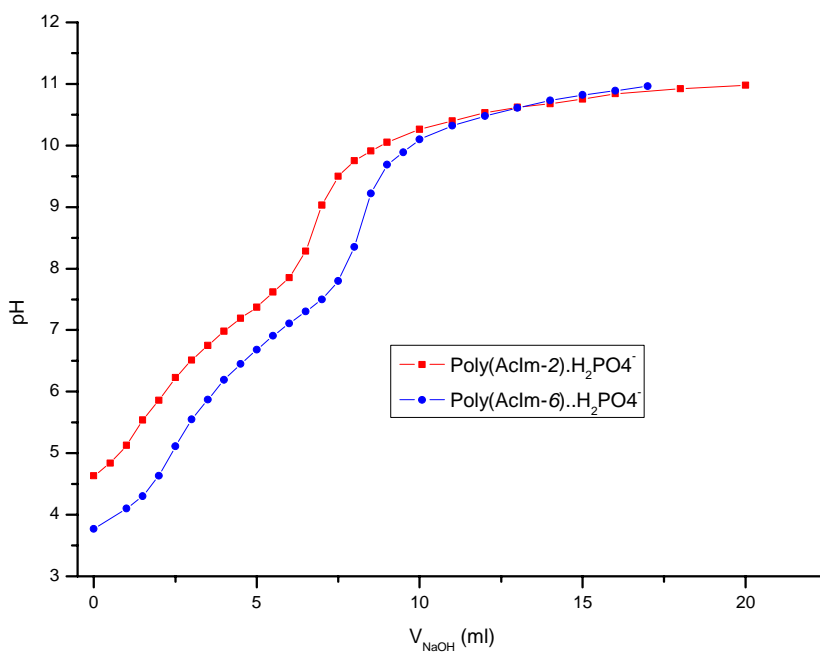


**Figure 3.4** Titration curves of polymers ( $4 \times 10^{-5}$  M) with NaOH (0.01N).

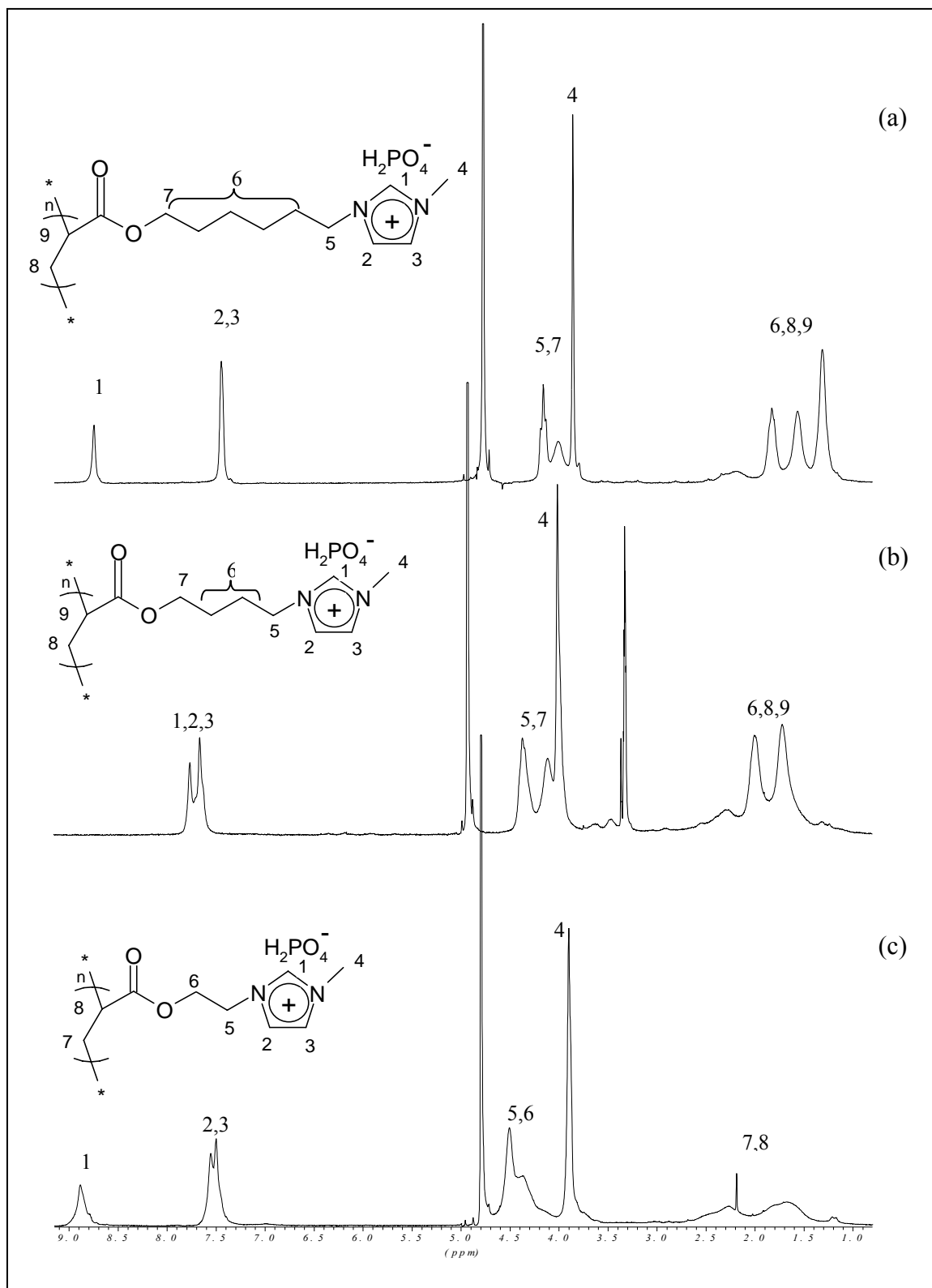
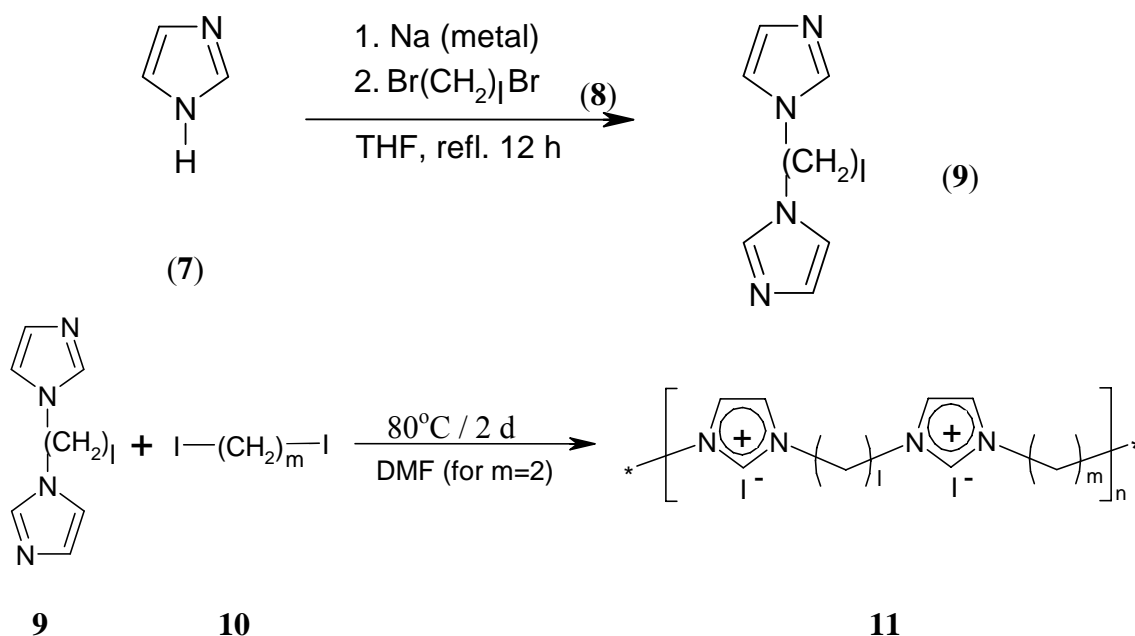


**Figure 3.5**  $^1\text{H-NMR}$  spectra of (a) Poly(AcIm-6) in  $\text{D}_2\text{O}$  (b) Poly(AcIm-4) in methanol (c) Poly(AcIm-2) in  $\text{D}_2\text{O}$ .

The  $^1\text{H-NMR}$  spectra of the polymers, Poly(AcIm-2), Poly(AcIm-4) and Poly(AcIm-6) with  $\text{H}_2\text{PO}_4^-$  anions are shown in Figure 3.5. The appearances of the signals at around 2 ppm are due to backbone protons of  $-\text{CH}_2-$  and  $-\text{CH}-$  groups. The signals of the N-CH-N protons are observed around 9 ppm. Other two protons at the imidazolium ring give a broad singlet with a shoulder at 7.5 ppm. The signals of the protons from O- $\text{CH}_2$ , N- $\text{CH}_2$  and  $-\text{CH}_3$  are found in between 3.5-4.5 ppm.

### 3.3.2 Synthesis of Ionenes

*N,N'*-bis(imidazolyl) alkanes (**9**) were synthesized by reacting imidazole (**7**) with dibromoalkane (**8**) (Scheme 3). The addition of alkyl halides to the reaction mixture just after the addition of the sodium metal to the solution of imidazole helped to shorten the time necessary for the metal to dissolve completely from several hours to one. This procedure avoided the use of a large volume of the solvent required to allow efficient stirring of the suspension [Sharma 00]. *N,N'*-bis(imidazolyl) alkanes (**9**) were reacted with diiodoalkanes (**10**) to obtain ionenes (**11**) (Scheme 3).



**Scheme 3.** Synthesis of ionenes.



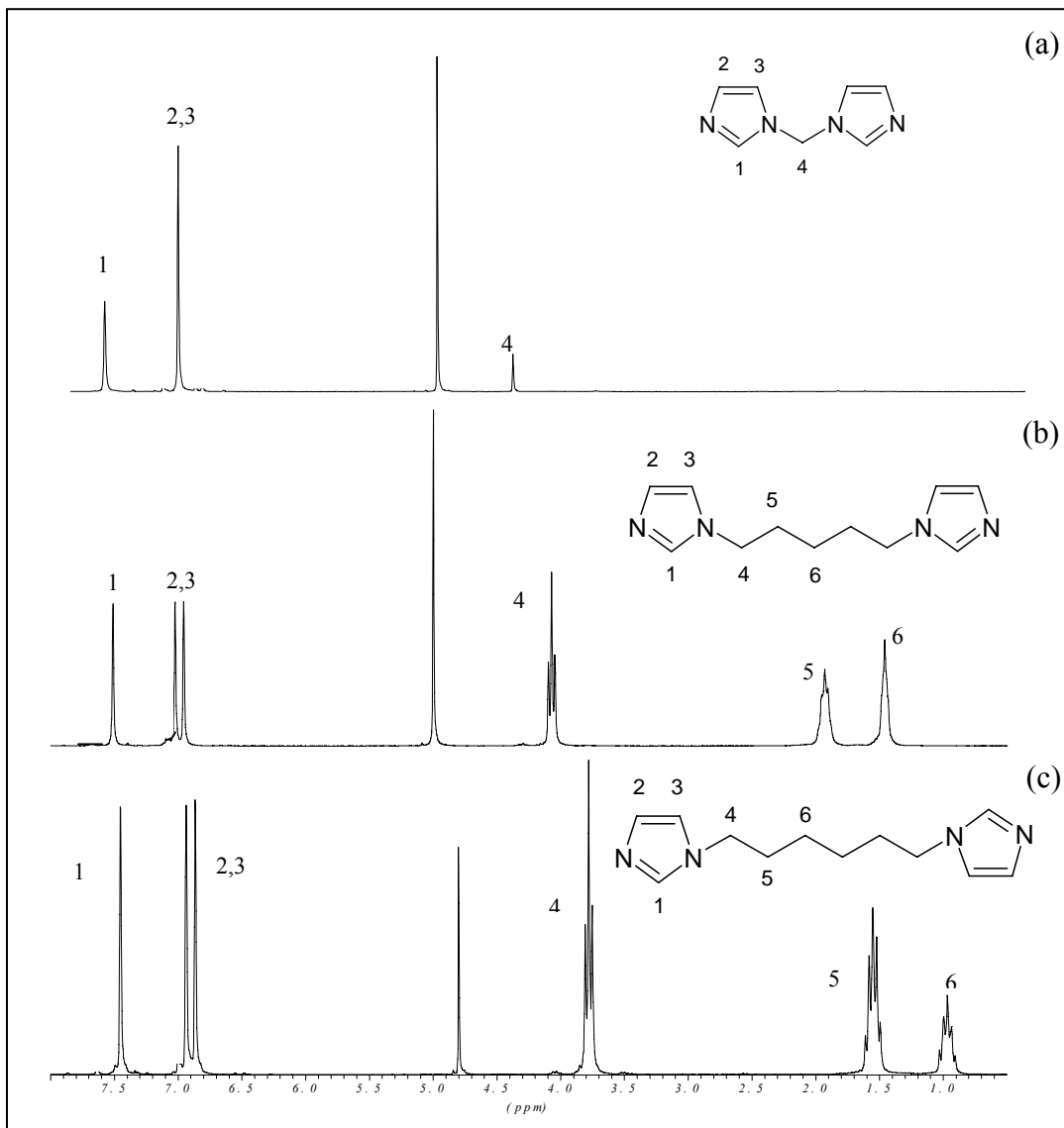


**Figure 3.6** The  $^1\text{H-NMR}$  spectra of the ionene precursor in  $\text{D}_2\text{O}$ .

The  $^1\text{H-NMR}$  spectra of the ionene precursor is shown in Figure 3.6. The  $-\text{CH}_2-$  groups which do not have nitrogen ( $-\text{N}-$ ) as a neighboring atom give two triplet signal around 1.0 and 1.5 ppm. The others, however, show signal around 4.0 ppm. It is due to the electronegative nitrogen atom since it is known that the resonance position of protons bonded to carbon is shifted down field by electronegative elements also bonded to the carbon. Two sharp singlets at around 7.0 ppm is assigned to the  $-\text{CH-N}-$  protons on the imidazol ring. The singlet at 7.5 ppm is attributed to the other proton ( $\text{N-CH-N}$ ) on the imidazol ring.

## Abbreviation for Synthesized Polymers

l	m	n	X = H <sub>2</sub> PO <sub>4</sub> <sup>-</sup>	X = N(SO <sub>2</sub> CF <sub>3</sub> ) <sub>2</sub> <sup>-</sup>	
		2	Poly(AcIm-2)	Poly(AcIm-2-Li)	
		4	Poly(AcIm-4)	Poly(AcIm-4-Li)	
		6	Poly(AcIm-6)		
5	2		Poly(Im-5-2)		
5	6		Poly(Im-5-6)		
6	6		Poly(Im-6-6)		

## 4. Thermal Analysis

The thermal properties of the samples were investigated by thermogravimetric analysis, (TGA) and differential scanning calorimetry (DSC). TGA measures continuously the weight change during a temperature scan. The information about degradation, oxidation, evaporation or sublimation reactions of the materials can be obtained from TGA thermograms [Craver 83]. The determination of moisture content in the polymer and determination of volatile additives in particular are also possible [Wundlich 90].

The determination of glass transition serves to characterize an important property of a polymeric material. The glass transition is the temperature,  $T_g$ , at which the polymer changes from a hard, glass like state to a rubber like state. DSC allows to identify the glass transition as a change in the heat capacity as the polymer matrix goes from the glassy state to the rubbery state (Figure 4.1).

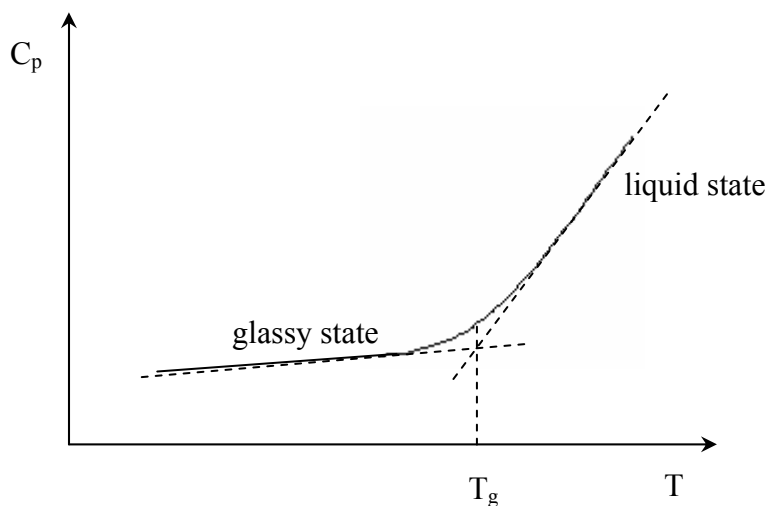


**Figure 4.1** Specific heat ( $C_p$ ) depending on temperature for a system undergoing glass transition.

$T_g$  can be significantly decreased by addition of plasticizers to the polymer. The molecules of the plasticizer become embedded within the polymer bulk, thus allowing chain segments to move past one another even at lower temperatures. The addition or sorption of species causes an enhancement of local segmental motion of the polymer chains. In polymer science, plasticization is generally considered as a positive and useful feature. The addition of plasticizers (low molecular weight additives) to polymers depresses the glass transition temperature below room temperature which enables the processing of polymers.

#### **4.1 Thermogravimetric Analysis (TGA) Results**

##### **4.1.1 TGA of the Poly(AcIm-n) x H<sub>3</sub>PO<sub>4</sub>**

The TGA thermograms of the Poly(AcIm-n) and their blends with H<sub>3</sub>PO<sub>4</sub> are shown in Figure 4.2. The blends were prepared by adding stoichiometric amount of H<sub>3</sub>PO<sub>4</sub> to the polymers, Poly(AcIm-n), in water. The blends were directly casted on the platinum electrode from the solution. Then, they were dried under vacuum prior to the measurements. All the measurement were performed under nitrogen with a heating rate of 10°C/min.

Although the first mass loss starts around 100°C due to the evaporation of physically bound water in those hygroscopic samples, the polymers are stable up to about 190°C. During the sample preparation, they might capture some moisture from the air. A hole was made in the pan to make it easier for the evaporation of water during heating process. As H<sub>3</sub>PO<sub>4</sub> content increases the weight loss becomes remarkable low at higher temperatures. Removal of bound water in these materials is very difficult. The stepwise decomposition after 200°C can be attributed to water liberation due to the self condensation of the phosphoric acid and also decomposition of the polymer main chain may contribute to further weight loss.

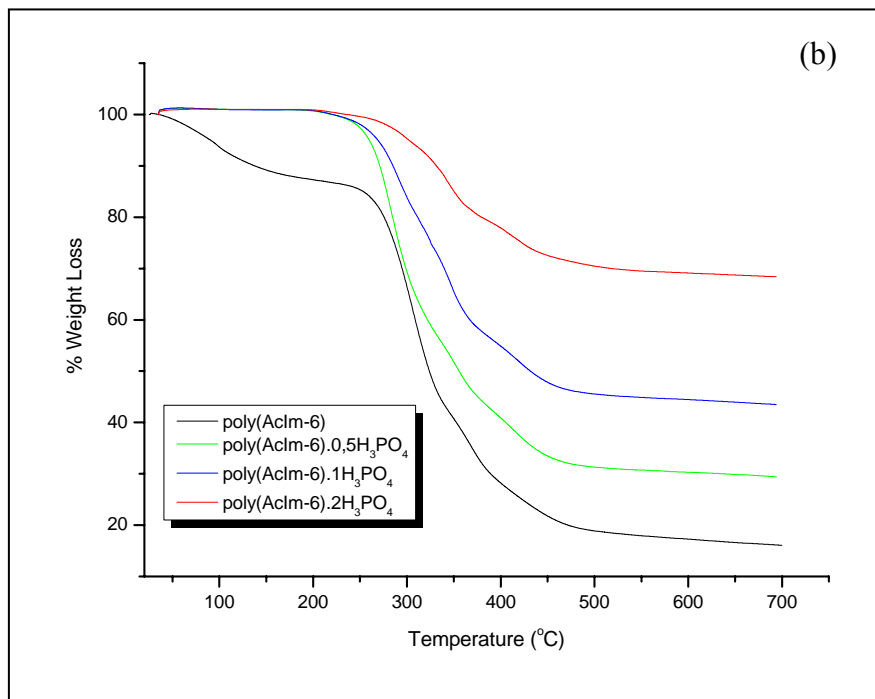
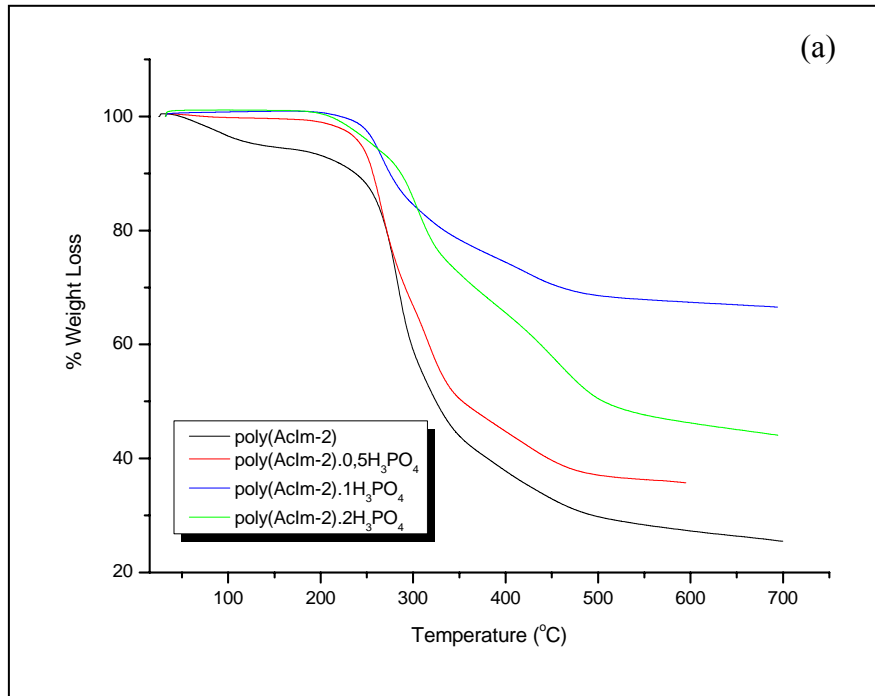


**Figure 4.2** TGA curves of (a) poly(AcIm-2) x H<sub>3</sub>PO<sub>4</sub> (b) poly(AcIm-6) x H<sub>3</sub>PO<sub>4</sub>.

#### 4.1.2 TGA of the Poly(AcIm-Li) x LiN(SO<sub>2</sub>CF<sub>3</sub>)<sub>2</sub>

Figure 4.3 presents the TGA thermograms of pure polymer of Poly(AcIm-Li) and its blends with lithium salt of trifluoromethylsulfonimide, LiN(SO<sub>2</sub>CF<sub>3</sub>)<sub>2</sub>. It is clearly seen that the polymer and blends are stable up to 200°C. The small weight loss observed between 180 and 230°C is due to the water absorbed in those hygroscopic samples. The addition of lithium salt does not have significant effect on the TG thermograms of the blends.

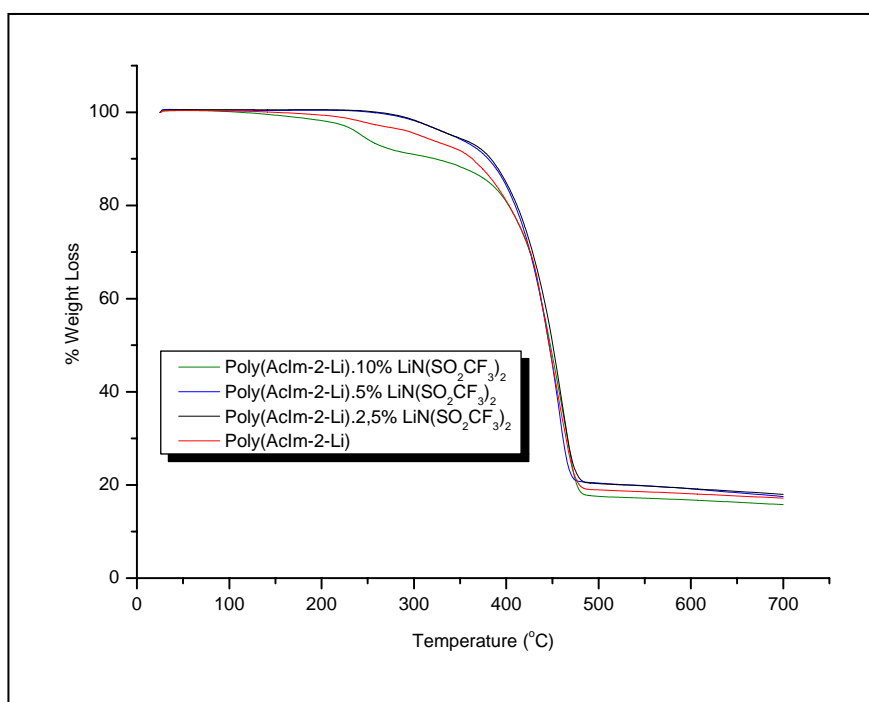


**Figure 4.3** TGA curves of poly(AcIm-2-Li) x LiN(SO<sub>2</sub>CF<sub>3</sub>)<sub>2</sub> recorded under N<sub>2</sub> atmosphere.

#### 4.1.3 TGA of the Poly(Im-*l-m*)

The thermogravimetric curves for the studied polymers are shown in Figure 4.4. The difference between the polymer with I<sup>-</sup> and H<sub>2</sub>PO<sub>4</sub><sup>-</sup> anion can be seen clearly. The polymers with H<sub>2</sub>PO<sub>4</sub><sup>-</sup> counter-ion showed a first degradation stage related to the bound water at a temperature range of 60–120°C. The stages corresponding to the

decomposition above for the materials with  $\text{H}_2\text{PO}_4^-$  must be related to the condensation of the  $\text{H}_2\text{PO}_4^-$  moieties. The profile of the TG curves associated with the percentage of mass loss suggests a higher stability up to approximately  $220^\circ\text{C}$  for the samples with  $\text{I}^-$  anion.

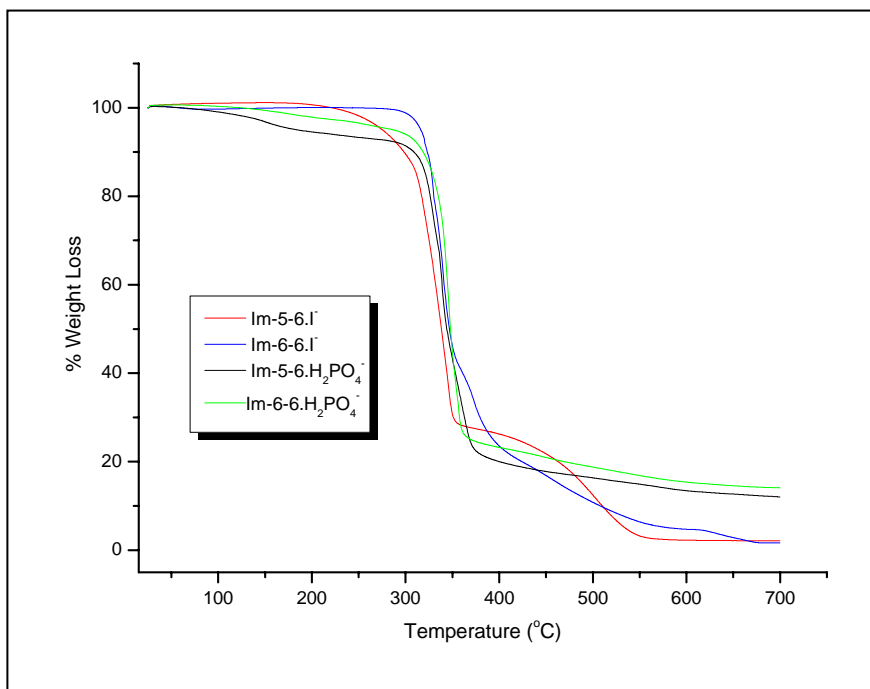


**Figure 4.4** TGA curves of ionenes recorded under  $\text{N}_2$  atmosphere.

## 4.2 Differential Scanning Calorimetry (DSC) Results

### 4.2.1 DSC Results of Poly(AcIm-n) x $\text{H}_3\text{PO}_4$

The DSC curves of all the samples presented here were monitored with a rate of 10 K/min. The DSC curves of polymeric ionic liquids and their blends are shown in Figures 4.5 and 4.6. The  $T_g$ 's of the blends obtained from the DSC thermograms are illustrated. Each sample was scanned several times to check the repeatability of the  $T_g$ . The glass transition temperatures are obtained from the intersection (onset) of the baselines before and after the glass transition. The lower  $T_g$  for longer side chain is expected since longer chains behave as spacer that causes easier segmental motion. Moreover, it has been

demonstrated that the glass transition temperatures are ranging from 7 to 83°C for poly(AcIm-2) x H<sub>3</sub>PO<sub>4</sub> and from -7 to 22 for poly(AcIm-6) x H<sub>3</sub>PO<sub>4</sub> with varying H<sub>3</sub>PO<sub>4</sub> content. H<sub>3</sub>PO<sub>4</sub> acts as plasticizer for the polymeric host and hence a decrease in the H<sub>3</sub>PO<sub>4</sub> concentration should lead to an increase in T<sub>g</sub>. This is a result of the restrictions of segmental motions of the polymer host.

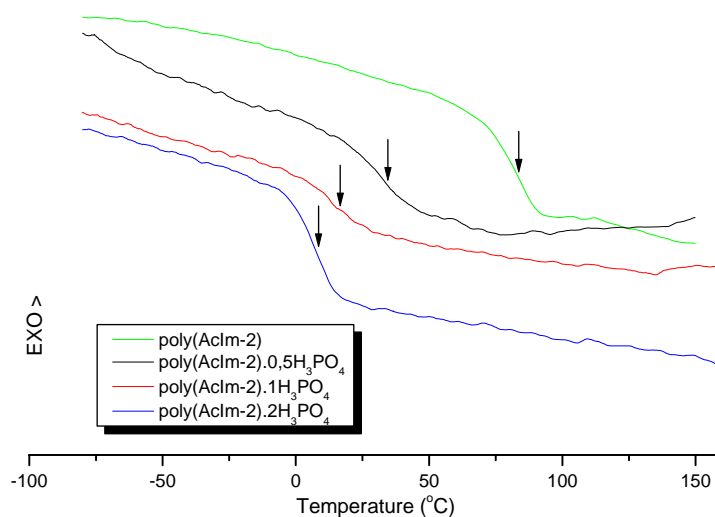


**Figure 4.5** DSC curves of poly(AcIm-2) x H<sub>3</sub>PO<sub>4</sub>.

It can be clearly seen that the addition of H<sub>3</sub>PO<sub>4</sub> leads to more change in T<sub>g</sub> for poly(AcIm-2) x H<sub>3</sub>PO<sub>4</sub>. Since poly(AcIm-6) x H<sub>3</sub>PO<sub>4</sub> already has longer side chain, and it has already plasticizing effect on T<sub>g</sub>. Therefore, the increase in the amount of H<sub>3</sub>PO<sub>4</sub> does not cause significant change as in poly(AcIm-2) x H<sub>3</sub>PO<sub>4</sub>. Figure 4.7 shows how T<sub>g</sub> of the polymer electrolytes change with H<sub>3</sub>PO<sub>4</sub> composition.



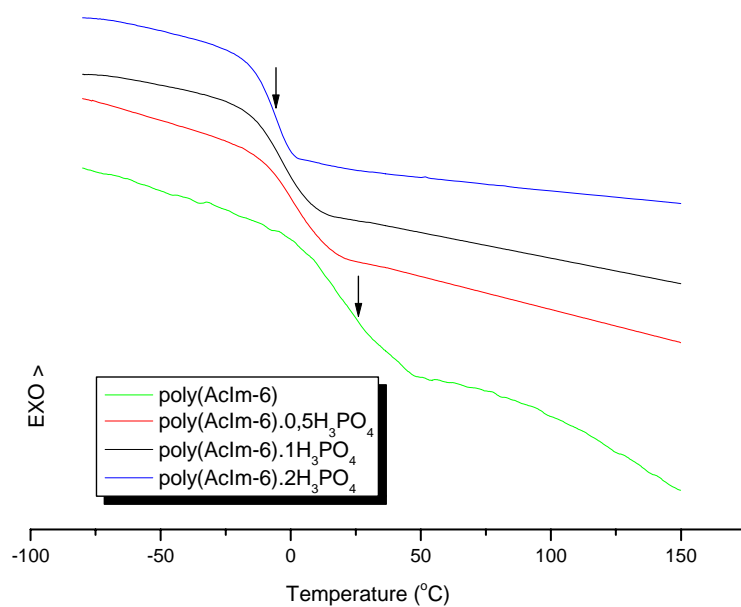


**Figure 4.6** DSC curves of poly(AcIm-6) x H<sub>3</sub>PO<sub>4</sub>.

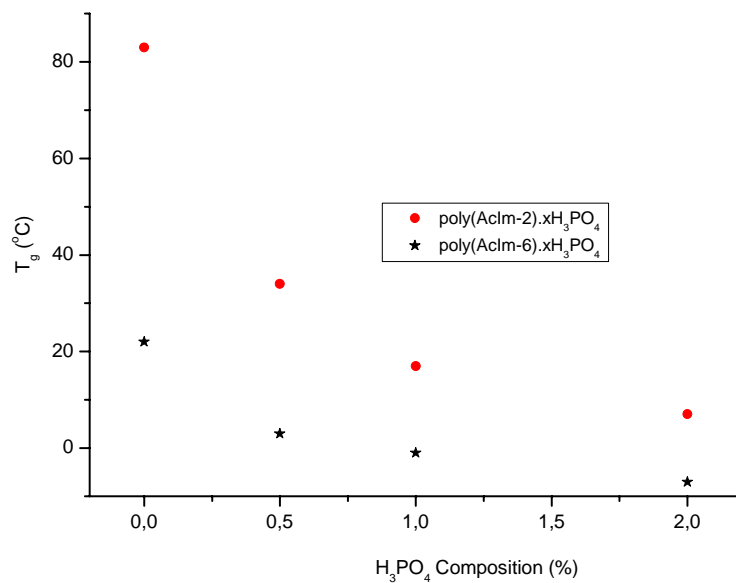


**Figure 4.7** Change of T<sub>g</sub>'s with H<sub>3</sub>PO<sub>4</sub> composition.

#### 4.2.2 DSC Results of Poly(AcIm-2-Li) x LiN(SO<sub>2</sub>CF<sub>3</sub>)<sub>2</sub>

Figure 4.8 shows the DSC curves of poly(AcIm-2-Li) x LiN(SO<sub>2</sub>CF<sub>3</sub>)<sub>2</sub>. Since the polymer, polymer blends and Li-salt itself have hygroscopic character, the samples were carefully dried before the measurements. A change in the sample weight has consequences in wrong specific heat capacity determination and changes the shape of thermal analysis curves. It typically has a strong affect on T<sub>g</sub>, too. From the curves, it is seen that the addition of salt slightly increases the T<sub>g</sub>. However, when the amount of Li-salt is more than 10% the T<sub>g</sub> decreases significantly. Although the samples were dried prior to measurements, small amount of water may be trapped inside.

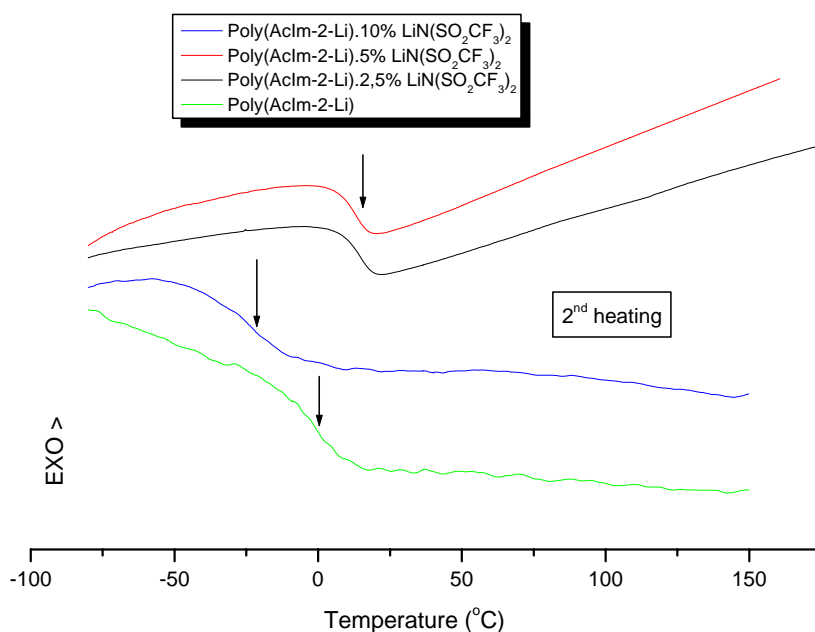


**Figure 4.8** DSC curves of Poly(AcIm-2-Li) x LiN(SO<sub>2</sub>CF<sub>3</sub>)<sub>2</sub>.

#### 4.2.3 DSC Results of Poly(Im-*l-m*)

Figure 4.9 presents the DSC curves of the ionenes. The T<sub>g</sub> of the samples increases from 8 to 30°C when the chain length between two imidazolium rings decreases. This is an expected result since longer chains gives the polymer backbone more freedom for the segmental motion at a given temperature, accordingly, shorter side chains gives rise for a higher T<sub>g</sub>.

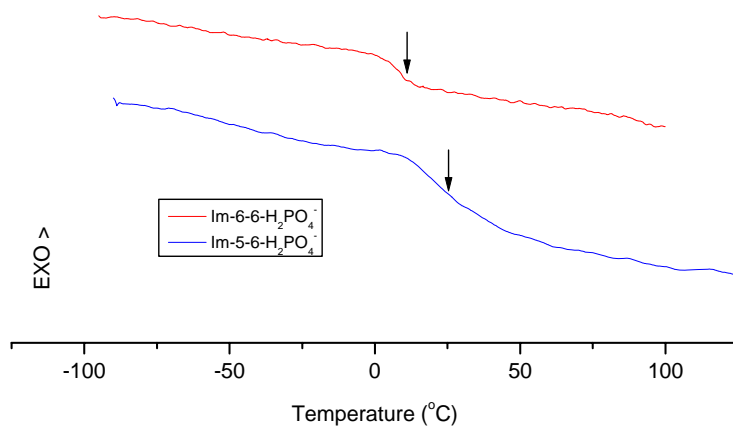


**Figure 4.9** DSC curves of ionenes Im-5-6-H<sub>2</sub>PO<sub>4</sub><sup>-</sup> and Im-6-6-H<sub>2</sub>PO<sub>4</sub><sup>-</sup>.

## 5. Dynamic Mechanical Analysis

Dynamic mechanical analysis (DMA), is a technique used to study and characterize the viscoelastic properties of polymers. DMA is particularly useful for measuring transitions in polymers that cannot be detected by other techniques. DMA measures the mechanical properties of materials while they are subjected to a periodic stress,  $\sigma$ , usually applied sinusoidally. The applied stress will cause a deformation measured by the strain ( $\epsilon$ ) which is the deformation per unit dimension.

$$\sigma(t) = \sigma_o \sin(\omega t + \delta) \quad 5.1$$

$$\epsilon(t) = \epsilon_o \sin(\omega t) \quad 5.2$$

where  $\omega$  is the angular frequency and  $\delta$  is the phase angle. DMA measures the amplitudes of the stress and strain as well as the phase angle ( $\delta$ ) between them. This is used to resolve the modulus into an in-phase component - the storage modulus ( $G'$ ) - and an out-of-phase component - the loss modulus ( $G''$ ).

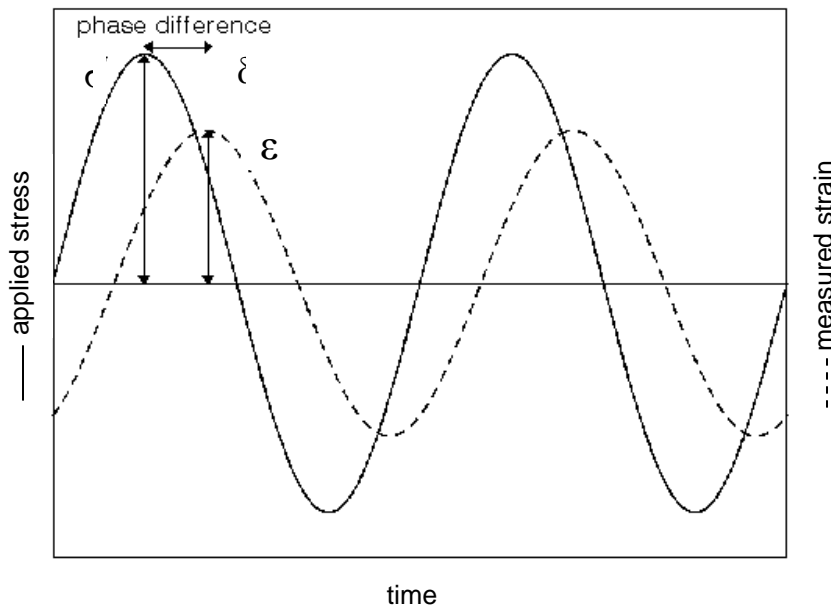


**Figure 5.1** Time dependence of stress and strain in a dynamic mechanical experiment.

$$\tan \delta = \frac{G'}{G''} \quad 5.3$$

Both stress  $\sigma^*(t)$  and strain  $\varepsilon^*(t)$  can be expressed in a complex form. Then the complex dynamic modulus,  $G^*(\omega)$  is defined as :

$$G^*(\omega) = \frac{\sigma^*(t)}{\varepsilon^*(t)} = G' + iG'' \quad 5.4$$

The real (storage) part describes the ability of the material to store potential energy and release it upon deformation. The imaginary (loss) part is associated with energy dissipation in the form of heat upon deformation.

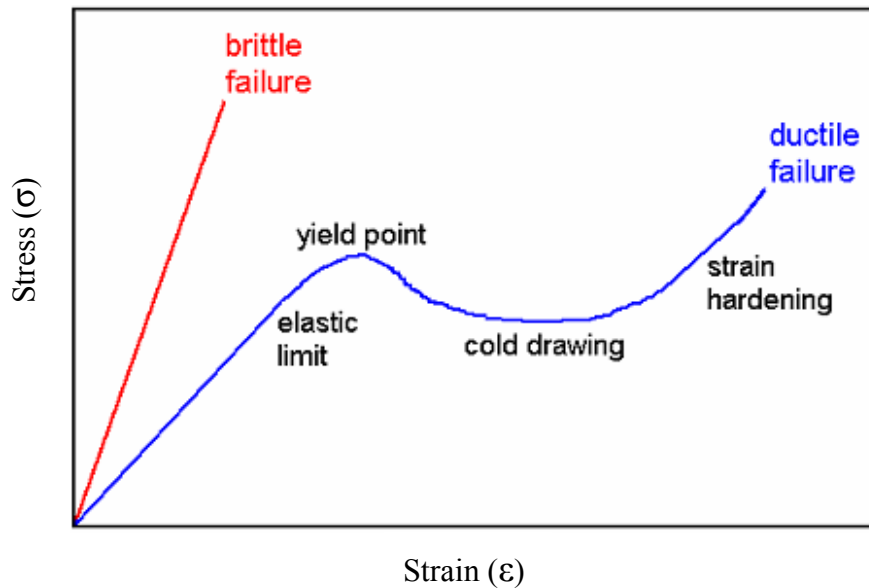


**Figure 5.2** Dynamic mechanical analysis curves of different materials.

If a material is subjected to a mechanical force it may behave in a variety of ways, illustrated in Figure 5.2. A brittle material will deform reversibly to a small amount and then fracture. A ductile material will also deform reversibly up to a certain amount and then yield and flow under the applied force until it begins to harden under load and then fail. Up to the elastic limit, the material will return to its former shape and size when the force is removed. Beyond this point deformation is irreversible i.e. creep has occurred.

The storage modulus is related with “stiffness” of a material. The dynamic loss modulus is often associated with “internal friction” and is sensitive to different kinds of molecular motions, relaxation processes, transitions, morphology and other structural heterogeneities. Therefore, the dynamic properties of materials provide information at the molecular level for understanding the polymer mechanical behaviour.

For polymer melts the viscosity is an important parameter and is expressed as :

$$\eta^* = \eta' - i\eta'' = \frac{\sigma}{\dot{\epsilon}} \sin(\omega t + \delta) \quad 5.5$$

where  $\eta^*$  is the complex dynamic viscosity and  $\dot{\epsilon}$  is the strain rate and it is defined as :

$$\dot{\epsilon} = \epsilon_o \omega \sin(\omega t) \quad 5.6$$

Measurement of beta ( $\beta$ ) and gamma ( $\gamma$ ) transitions in polymers are very difficult to observe by DSC. These transitions, which are often very important in determining the impact resistance of the polymer, are caused by local motion of the polymer chains as opposed to large scale co-operative motion that accompany the glass transition. The  $T_g$  is often measured by DSC (Differential Scanning Calorimetry), but the DMA technique can also yield data which can be used to investigate the frequency (and therefore time) dependent nature of the transition.

### 5.1 Mechanical Properties of Poly(AcIm-*n*)

The schematic representation of the parallel plate rheometer is shown in Figure 5.3.

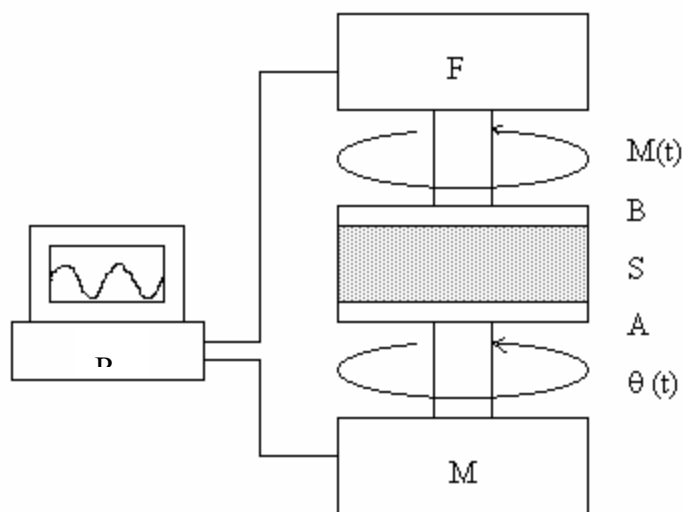


**Figure 5.3** Parallel Plate Rheometers: A,B are parallel plates, S sample, M motor, angular frequency of motor  $\omega$ , the rotor (F), rotor frequency  $M(t)$  and (R) recorder.

The samples were prepared as cylindrical films by melting on a hot plate. Then, they are placed between two parallel plates in a chamber filled with nitrogen. An oscillating force is applied to the sample and the resulting displacement of the sample is measured at a rate of 10 rad/s. From this the stiffness of the sample is determined, and the sample modulus is calculated.

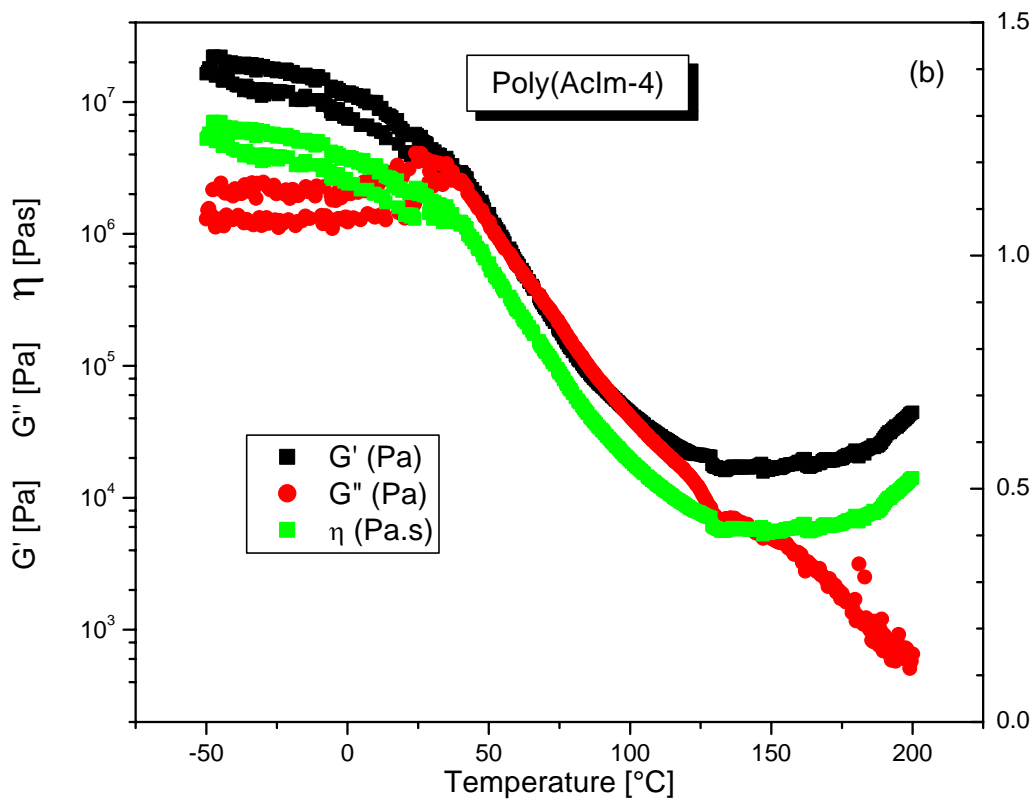
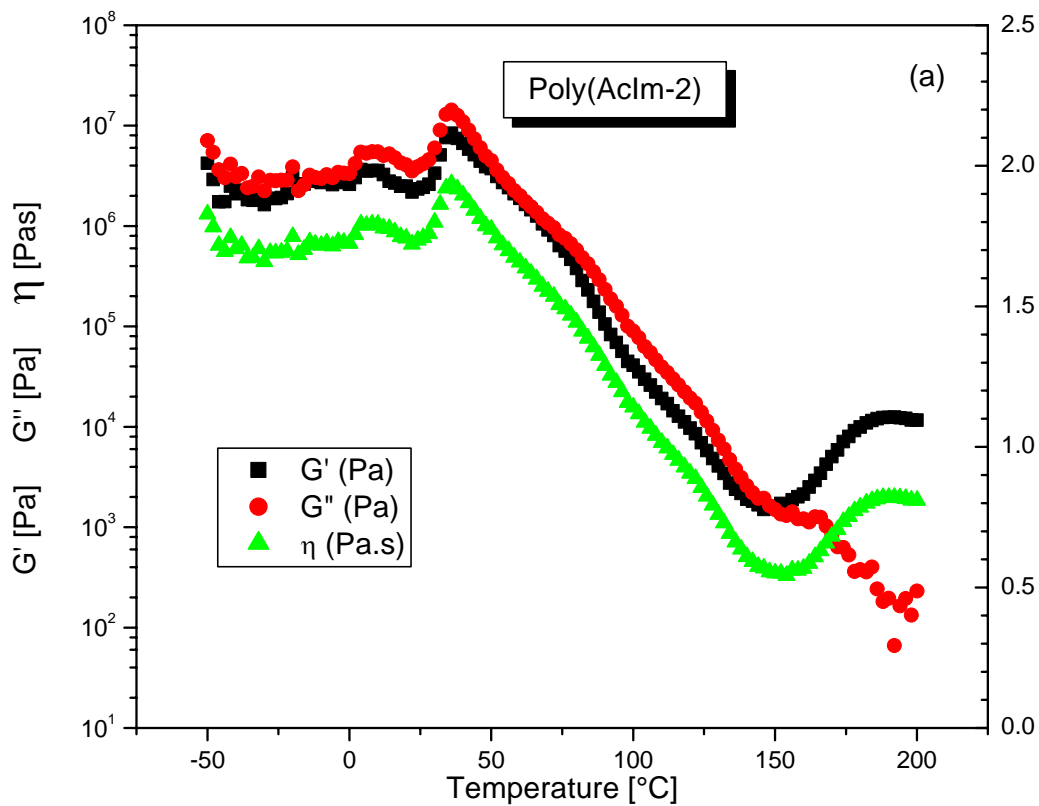
Figure 5.4 shows the storage ( $G'$ ) and loss ( $G''$ ) moduli curves of the samples as a function of temperature. The shape of the curves reveals some features which can be qualitatively assessed as follows: At lower temperatures, the membranes showed glassy properties with high value of  $G'$  about  $10^7$ - $10^9$  Pa. Small peaks at this frequency zone may correspond to secondary relaxations, i.e.,  $\beta$ -relaxation which disappears as  $n$

increases. At intermediate temperature zone (0 to 90°C), storage modulus decreases due to cooperative segmental relaxations in these amorphous polymer electrolytes. At higher temperatures, a severe drop in both  $G'$  and  $G''$  values is observed until values are reached to about  $10^3$ - $10^4$  Pa which are typical for a highly viscous melt. The onset of this loss of mechanical strength shifts to lower temperatures with increasing  $n$ , which is consistent with the  $T_g$  shift. The reason of two broad peaks of  $G'$  in the glass transition zone around  $10^4$  and  $10^6$  Pa for Poly(AcIm-2) is unclear yet.

A curvature is observed around 150°C at which the polymers undergo cross-linking due to condensation of phosphate moieties. The mechanical properties, however, do not start to change suddenly until certain time into the cross-linking process as a network of polymer molecules begins to form. The  $G'$  modulus and  $\eta^*$ , therefore, stay constant at temperatures around 150°C. Since the membranes are already in the melt at this temperature the cross-linking process occurs in the liquid state. It is clearly seen that the chain length of the electrolytes for Poly(AcIm- $n$ ) does not have any effect on the cross-linking temperature. The cross-linking starts around 150°C for all of these electrolytes. A marked increase when  $T > 160^\circ\text{C}$  suggests an increase in cross-linking density with increasing temperature by time.

After the process was completed the cylindrical polymer films expanded to form foam like structure indicating evaporation of the water. The water is the result of the cross-linking due to condensation of the acidic units.





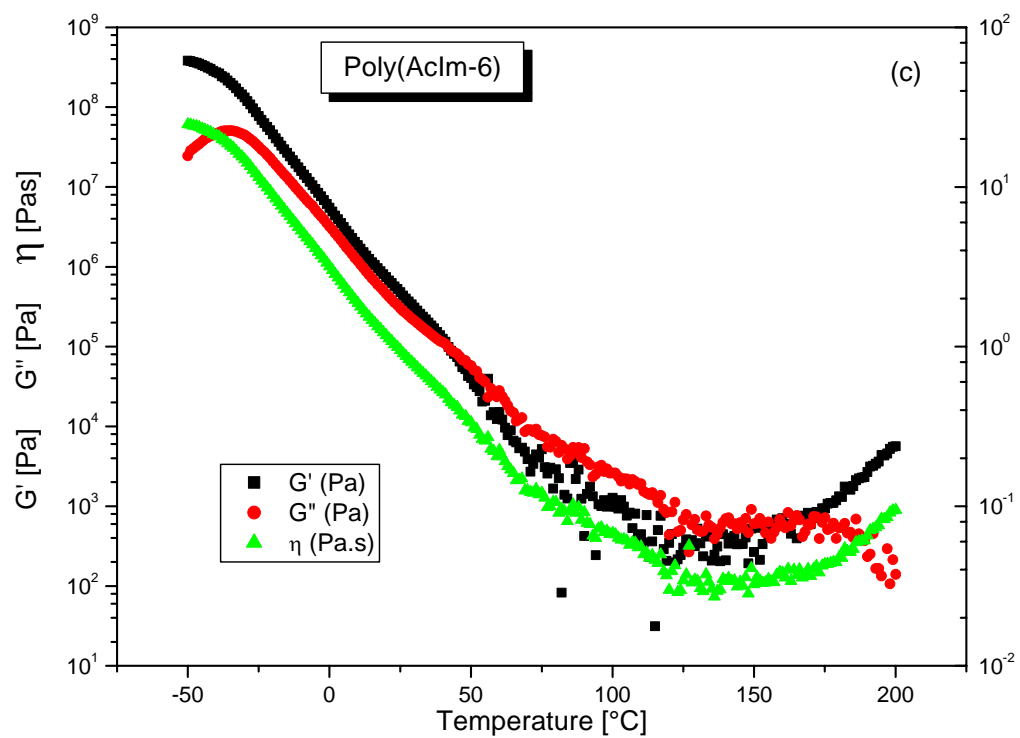
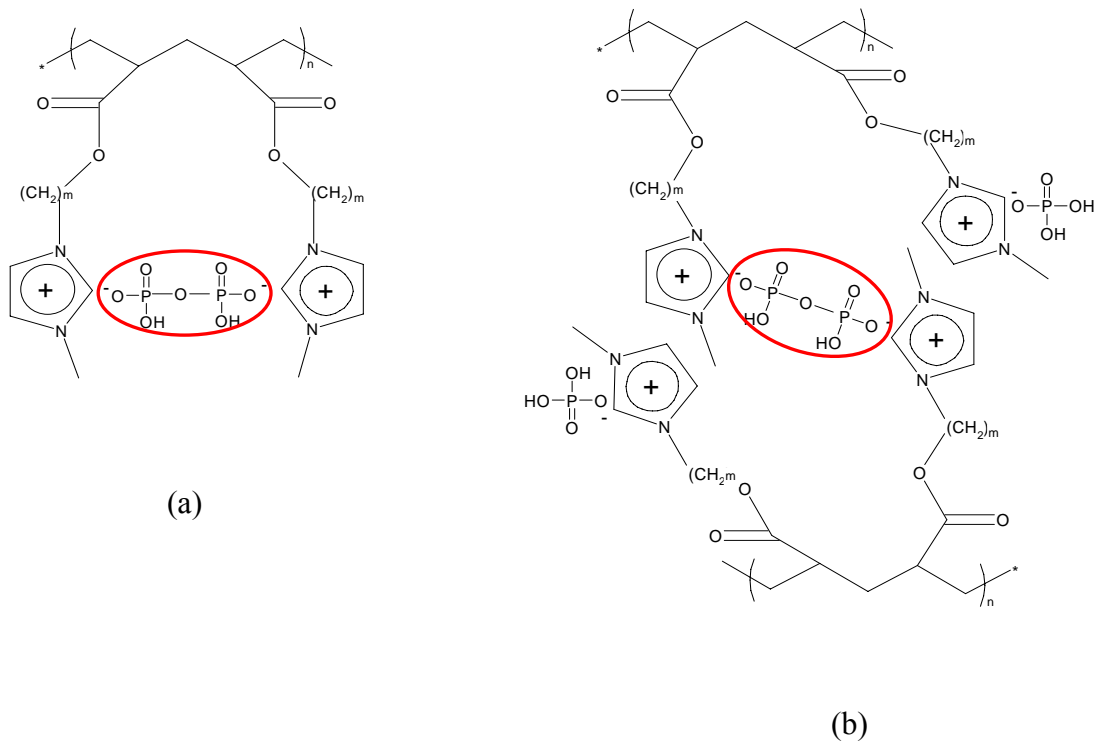


**Figure 5.4** DMA of Poly(AcIm- $n$ ),  $n$  is 2, 4, and 6 for (a), (b), and (c), respectively.

Both inter and intra-cross-linking are supposed to occur within the polymers according to following scheme:



**Scheme 4.** Cross-linking of the Poly(AcIm-n) membranes (a) intra-chain (b) inter-chain cross-linking.

The cross-linking of the polymer electrolytes was also proved by solid state NMR which is discussed in section 7.3.4 in details.

## 6. Dielectric Spectroscopy

The interaction of electromagnetic radiation with matter is of fundamental importance for polymer-based electrolytes. The frequency regime between  $10^{-6}$  and  $10^{12}$  Hz is the domain of broadband dielectric spectroscopy. Spectroscopic dispersion of dielectric permittivity and associated energy absorption regions may be observed for a material over the entire range from  $10^{-6}$  to  $10^{11}$  Hz due to classical electric polarization and electrical conduction processes. The magnitude of the effects and the frequency location of the energy absorption features the relaxation associated with these processes which will depend markedly upon the chemical and physical nature of a material and the temperature and pressure at which it is studied. Studies of electric polarization and conduction processes are made under the titles ‘Dielectric Relaxation Spectroscopy’ (DRS), ‘Impedance Spectroscopy’ (IS), ‘Electrical Impedance Spectroscopy’ (EIS) and ‘Electrical Relaxation Spectroscopy’ (ERS). The diversity of the techniques is due to the studies made for different reasons with different classes of materials and different techniques. DRS is a good method for the study of dipolar molecular motions in solids. DRS probes the interaction of a macroscopic sample with a time-dependent electric field [Kremer 02]. The resulting polarization either expressed by the frequency-dependent complex permittivity and conductivity or as an impedance spectrum, characterizes amplitude and timescale (via the relaxation time) of the charge-density fluctuations within the sample. Such fluctuations generally arise from the reorientation of the permanent dipole moments of individual molecules or from the rotation of dipolar moieties in flexible molecules, like polymers. Other possible mechanisms include the transport of ions or the appearance of interfacial charges in heterogeneous systems. The timescale of these fluctuations depends on the sample and on the relevant relaxation mechanism. Relaxation times range from several picoseconds in low-viscosity liquids to hours in glasses, probably marking DRS as the technique with the most extensive coverage of dynamical processes. The corresponding measurement frequencies range from  $10^{-4}$  Hz to  $10^{12}$  Hz, which requires a series of instruments for complete coverage. However, it is generally sufficient to concentrate on a smaller frequency range adapted to the sample properties [Williams].

In contrast to conventional spectroscopic methods, like NMR or vibrational spectroscopy, DRS is especially sensitive to intermolecular interactions (Figure 6.1). DRS is able to monitor cooperative processes and thus provides a link between molecular spectroscopy, which monitors the properties of the individual constituents, and techniques characterizing the bulk properties of the sample, especially the viscoelastic and rheological behaviour. The decomposition of the dielectric spectrum into its individual relaxation processes informs on the relative amplitudes and characteristic times of the underlying molecular motions.

DRS is widely applied in the characterization of ion-conducting solids, polymers and mesophases [Kremer 02, Jonscher 83, Dominguez 88, Rietz 93-94, Ku 87].

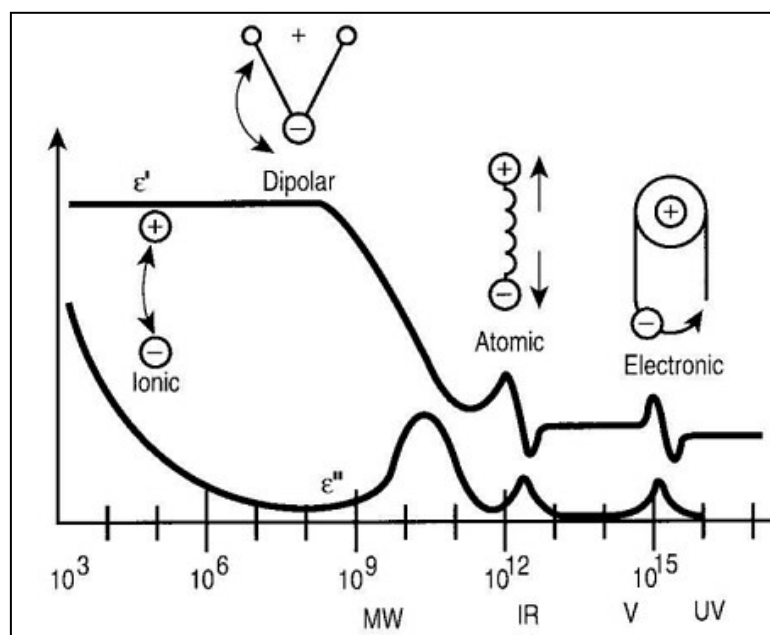


**Figure 6.1** A dielectric permittivity (real and imaginary parts) spectrum over a wide range of frequencies [Kremer 02].

The electrical conductivity measurements of the polymers are performed with both, direct current (DC) and alternating current (AC) measurements. In DC methods, the

sample is sandwiched between two nonblocking electrodes and a DC voltage is applied. Direct current techniques seem to be the most straightforward methods. However, their use is less common in ionic conductivity studies due to the problems arising from the electrode contacts on the measured electrolyte conductivity. The effect of blocking electrodes is caused by the simple effect that ions usually can not be discharged at the surface of a metal electrode, which is conventionally used. Thus, an electrical potential is constructed caused by the formation of an ion gradient. AC measurements are the most popular approach for the determination of electrical properties of polymer electrolytes [MacDonald 74]. In this method a sinusoidal voltage is applied to a cell which functions as a capacitor and the resulting impedance is determined. The information about polarization phenomena occurring within the cell can be obtained with AC-data.

The principle of a dielectric measurement is shown in Figure 6.2. The sample is placed between two round electrode plates in order to act as a capacitor as shown in Figure 6.3.

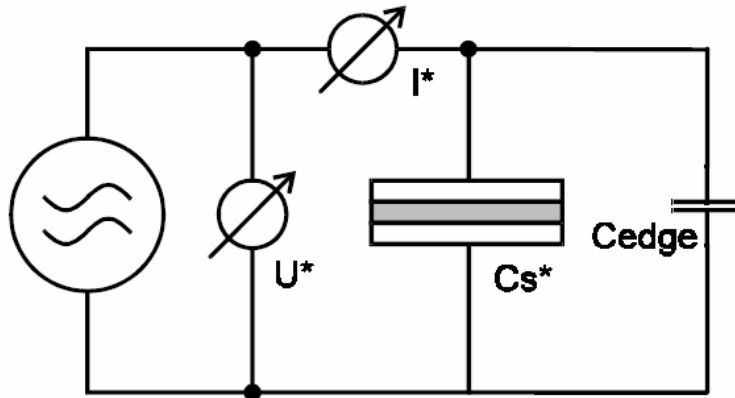


**Figure 6.2** Principle arrangement for a dielectric measurement.

A generator applies an ac voltage  $U(\omega)$  of the frequency  $\omega/2\pi$  to one of the capacitor plates. The sample current  $I(\omega)$  is determined by means of a vector current meter. The current amplitude  $I_0$ , and the phase shift  $\phi$  of the current with respect to the voltage is measured as well. For easy calculation and representation of the formulas it is convenient to use complex notations.

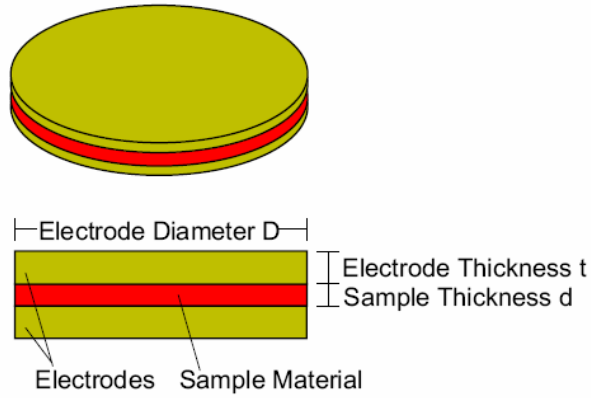


**Figure 6.3** External electrodes with the sample material in sandwich arrangement.

$$U(\omega) = U_o \sin(\omega t) = \text{Re}(U^* \exp(i\omega t)) \quad 6.1$$

$$I(\omega) = I_o \sin(\omega t + \varphi) = \text{Re}(I^* \exp(i\omega t)) \quad 6.2$$

with

$$U^* = U' + i U'' = U_o \quad 6.3$$

and

$$I^* = I' + i I''$$

$$I_o = \sqrt{I'^2 + I''^2}$$

$$\tan(\varphi) = \frac{I''}{I'} \quad 6.4$$

From this, the complex measured sample capacity  $C_m$  is evaluated by

$$C_m^* = -i \frac{I^*}{\omega U^*} \quad 6.5$$

On the other hand, the dielectric function of the sample material is related to the complex capacity of an ideal sample capacitor by

$$\varepsilon^* = \varepsilon' - i\varepsilon'' = \frac{C_s^*}{C_o} \quad 6.6$$

where  $C_o$  is the vacuum capacity of the empty sample capacitor and it's defined by

$$C_o = \varepsilon_o \frac{A}{d} \quad 6.7$$

$\varepsilon_o$  is the vacuum permittivity ( $\varepsilon_o = 8,852.10^{-14}$  F/cm),  $A$ , and  $d$  are the area and distance between the electrode plates respectively.

Experimental results rely on the determination of the complex impedance of a measured system. For a sample with linear characteristics the complex impedance  $Z$  is:

$$Z(\omega) = \frac{U_o}{I_o} e^{i\varphi} = Z' + iZ'' \quad 6.8$$

impedance can be related to the current and voltage by

$$\frac{I(\omega)}{U(\omega)} = \frac{1}{Z(\omega)} = \omega C_o (\varepsilon' + i\varepsilon'') \quad 6.9$$

It is convenient to consider the sample as being a frequency dependent capacitance,  $C_p$  and the resistance,  $R_p$  in an electrically equivalent parallel circuit. The complex impedance is  $Z(\omega)$  given as

$$\frac{1}{Z(\omega)} = \frac{1}{R_p} + i\omega C_p \quad 6.10$$

the real and imaginary parts of  $\varepsilon^*$  are obtained with parallel capacitor  $C_p$  and parallel resistor  $R_p$

$$\varepsilon' = \frac{C_p}{C_o} \quad \varepsilon'' = \frac{1}{R_p \omega C_o} \quad 6.11$$

The loss factor (6.12) which is related with the heat loss in the material due to the



motions of charges and dipoles is

$$\tan \delta = \frac{\varepsilon''}{\varepsilon'} \quad 6.12$$

and the complex conductivity is

$$\sigma^* = \sigma' + i\sigma'' = i\omega\varepsilon_0\varepsilon^* \quad 6.13$$

The frequency dependent AC conductivity,  $\sigma_{ac}$  is defined by the equations

$$\sigma(\omega) = \text{Re } \sigma^*(\omega) \quad 6.14$$

$$\sigma_{ac}(\omega) = \sigma'(\omega) = \varepsilon''(\omega)\omega\varepsilon_0 \quad 6.15$$

Figure 6.4 shows the relations of real and imaginary parts of the permittivity with frequency for a typical material. In the case of materials which exhibit only polar relaxations the real part of the permittivity  $\varepsilon'(\omega)$  decreases with increasing frequency and the imaginary part of permittivity  $\varepsilon''(\omega)$  shows a peak as shown in Figure 6.4a. For pure conducting materials the real permittivity  $\varepsilon'(\omega)$  is independent from frequency and the imaginary part  $\varepsilon''(\omega)$  decreases monotonically with increasing frequency as shown in Figure 6.4b.

There may be several distinct conformational relaxations in polymeric materials. The glass transition is assigned as  $\alpha$  relaxation and describes the onset of the motion of the segments of macromolecules when the material is heated. It is observed in the low frequency range and/or at higher temperatures (Time-Temperature Superposition TTS). The  $\beta$  and  $\gamma$  relaxations describe localized motions of dipoles associated with subunits of the molecules. They occur in the higher frequency range [Blythe 79].

Figure 6.5 shows the typical frequency dependence of ionic conductivity  $\sigma$ . The ion-motions averaged over individual hops of individual ions takes place in the regime III. In the regime II correlations between forward and backward hops are observed. Successful hops contributing to the total conduction are observed in the regime I.

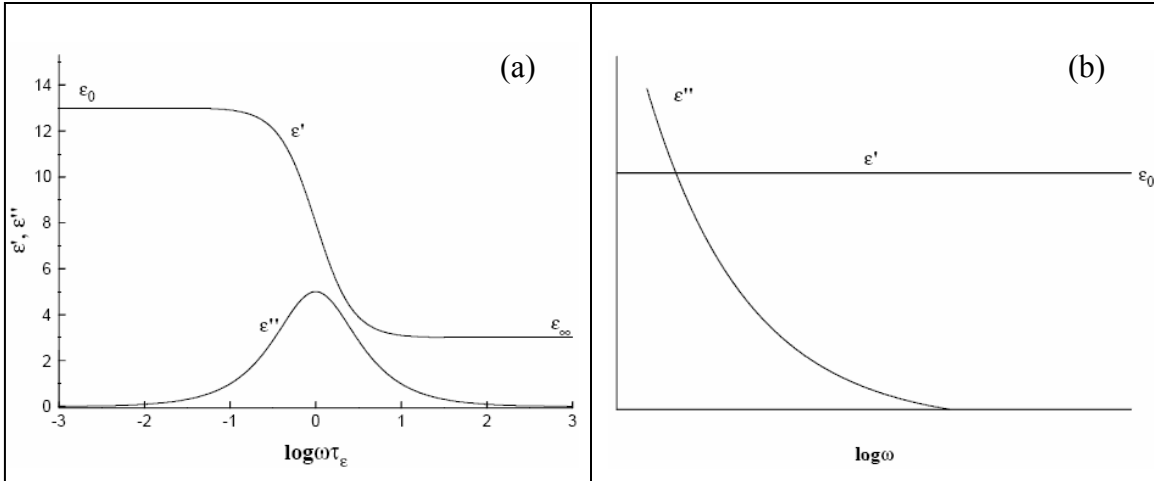


**Figure 6.4** Schematic plots of the dispersion of  $\epsilon'(\omega)$  and  $\epsilon''(\omega)$  in the frequency domain for: a) samples that exhibit dielectric relaxation b) samples that exhibit conduction [Williams].

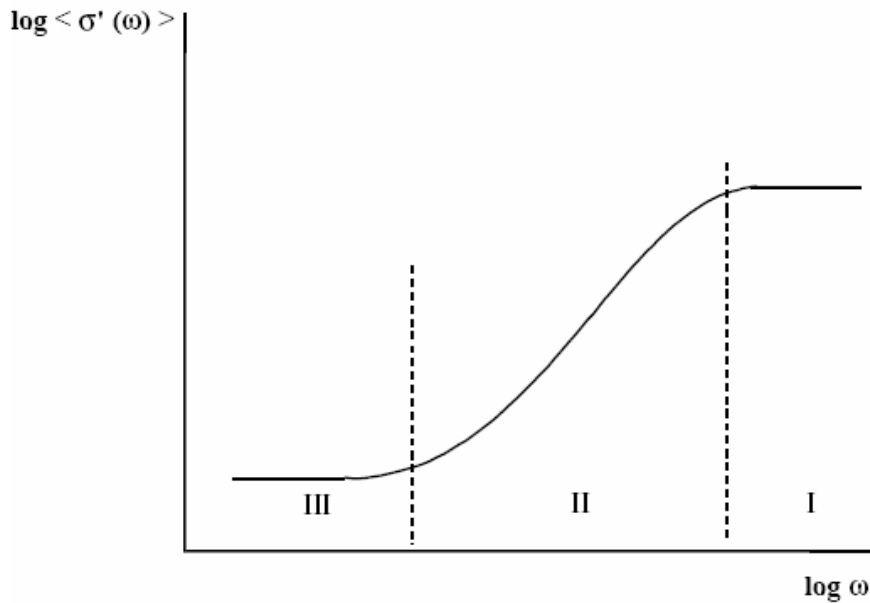


**Figure 6.5** Plot of  $\log \sigma'(\omega)$  vs  $\log \omega$  for model system exhibiting ionic conduction [Williams].

Typically, in polymers a conductivity contribution can be observed besides a relaxation contribution. To separate both the Havriliak-Negami equation can be used [Havriliak 67-96, Ratner 88]. The conductivity region is separated from the relaxation part and the corresponding ionic conductivity is obtained. Generally, the observation of conductivity plateaus at low frequencies corresponds to the DC conductivity,  $\sigma_{dc}$  (Figure 6.6). The  $\sigma'$  can be written [Almond 84, Chen 92, Chowdari 87, Rietz 93] as:

$$\sigma' = \sigma(0) + \sigma(0) \frac{\omega^p}{\omega_s^p} \tag{6.16}$$

$\sigma(0)$  represents the DC conductivity when frequency is extrapolated to zero

$$\lim_{\omega \rightarrow 0} \sigma'(\omega) \rightarrow \sigma_{dc} \tag{6.17}$$

and  $\omega_s$  is the critical frequency at which dispersion of conductivity begins and  $p$  represents the slope of the dispersion region at higher frequencies and it is related to the carrier hopping rate. The conductivity at  $\omega_s$  is given by

$$\sigma(\omega_s) = 2\sigma(0) \tag{6.18}$$

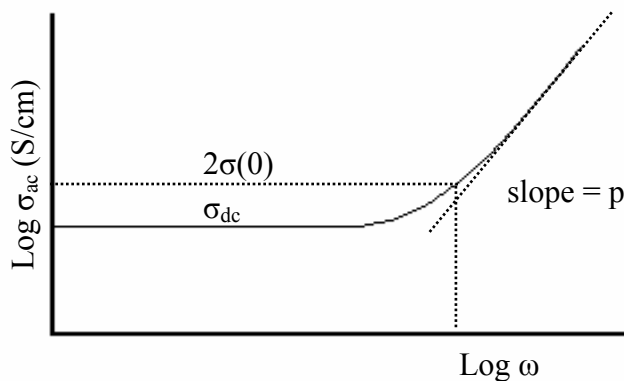


**Figure 6.6** A plot of  $\sigma'$  (T) vs. frequency with arbitrary parameters.

## 6.1 Theoretical Treatment of Ion Conduction in Solid Electrolytes

Ionic compounds and polymers can be categorized according to their conductivity: (i) *insulators* with ionic conductivity lower than  $10^{-10}$  S/cm, (the electronic contribution to the conductivity is in the same range). (ii) *ionic conductors*; the presence of charge carriers increases the conductivity up to  $10^{-5}$  S/cm. (iii) *superionic conductors* with conductivity of at least  $10^{-4}$  S/cm.

### 6.1.1. Ion Conduction in Solid Electrolytes

The bulk conductivity in solid electrolytes depends on the concentration of free ions (6.19). The concentrations of these charge carriers and their mobilities should be high since;

$$\sigma = \sum n_i (z_i e) \mu_i \quad 6.19$$

$n_i$  is the number of carriers of type  $i$ ,  $z_i e$  is the net electronic charge on the ion or aggregate, and  $\mu_i$  is mobility. The energies of activation of the formation and diffusion of these charge carriers should be higher than that of potential barriers to transport the ions. The ionic mobility,  $\mu_i$  is related to the diffusion coefficient  $D_i$  by the (NE) equation (6.20);Nerst-Einstein

$$\mu = \frac{z_i e D_i}{kT} \quad 6.20$$

this yields with (6.19) the conductivity (6.21)

$$\sigma = \frac{n_i (z_i e)^2 D}{kT} \quad 6.21$$

The conductivity in the glassy state may sometimes be expressed by the Arrhenius equation (6.22)

$$\sigma = \sigma_0 \exp(-E_a/kT) \quad 6.22$$

$E_a$  is activation energy for conductivity and  $\sigma_0$  is the preexponential factor.

### 6.1.2. Ion Conduction in Amorphous Polyelectrolytes

The multiphase behavior in a material influences the ion conductivity since the presence of both, crystalline and amorphous regions introduce phase boundary effects. The ion conductivity is usually higher in the amorphous region. The conductivity of the crystalline material increases rapidly when it melts. In order to understand the ionic motion in solid electrolytes, fully homogeneous amorphous polymer-salts or polyelectrolytes are considered. In this type of conductor the ion transport strongly depends on the ion diffusion, which is cooperative rearrangement of the polymer segments, i.e., associated with a local free volume or viscosity of the material.

The temperature (and frequency) dependent viscosity of amorphous polymers can be described by the VTF (Vogel-Tamman-Fulcher) equation (6.23) [Maccallum 87<sup>1</sup>, Vogel 26].

$$\eta = C \exp\left(\frac{-B}{k(T-T_0)}\right) \quad \text{with } C \propto T^{1/2} \quad 6.23$$

The empirical relationship (Doolittle Eq.) between viscosity and the free volume of the material can be represented by the formula 6.24 [Doolittle 51, Cohen 59]

$$\eta = A \exp(b_0 v_0 / v_f) \quad 6.24$$

$b_0$  is a dimensionless constant,  $v_0$  is the Van der Waals volume and  $v_f$  is the average Free Volume. From the Stokes-Einstein relation [Angell 92, Ratner 92] the VTF conductivity equation (6.25) results

$$\sigma = \sigma_0 \exp \left( \frac{-B}{k(T-T_0)} \right) \quad 6.25$$

where  $T_0$  is the Vogel temperature generally placed  $\sim 50$  K below the glass transition temperature which is idealized as the temperature at which all “free volume” vanishes or all polymer segmental motions disappear or the configurational entropy of the material vanishes. The  $\sigma_0$  contains a  $T^{-1/2}$  term and some other constants,  $B$  is proportional to a characteristic hard sphere volume of the moving polymer chain segment or to the inverse expansivity of the material. This equation shows the conductivity and viscosity relation as a function of temperature. The WLF (Williams-Landel-Ferry) [Williams 55] (Eq 6.26) equation includes both the viscosity and relaxation processes in amorphous systems.

$$\sigma = \sigma(T_r) \exp \left( \frac{C_1 [T - T_r]}{C_2 + T - T_r} \right) \quad 6.26$$

where  $C_1$  and  $C_2$  are WLF parameters for the temperature dependence of the ionic conductivity obtained experimentally,  $T_r$  is a reference temperature.

Both WLF and VTF equations are identical when  $C_1 C_2 = B$  and  $C_2 = T_r - T_0$ . These two equations offer several advantages: they describe the temperature dependent conductivity and transport properties including, viscosity and conductivity. They allow for an interpretation of several parameters such as  $T_0$  (VTF temperature) and  $V_f$  (free volume). However, they don't give information about the microscopic structure such as molecular weight dependence of ion transport and the mechanism of ion transport. To understand the microscopic transport the “Dynamic Bond Percolation” model was suggested [Ratner 92] for amorphous materials. The static percolation model can be defined as the set of sites at which the moving ions can reside (hopping process). This is valid in the glassy framework of solid electrolytes. When the  $T > T_g$ , then the static bond percolation model can not characterize the ion motion, in this case the motion of ions occurs dynamically by means of coordinated segmental motions of the polymer host timescales.

## 6.2 Proton Conduction in Polymer-Phosphoric Acid Systems

The proton transport mechanisms in liquid phosphoric acid have been already proposed by Kreuer et al. [Dippel 93]. There are two main mechanisms that contribute to the proton conductivity in phosphoric acid doped polymer electrolytes. The first mechanism can be explained by correlated proton jumps (in opposite direction) so called structural diffusion (Grotthus mechanism) in which the proton transport occurs through phosphate ions, i.e.  $\text{H}_4\text{PO}_4^+$ ,  $\text{H}_2\text{PO}_4^-$ . This leads to structure diffusion of both species in the same direction until they finally neutralize (Figure 6.7a)

The second is the vehicle mechanism where the protons travel through the material associated with neutral or charged molecules (Figure 6.7b). Several studies were reported about the contribution of these mechanisms on the proton conductivity of pure phosphoric acid and it was indicated that the character of conduction mechanism is mainly controlled by the structural diffusion rather than vehicle mechanism [Dippel 93, Bozkurt 99].

In systems with small vehicle species such as water, the vehicle excitation required to induce proton transfer is of the same order as the one required for the diffusion of the vehicle as a whole (structure diffusion activated by molecular diffusion [Dippel 91]). For larger vehicles, however, such as the different phosphate species, the proton transfer mode can be induced by some local dynamic of the vehicle species.

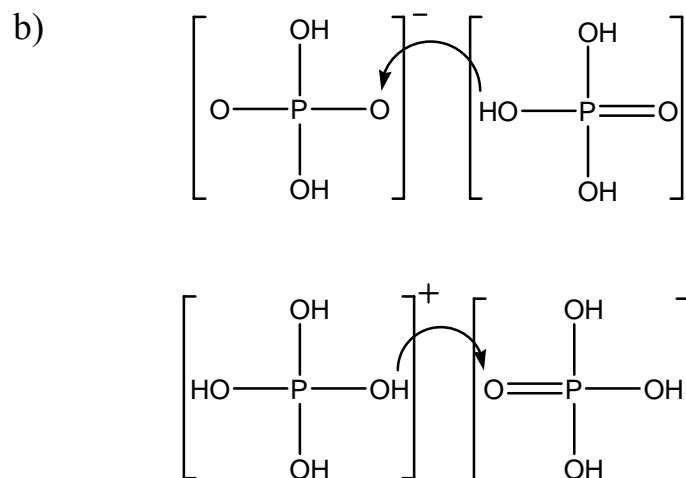
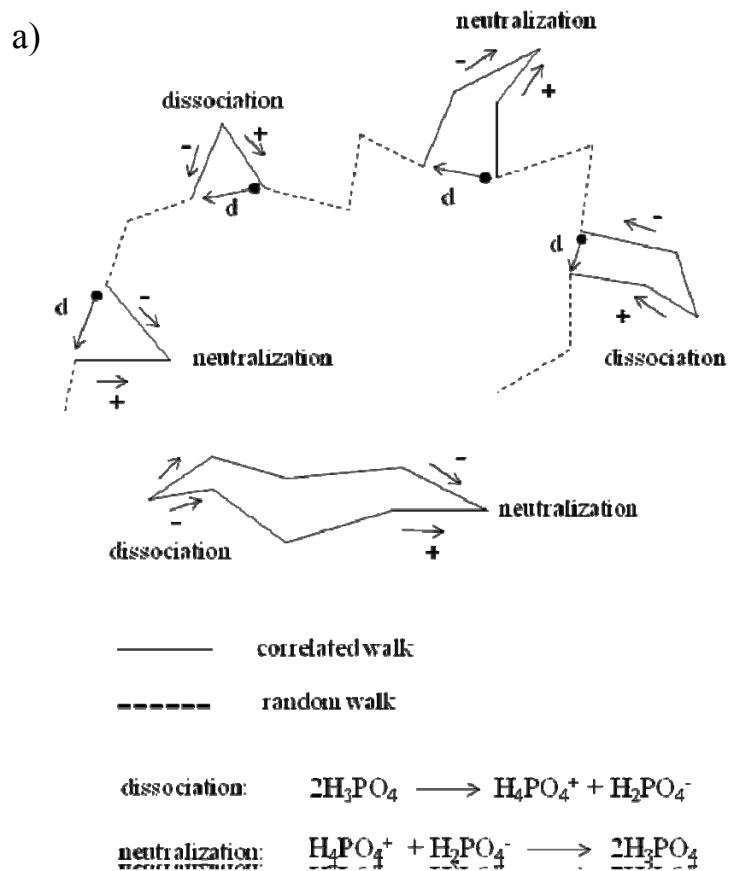


**Figure 6.7** Suggested features of proton diffusion and conductivity in fused  $\text{H}_3\text{PO}_4$  [Dippel 93].



### 6.3 Dielectric Relaxation of Polymeric Ionic Liquids

Polymeric ionic liquids as mentioned in the synthesis part can be good candidates for being used in PEMs since they represent some properties of both ionic liquids and polymer electrolytes. Conductivity properties of this kind of polymer electrolytes were studied previously [Ohno 02, Every 00, Ito 00, Susan 03<sup>1</sup>, Noda 03]. However, in all these publications the authors describe only the conductivities of pure electrolytes. In this part, we present the conductivities of blends  $\text{H}_3\text{PO}_4$  as well. Conductivities of the samples were obtained by means of the complex impedance method. The films were obtained by melting the samples between platinum electrodes. Then the films were sandwiched between two platinum blocking electrodes and placed in a temperature-controlled measuring cell. The impedance measurements were carried out over the  $10^{-1}$ - $10^6$  Hz frequency range and with variable temperatures.

#### 6.3.1 Conductivities of Poly(AcIm-n) x $\text{H}_3\text{PO}_4$

The use of polymerizable cation was considered to be effective to maintain high mobility of imidazolium to obtain higher ionic conductivity for the polymerized ionic liquid. The ionic conductivities of poly(AcIm-n) x  $\text{H}_3\text{PO}_4$  were measured in the temperature range of -10 and 150°C. Figs. 6.8-11 and 6.13-16 display the frequency dependence of the specific conductivity, ac conductivity ( $\sigma_{ac}$ ) of poly(AcIm-2) x  $\text{H}_3\text{PO}_4$  and poly(AcIm-6) x  $\text{H}_3\text{PO}_4$  as a function of temperature, respectively.

The  $\sigma_{dc}$  of the samples which are illustrated in Figures 6.12 and 6.17 were obtained by linear extrapolation of the the  $\sigma_{ac}$  plateau values to zero frequency in the frequency plot. Since the polymeric ionic liquids are highly concentrated in terms of ions, ion diffusion depends on several parameters. The influence of columbic interaction between ionic species, i.e., attractive and repulsive interaction, and the equilibrium between dissociated ions and associated ions also seem to be important for ion conduction. Hussey et al. showed the importance of the ionic charge which affects the transport properties [Hussey 90].

In all samples the conductivity exhibits a plateau at medium frequencies and a strong increase on the high frequency side at low temperatures which can be attributed to the 'normal' dispersion in polymers [McCrum 91]. The irregularities at low frequency side are due to the electrode polarization. It has been already shown that doping of polymer electrolytes with strong acids such as  $\text{H}_3\text{PO}_4$  or  $\text{H}_2\text{SO}_4$  enhances the conductivity with increasing the number of moles of acid (x) per polymer repeat unit [Rodriguez 93, Bozkurt 99]. The conductivities in poly(AcIm-n) $\text{H}_3\text{PO}_4$  are about one orders of magnitude higher than in poly(AcIm-n) $2\text{H}_3\text{PO}_4$ . The conductivity difference between the samples becomes smaller with increasing temperature and frequency.

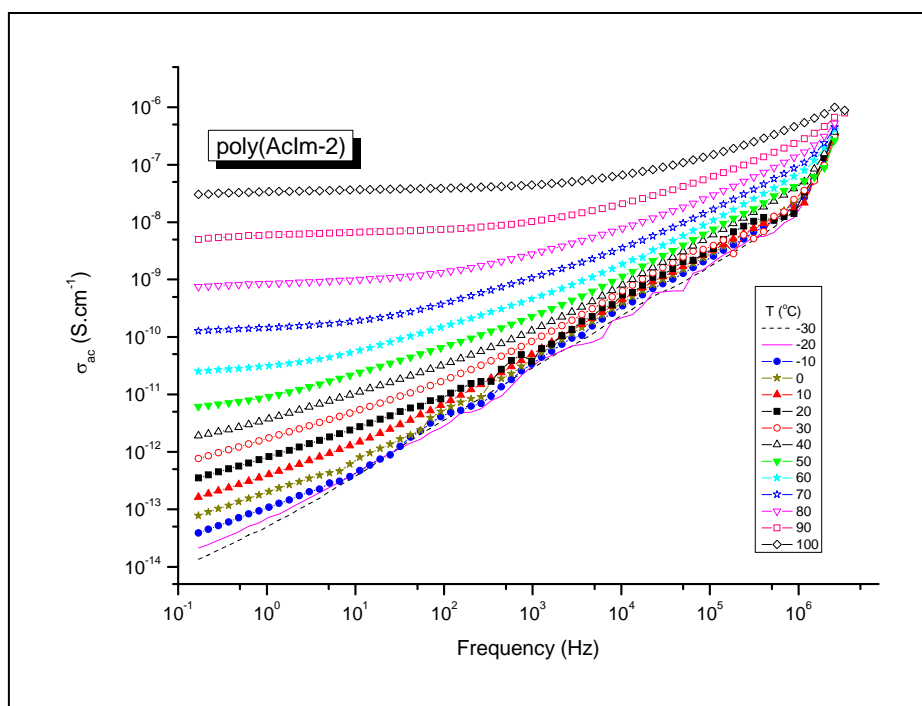


**Figure 6.8** Plot of  $\sigma_{ac}$  vs frequency (Hz) for Poly(AcIm-2).

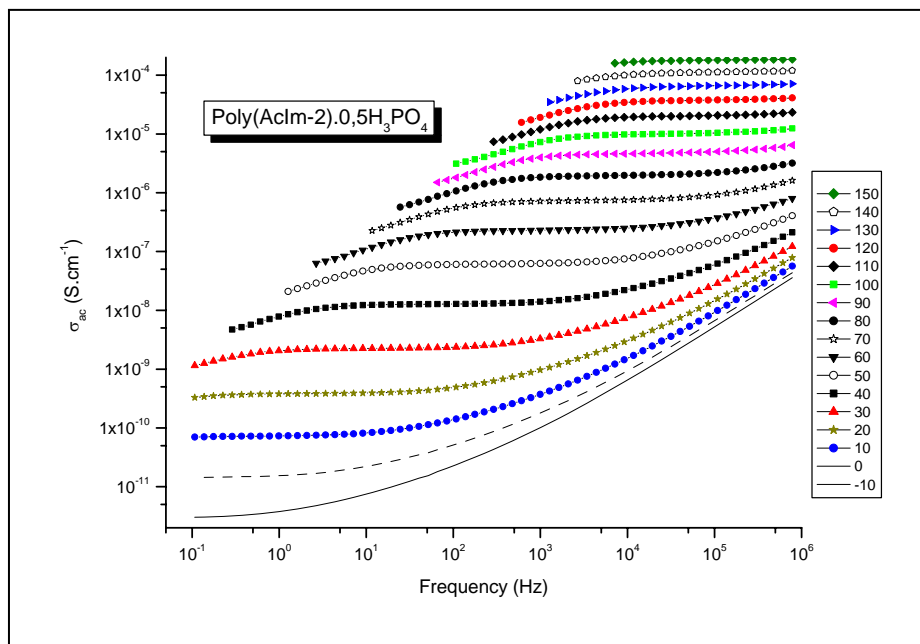


**Figure 6.9** Plot of  $\sigma_{ac}$  vs frequency (Hz) for Poly(AcIm-2) 0,5  $H_3PO_4$ .

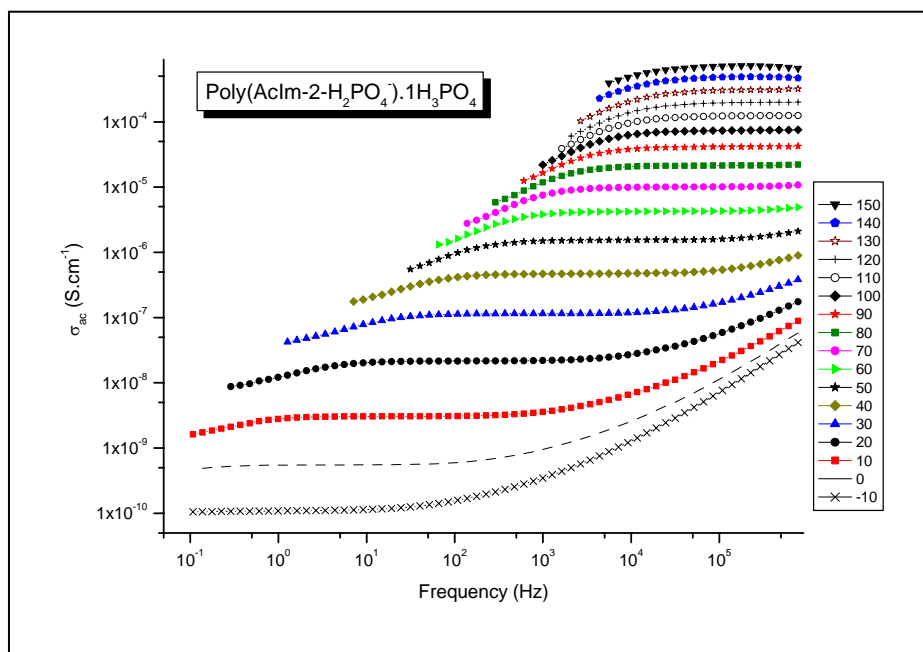


**Figure 6.10** Plot of  $\sigma_{ac}$  vs frequency (Hz) for Poly(AcIm-2) 1  $H_3PO_4$ .

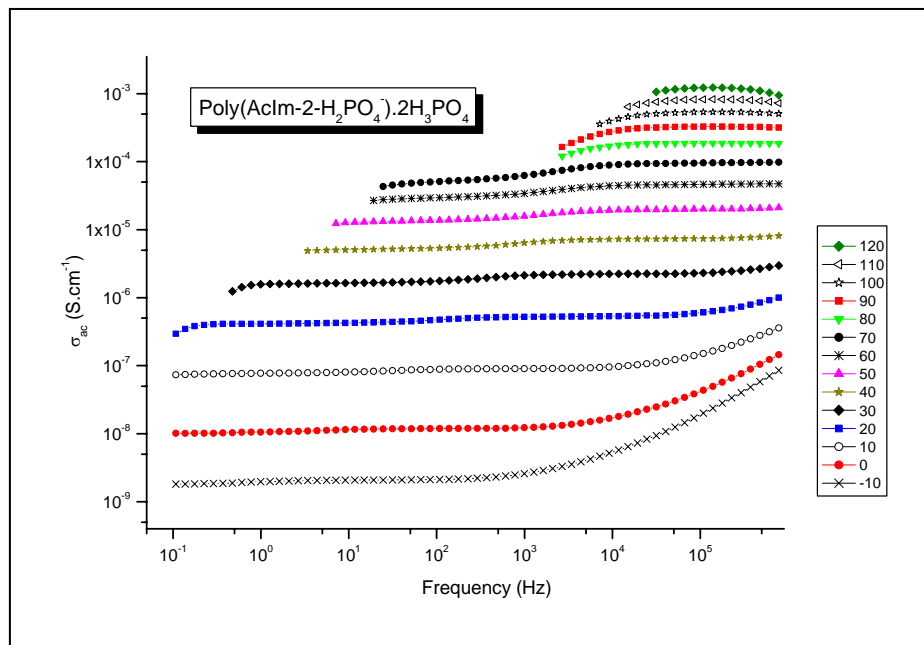


**Figure 6.11** Plot of  $\sigma_{ac}$  vs frequency (Hz) for Poly(AcIm-2)  $2H_3PO_4$ .

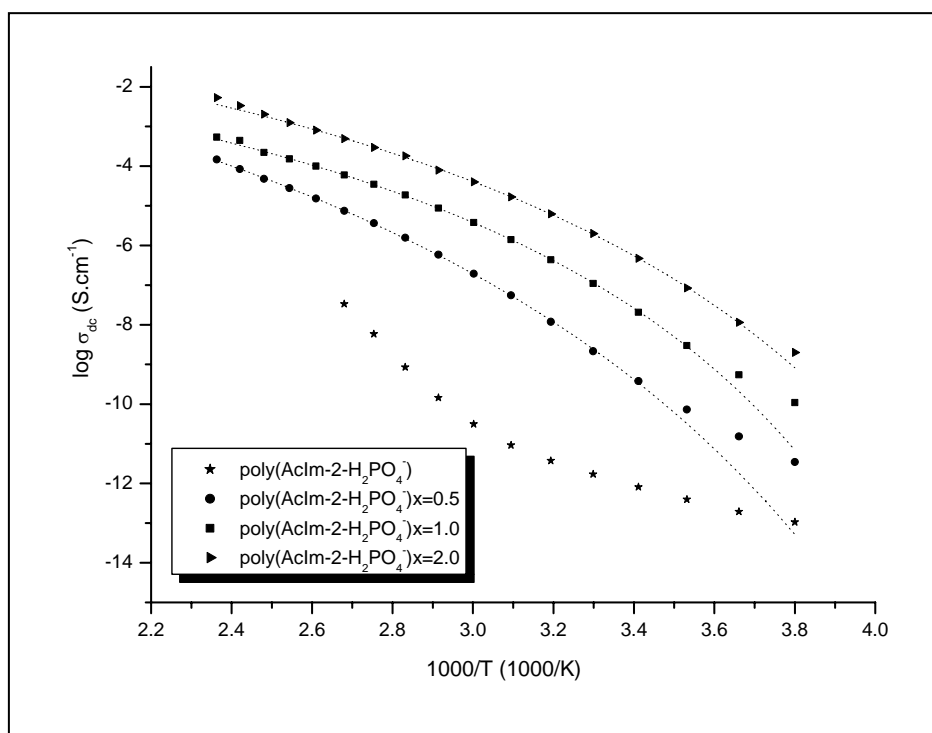


**Figure 6.12** DC conductivities,  $\sigma_{dc}$ , of Poly(AcIm-2)  $x H_3PO_4$  with temperature (dotted lines represent the fit of the data to the VTF equation).

The temperature dependence of the d.c. conductivities of the various blends and of the pure polyelectrolyte are compared in Figures 6.12 and 6.17. It is clear that the conductivity of the blends increases with temperature and with increasing  $x$ . Influence of alkyl spacer on the ionic conductivity for polymerized ionic liquids was evaluated. Both systems, poly(AcIm- $n$ )  $\times$  H<sub>3</sub>PO<sub>4</sub> with  $n=2$  and 6, showed the similar ionic conductivity of about  $10^{-7}$  S/cm at room temperature for  $x=1$ . This shows that the length of the alkyl spacer does not have a significant effect on ionic conductivity above glass transition temperatures.

The d.c. conductivities of the blends, poly(AcIm- $n$ )  $\times$  H<sub>3</sub>PO<sub>4</sub>, at 20 and 100°C are plotted as a function of the phosphoric acid content ( $x$ ) in Fig. 6.18 for comparison. It seems that the conductivities of the blends are comparable particularly at  $x=2$ .

Obviously, the conductivities increase with increasing  $x$ , seemingly approaching about  $10^{-3}$  S/cm at 100°C and  $10^{-6}$  S/cm at 20°C.

The analysis of the temperature dependence of the conductivity shows that the behaviors that can be adjusted by typical curves of amorphous systems and the ionic conductivity can be explained by mechanism that follows the free volume theory represented by VTF or WLF models. These theories predict that the segmental motion of the elastomeric polymer assures the ion transport. According to these considerations, typical d.c. conductivity curves are interpreted with the VTF equation (Eq. 6.25) and this is verified by inserting the appropriate VTF fits into Figures 6.12 and 6.17.

$$\sigma = \sigma_o \exp\left(-\frac{B}{k(T - T_o)}\right)$$

where  $\sigma_o$ ,  $B$  and  $T_o$  are the parameters explained before. Clearly, at lower temperatures the blends display less temperature sensitive behavior which may correspond to the effect of the onset of a relaxation process. It has been shown that there are two main proton transport mechanisms that contribute to the proton conductivity in phosphoric acid doped

polymer systems [Bozkurt 99, Dippel 93]. The first is the structural diffusion in which the proton diffusion occurs through phosphate ions, i.e.  $\text{H}_4\text{PO}_4^+$ ,  $\text{H}_2\text{PO}_4^-$ . The second is the vehicle mechanism where the protons travel through the material on neutral or charged molecules. Generally, the increase of  $T_g$  causes considerable drop in the ionic conductivity owing to the restriction of the diffusion processes [Wilkes 82].

The samples,  $\text{poly}(\text{AcIm-n}) \times \text{H}_3\text{PO}_4$ , maintained the ionic conductivity of over  $10^{-6}$  S/cm at room temperature and showed the highest ionic conductivity of about  $10^{-2}$  S/cm at  $120^\circ\text{C}$  for  $x=2$ .

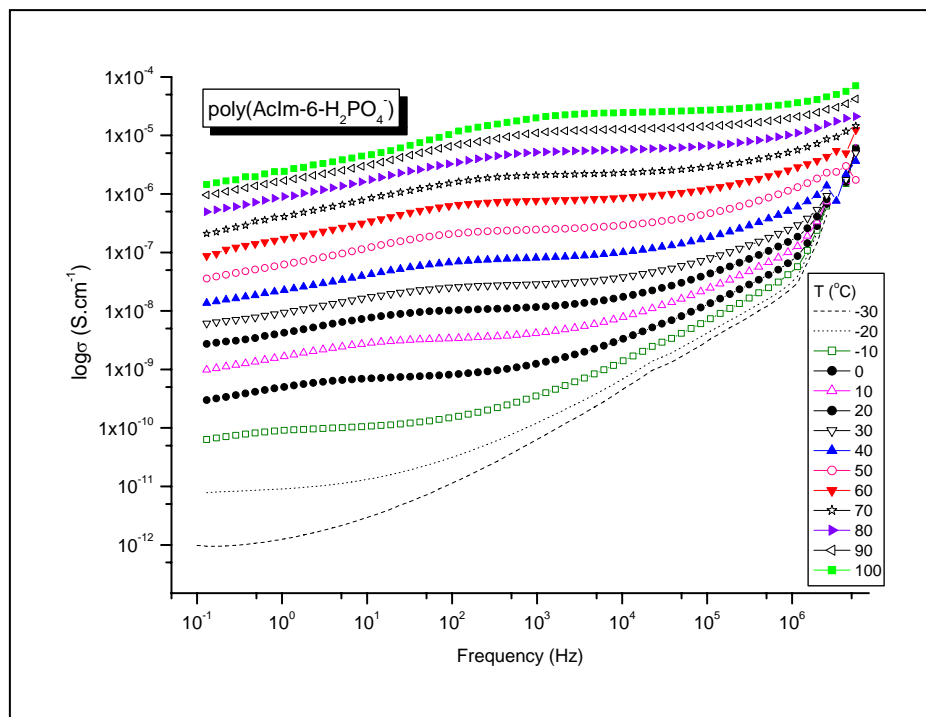


**Figure 6.13** Plot of  $\sigma_{ac}$  vs frequency (Hz) for Poly(AcIm-6).

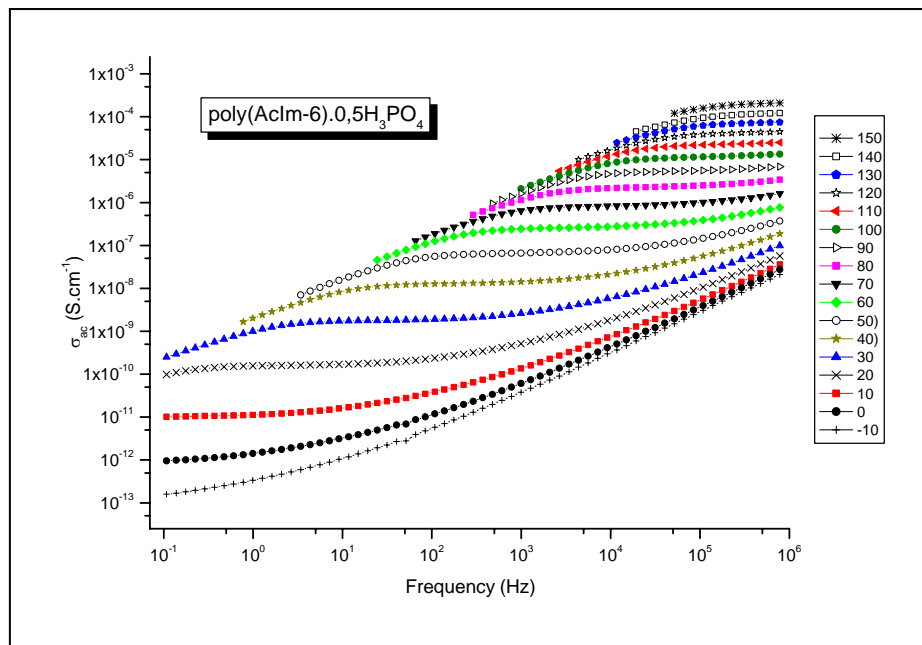


**Figure 6.14** Plot of  $\sigma_{ac}$  vs frequency (Hz) for Poly(AcIm-6).0.5H<sub>3</sub>PO<sub>4</sub>.

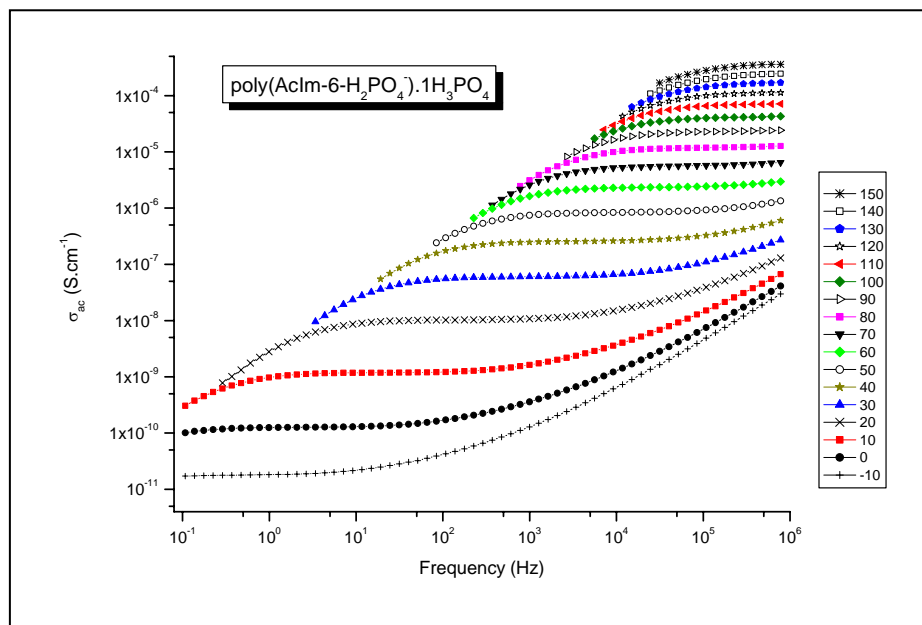


**Figure 6.15** Plot of  $\sigma_{ac}$  vs frequency (Hz) for Poly(AcIm-6).1H<sub>3</sub>PO<sub>4</sub>.

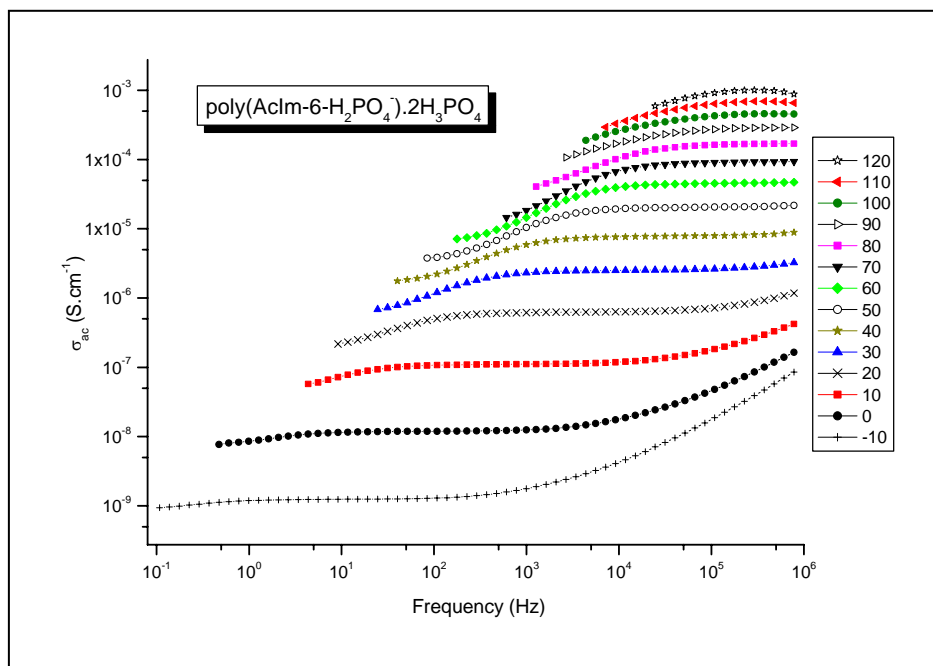


**Figure 6.16** Plot of  $\sigma_{ac}$  vs frequency (Hz) for Poly(AcIm-6). $2H_3PO_4$ .

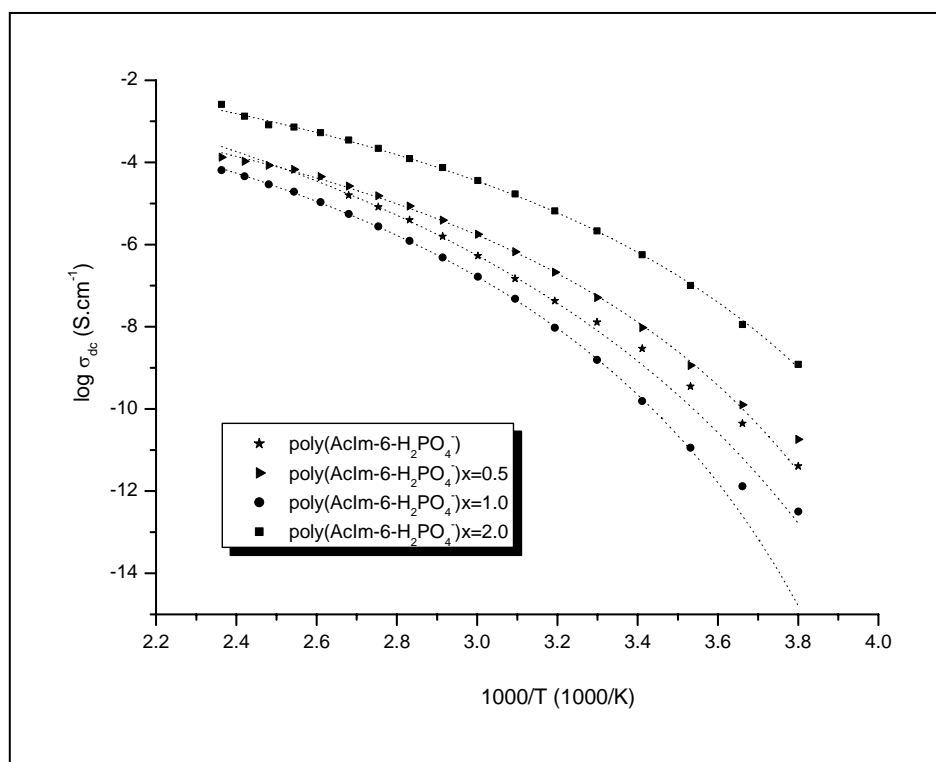


**Figure 6.17** DC conductivities,  $\sigma_{dc}$ , of Poly(AcIm-6)  $\times$   $H_3PO_4$  with temperature (dot lines represent the fit of the data to VTF equation).



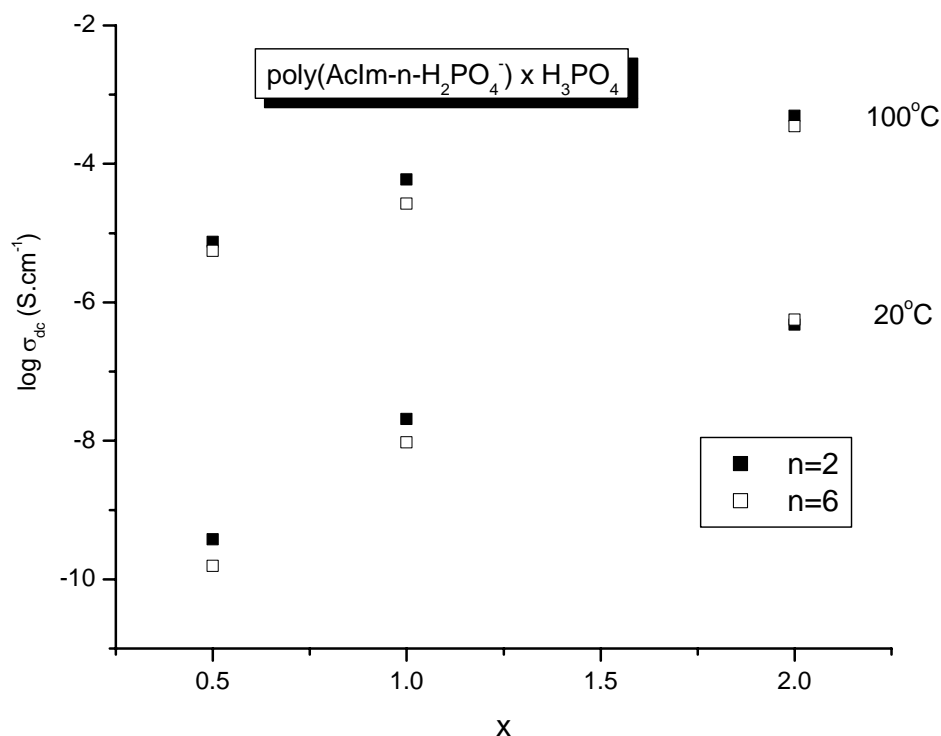


**Figure 6.18** dc conductivities of poly(AcIm-*n*) x H<sub>3</sub>PO<sub>4</sub> at 20 and 100°C as a function of the phosphoric acid content (*x*).

### 6.3.2 Conductivities of Poly(AcIm-2-Li) x LiN(SO<sub>2</sub>CF<sub>3</sub>)<sub>2</sub>

The counter ion of the polymeric ionic liquids was exchanged to trifluoromethanesulfonimide (N(SO<sub>2</sub>CF<sub>3</sub>)<sub>2</sub>) ion in order to study Li<sup>+</sup> conduction in this type of electrolytes. The electrolytes were blended with excess amounts of Li-salt (lithium trifluoromethanesulfonimide (LiN(SO<sub>2</sub>CF<sub>3</sub>)<sub>2</sub>)). Figures 6.19-22 show the variation of dielectric loss ( $\epsilon''$ ) with frequency at different temperature for pure and doped electrolytes. It is clear from the figures that in the low frequency region the plots are nearly linear. This reflects d.c. conductivity which is characterized by the equation  $\epsilon''_{dc} = \sigma_{dc}(\omega C_0)$ , where  $\sigma_{dc}$  is the d.c. conductance and  $C_0$  is the vacuum capacitance for the unfilled cell in which the electrode plate spacing is equal to the sample thickness [McCrum 91].

The electrolytes exhibits a relaxation process around  $1 \times 10^3$  Hz. This relaxation process so called  $\beta$ -relaxation may be caused by some local movement of side group dipoles [Williams 79, 94]. This relaxation is clearer for the blends which may be due to the plasticization effect of the added lithium salt. At higher temperatures and in high frequency range, the plot comprises a broad relaxation curves which is the contribution of  $\alpha$ -relaxation. The  $\alpha$ -relaxation process is the result of movement of main chain dipole segments [McCrum 91]. The appearance of two sets of relaxation peaks indicates that this materials show two different types of relaxation processes having different relaxation times and temperatures. It is observed from the figures that the dielectric loss continuously decreases with increasing frequency. A rapid decrease in dielectric loss may be noticed over the frequency range  $10^3$ - $10^6$  Hz. This may be attributed to the tendency of dipoles in macromolecules to orient themselves in the direction of the applied field in the low frequency range. However, in the high frequency range the dipoles will hardly be able to orient themselves in the direction of applied filed and hence the value of dielectric loss decreases [Reicha 91]. This phenomena is called “conductivity relaxation” [Dyre 91]. In order to check the effect of temperature on the relaxation process for pure and blended electrolytes the Figures 6.23 (a, b) were plotted. They depict the dielectric relaxation spectra at different temperatures. As the temperature increases the peak of the relaxation shifts towards a higher frequency region showing that the relaxation is strongly temperature and frequency dependent.

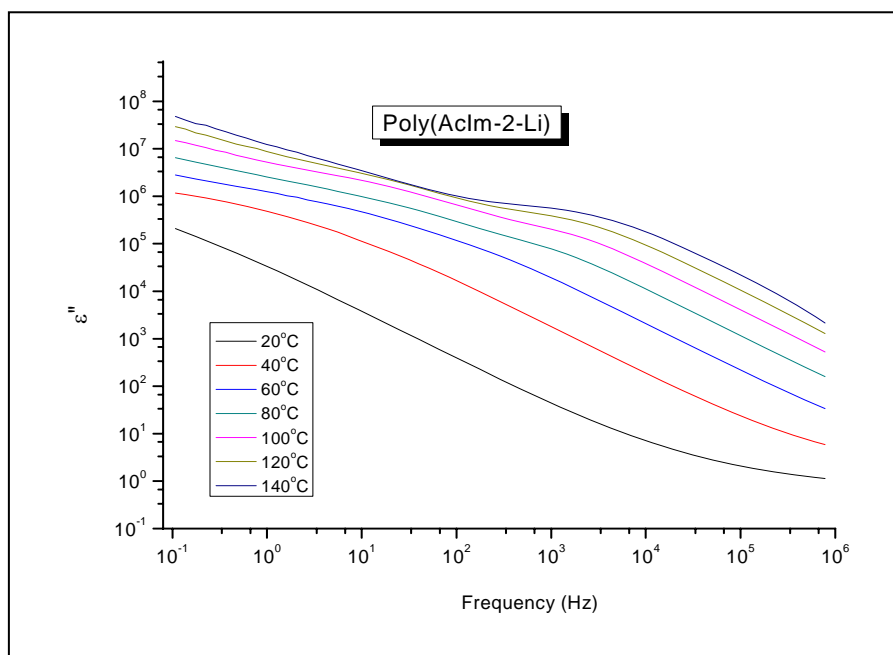


**Figure 6.19** Variation of dielectric loss ( $\epsilon''$ ) with frequency at different temperatures for poly(AcIm-2-Li).

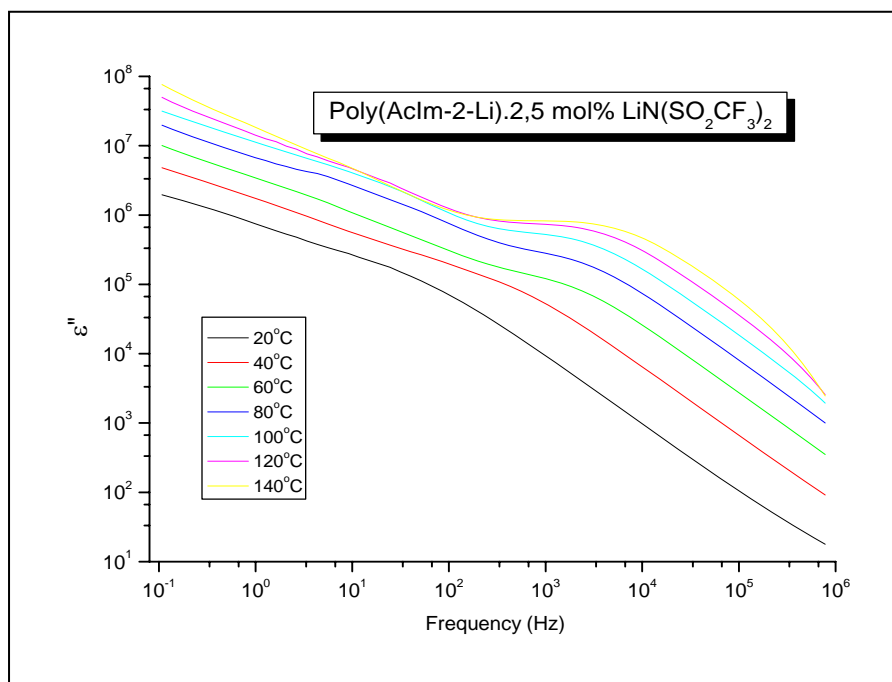


**Figure 6.20** Variation of dielectric loss ( $\epsilon''$ ) with frequency at different temperatures for poly(AcIm-2-Li) with 2,5 mol %  $\text{LiN}(\text{SO}_2\text{CF}_3)_2$ .

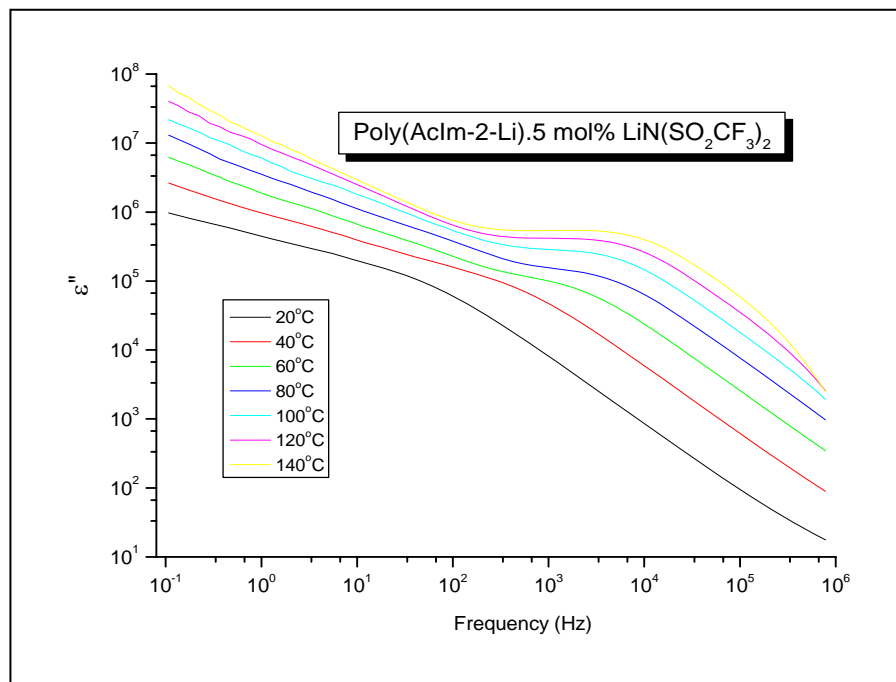


**Figure 6.21** Variation of dielectric loss ( $\epsilon''$ ) with frequency at different temperatures for poly(AcIm-2-Li) with 5 mol % LiN(SO<sub>2</sub>CF<sub>3</sub>)<sub>2</sub>.

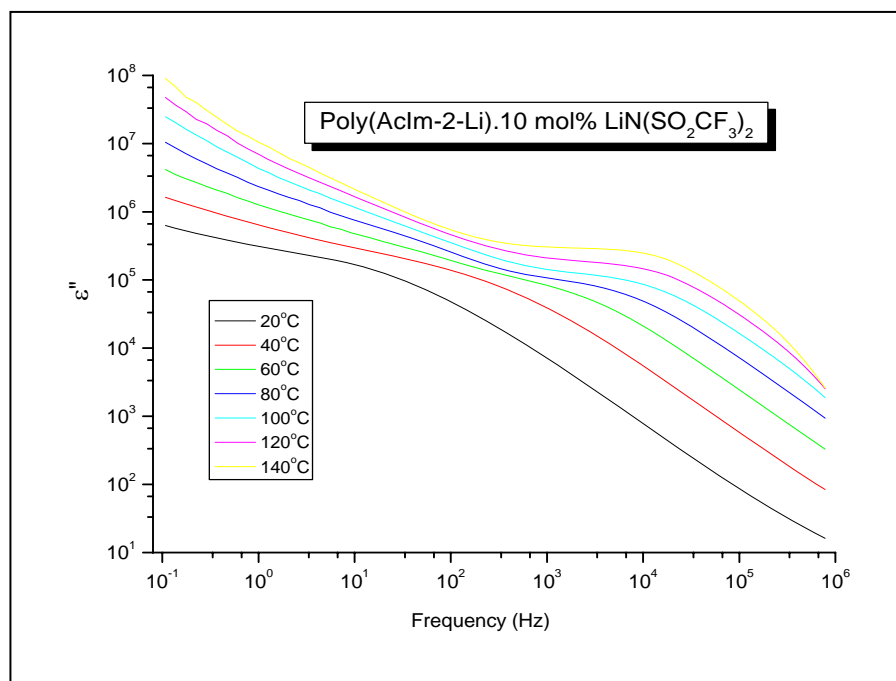


**Figure 6.22** Variation of dielectric loss ( $\epsilon''$ ) with frequency at different temperatures for poly(AcIm-2-Li) with 10 mol % LiN(SO<sub>2</sub>CF<sub>3</sub>)<sub>2</sub>.

The d.c. conductivities of the materials are shown in Figure 6.24. These conductivities were obtained by the extrapolation of the plateau region of the plot of  $\sigma_{ac}$  vs frequency which are not shown here to zero frequency according to equation 6.15. Figure 6.25 shows the fitted curves of the d.c. conductivities of these materials which are obtained by using the VTF equation (Eq. 6.25) and the calculated parameters are shown in Table 6.1. The films were prepared by casting the sample solutions on the platinum electrodes then the solvent, DMF, was evaporated by heating. It is important to obtain nicely smooth films in order to minimize the obscuring effect of d.c. conductivity due to residual water (the samples are very hygroscopic, and it becomes more with increasing salt content). This procedure is also critical for removing surface voids which would affect the contact between the sample and the electrode. It can be seen that ionic conductivity increases with blends up to certain point and reaches nearly constant value for all blend content. It is known that the polymer electrolytes obtained by dissolution of salts in poly(ethylene oxide), PEO, undergo partial crystallization with formation of crystalline PEO or crystalline PEO-salt complexes [Gray 97]. Ionic conductivity decreases with increasing content of crystalline phase. However, the low lattice-energy lithium salt with large flexible anion:  $\text{LiN}(\text{CF}_3\text{SO}_2)_2$  (lithium bis(trifluoromethanesulfone) imide, inhibits crystallization of the system [Dygas 03]. In our case, no crystallization process was observed by thermal analysis. It is known also that in the typical salt-polymer blends, so-called salt-in-polymer electrolytes, the number of carrier ions increases, but their mobility decreases with increasing the electrolyte concentration. Thus, the reason for this constant conductivity may be due to the ionic association when the salt content is higher than some extent.

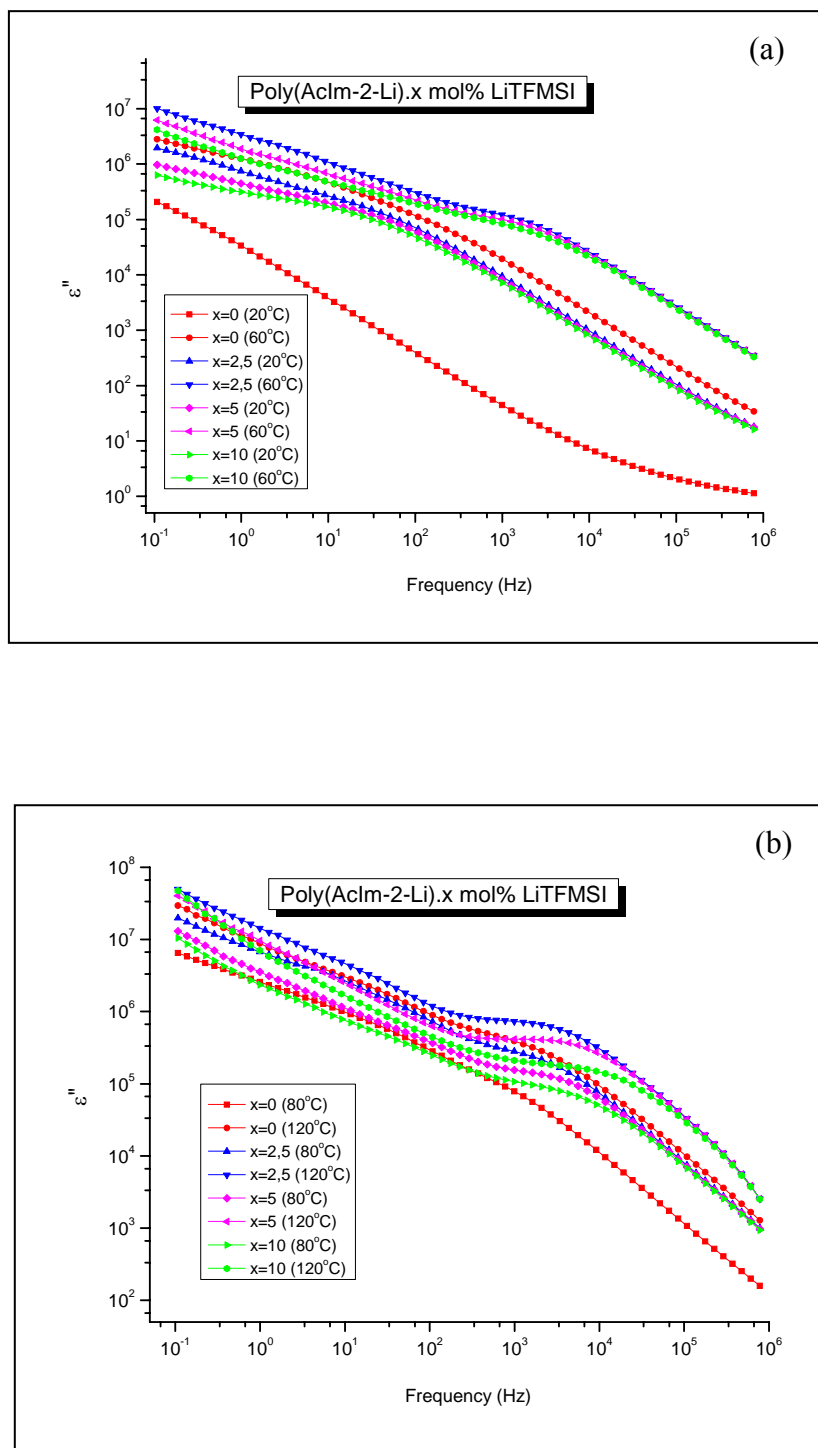


**Figure 6.23** Variation of dielectric loss ( $\epsilon''$ ) with frequency at different temperatures for pure and blended Poly(AcIm-2-Li) (a) at 20 and 60°C (b) 80 and 120°C.

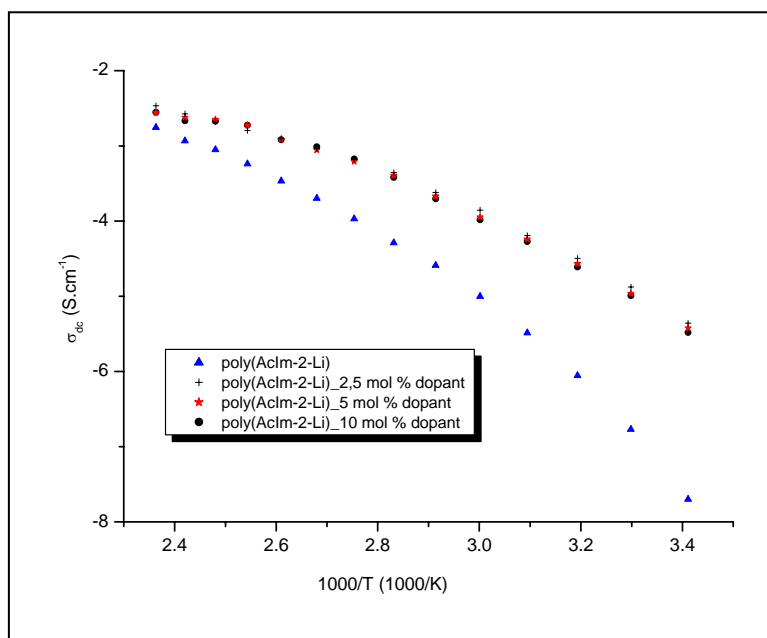


**Figure 6.24** Plot of  $\sigma_{dc}$  vs temperature (Hz) for Poly(AcIm-2-Li) and blends.

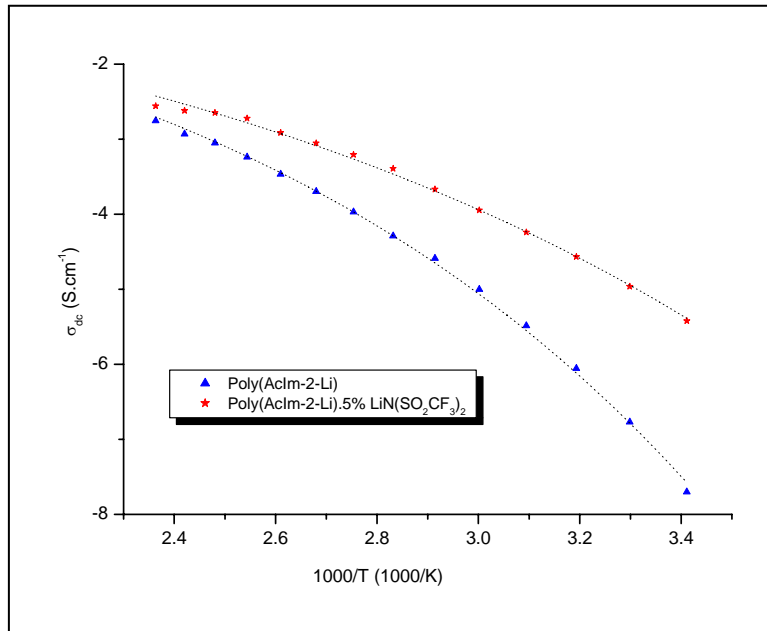


**Figure 6.25** Plot of  $\sigma_{dc}$  vs temperature (Hz) for Poly(AcIm-2-Li) and blend. (dotted lines represent the fit of the data to the VTF equation).

#### 6.4 Conductivity of Poly(Im-6-6)

Ionenes, cationic polyelectrolytes with quarternary imidazolium groups in the repeat unit, can be considered as models for polyelectrolytes. The charge density of the ionene is chemically changeable in the synthesis by using various kinds of reagents which consist of different numbers ( $l,m$ ) of (-CH<sub>2</sub>-) groups between quaternized nitrogen (imidazolium), expressed as  $l,m$ -ionene. The polymers were synthesized and purified as described previously in Chapter 3. However, the yield of the 6-6-ionene was only adequate to be processed for ionic conductivity.

The conductivity was measured with impedance spectroscopy using a Novocontrol Impedance spectrometer. Sample preparation was carried out by casting the polymer solution in DMF on platinum electrode. The solvent was evaporated by heating around 100°C. The evaluation of ionic conductivity by means of dielectric spectroscopy is well established and the application of this method with respect to ammonium type of ionenes was recently described [Kremer 89, Reisinger 98<sup>1</sup>].

The temperature dependence of free volume should follow a VTF behavior for the alpha process, which therefore obeys temperature dependence according to

$$\log \tau = -\frac{B}{T - T_0} \quad 6.27$$

where  $B$  is a pseudo activation energy,  $T_0$  is the Vogel temperature and  $\tau$  is the relaxation time, but might also be another dynamic value like conductivity as long as this is related to the alpha process [Reisinger 98<sup>1</sup>]. In the case of conductivity, this relation has been confirmed for the conductivity case [Ratner 87] and it turns out that  $\sigma \propto 1/\tau$ . The alpha relaxation in ionenes cannot be observed in dielectric spectroscopy since it is too small compared to the conductivity contribution [Reisinger 98<sup>1</sup>]. Hence conductivity is the only means to investigate the temperature dependence of dynamic values around the glass transition. Figure 6.26 shows this temperature dependency and a conductivity spectrum,



with its typical behavior: low frequency dispersion due to electrode polarization, a conductivity plateau and a high frequency dispersion. The temperature behavior could either be observed in the ac conductivity modulus or at a constant frequency in the conductivity plateau. The curvature of the Arrhenius plot indicates that there is no Arrhenius dependence. The empirical VTF was fitted well to the data. The fit parameters are displayed in Table 6.1. This temperature relationship can be explained with the free volume model. This model was successfully applied to ionic conductivity of ionenes [Reisinger 98<sup>2</sup>].

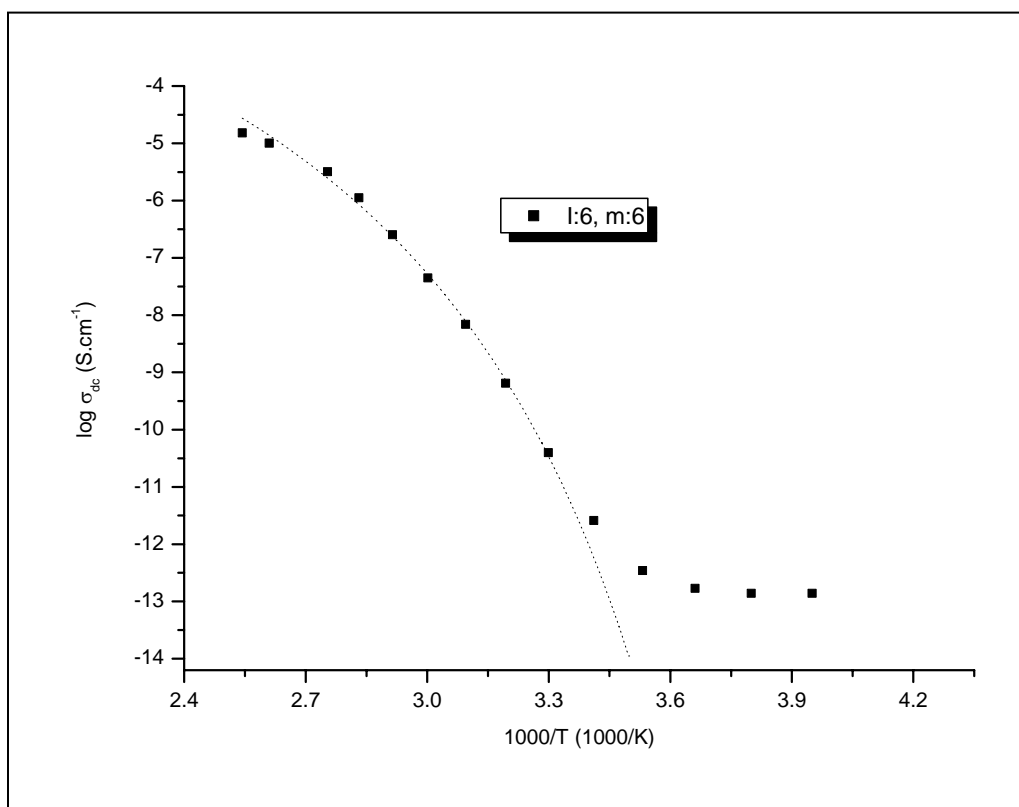


**Figure 6.26** Temperature dependency of conductivity of Poly(Im-6-6).

**Table 6.1.** VTF fitting parameters for the DC conductivities of Poly(AcIm-n) .x H<sub>3</sub>PO<sub>4</sub>, Poly(AcIm-2-Li) .x LiN(SO<sub>2</sub>CF<sub>3</sub>)<sub>2</sub> and Poly(Im-6-6)

Poly(AcIm-n) .x H <sub>3</sub> PO <sub>4</sub>	x	T <sub>g</sub> (°C)	log σ <sub>0</sub>	B(eV)	T <sub>0</sub>
n : 2	0.5	30	1.759	0.289	-111.470
	1.0	20	-0.191	0.139	-73.990
	2.0	7	0.828	0.153	-88.220
n : 6	0.0	22	0.317	0.178	-78.950
	0.5	10	-0.330	0.163	-87.260
	1.0	0	-0.557	0.140	-74.710
	2.0	-7	-0.430	0.102	-68.190
Poly(AcIm-2-Li) .x LiN(SO <sub>2</sub> CF <sub>3</sub> ) <sub>2</sub>	0.0	0	-0.408	0.090	4.630
	5.0	12	0.151	0.120	4.910
Poly(Im-6-6)		6	0.3947	0.169	-50.3239

## 7. Solid State NMR

Information about hydrogen bonding in solids can be obtained by a variety of methods. NMR spectroscopy is one of them and has the advantage of allowing the direct probing of the hydrogen-bonded protons themselves. However,  $^1\text{H}$  NMR spectroscopy of rigid solids is complicated by the homonuclear proton-proton dipolar interaction [Mehring 83]. Hydrogen bonds are known to play an important role in determining the properties of a range of materials [Brunet 97, Castellano 98].

The hydrogen-bonding interaction play a role for the changes in glass transition temperatures and is a crucial precondition for  $\text{H}^+$  transport in our polymer [Wirasate 98]. To better investigate these interactions solid state  $^1\text{H}$  NMR measurements were carried out.

The purpose of this  $^1\text{H}$  NMR study is to show that recently developed fast magic-angle spinning (MAS) and double-quantum (DQ) NMR methods outlined below can provide further information on the hydrogen bonding in our samples, which is both unique and complementary to that achievable by other approaches.

### 7.1 Nuclear Spin Interactions in the Solid Phase

#### 7.1.1 Chemical Shielding

The chemical shielding is a local property of each nucleus, and depends on the chemical environment of the individual nucleus.

Specifically, the external magnetic field induces currents of the electrons in molecular orbitals. These induced currents create local magnetic fields that often vary across the entire molecular framework such that nuclei in distinct molecular environments usually experience unique local fields from this effect.

Under sufficiently fast magic angle spinning, or in solution-state NMR, the directionally dependent character of the chemical shielding is removed, leaving the isotropic chemical shift, which is dispersed in a region of around 20 ppm.

### 7.1.2 J-Coupling (Scalar Coupling)

The J-coupling or scalar coupling describes the interaction of nuclear spins through chemical bonds. This interaction is not very pronounced in solid state  $^1\text{H}$  NMR, because of the exceeding dipolar interactions.

### 7.1.3 Dipolar Coupling

Nuclear spins exhibit a dipole moment, which interacts with the dipole moment of other nuclei (dipolar coupling). The magnitude of the interaction is dependent on the spin species, the internuclear distance, and the orientation of the vector connecting the two nuclear spins with respect to the external magnetic field  $B$  (Figure 7.1).

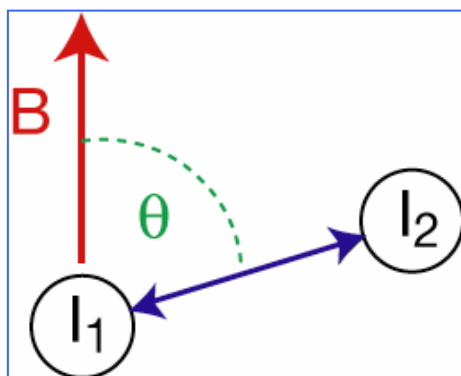


**Figure 7.1** Dipolar coupling vectors.

The maximum dipolar coupling is given by the dipolar coupling constant  $d$ ,

$$d = \frac{h\mu_0}{4\pi} \frac{\gamma_1\gamma_2}{r^3}$$

where  $r$  is the distance between the nuclei, and  $\gamma_1$  and  $\gamma_2$  are the gyromagnetic ratios of the nuclei,  $h$  is the Planck's constant and  $\mu_0$  is the clumy factor ( $4\pi \times 10^{-7} \text{ Hm}^{-1}$ ). In a strong magnetic field, the dipolar coupling depends on the orientation of the internuclear vector with the external magnetic field by

$$D \propto 3\cos^2\theta - 1$$

Consequently, two nuclei with a dipolar coupling vector at an angle of  $\theta_m = 54.7^\circ$  to a

strong external magnetic field, which is the angle where  $D$  becomes zero, have zero dipolar coupling.  $\theta_m$  is called the magic angle. One technique for removing dipolar couplings, at least to some extent, is magic angle spinning. The dipolar interactions of  $^1\text{H}$  in solid supramolecular systems may be as much as hundreds kHz.

## 7.2 Modern Solid-State NMR spectroscopy

### 7.2.1 $^1\text{H}$ NMR

For the investigations of supramolecular systems solid-state  $^1\text{H}$  NMR spectroscopy exhibits attractive features. The subjected nucleus,  $^1\text{H}$ , can be observed directly with excellent sensitivity and resolution. The information of the proton environment is understood by the specific chemical shift values, which are a result of the electronic environment of the individual proton.

Molecular mobility can also be monitored by measuring the strength of the  $^1\text{H}$ - $^1\text{H}$  dipolar interactions, which exist at full strength in rigid systems but is reduced in mobile systems as a consequence of molecular motion occurring on the timescale of 10-100  $\mu\text{s}$ . To investigate  $^1\text{H}$ - $^1\text{H}$  dipolar couplings, one dimensional Double Quantum Filtered and two dimensional Double Quantum NMR spectroscopy will be applied. In these techniques dipolar double-quantum (DQ) coherences between pairs of protons are generated. By these methods it will be possible to differentiate signals coming from rigid and mobile molecules in the material. The so called Back-to-Back pulse sequence is used for the generation of double quantum coherences [Schnell 1998]. Observation of DQ signal implies the existence of a dipole-dipole coupling  $D_{ij}$ , between the pair of nuclei on the timescale of the experiment (typically between 10-100  $\mu\text{s}$ ). Absence of a DQ signal indicates a lack of dipole-dipole coupling (less than 2 kHz) which can either be due to long  $^1\text{H}$ - $^1\text{H}$  distance or due to molecular motion on the timescale  $< 100 \mu\text{s}$ .

To achieve spectral resolution in these strongly dipolar coupled  $^1\text{H}$  spectra, high speed specimen rotation will be applied (MAS) which will be around 30 kHz.

A comparison of single pulse  $^1\text{H}$  MAS spectra to DQF  $^1\text{H}$  spectra allow us to distinguish mobile and rigid domains. Variable temperature  $^1\text{H}$  MAS spectra are used to characterize

the local proton mobility with the observed line narrowing, which may be compared to the conductivity measurements of the samples [Goward 2002].

### 7.2.2 Cross Polarization MAS NMR

A fundamental RF pulse sequence and building-block in most solid-state NMR experiments is cross-polarization (CP) [Pines, 1973] (Figure 7.2). It can be used to enhance the signal of nuclei with a low gyromagnetic ratio (e.g.  $^{13}\text{C}$ ,  $^{15}\text{N}$ ) from a transfer of nuclei with a high gyromagnetic ratio (e.g.  $^1\text{H}$ ), or as spectral editing method (e.g. directed  $^{15}\text{N} \rightarrow ^{13}\text{C}$  CP in protein spectroscopy).

In order to establish magnetization transfer, the RF pulses applied on the two frequency channels must fulfill the Hartmann–Hahn condition [Hartmann, 1962]. Under MAS, this condition defines a relationship between the voltage through the RF coil and the rate of sample rotation. Experimental optimization of such conditions is one of the routine tasks in performing a (solid-state) NMR experiment.

CP is a basic building block of most pulse sequences in solid-state NMR spectroscopy. Given its importance, a pulse sequence employing direct excitation of  $^1\text{H}$  spin polarization, followed by CP transfer to and signal detection of  $^{13}\text{C}$ ,  $^{15}\text{N}$  or similar nuclei, is itself often referred to as CP experiment, or, in conjunction with MAS, as CP-MAS [Schaefer 1976]. It is the typical starting point of an investigation using solid-state NMR spectroscopy.

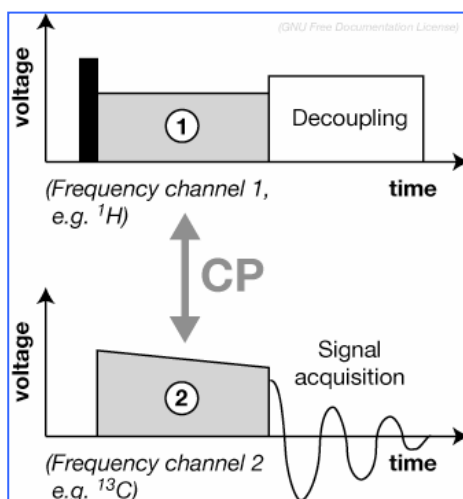


**Figure 7.2** CP pulse sequence.

### 7.3 Results of NMR Spectroscopy

#### 7.3.1 Results of $^1\text{H}$ -MAS and $^1\text{H}$ -DQF NMR Spectroscopy

The structures of the materials in the solid state can be significantly different from the structures in solution, and these differences have remarkable effects on the spectra of the materials [Brown 2001]. For example, hydrogen bonding and pi-pi stacking will cause one of these differences. For example, in the sample Poly(AcIm-6) there is a shift to high ppm values in solid state of 1 ppm for the peak appearing at around 9 ppm in solution state.

When the  $^1\text{H}$  MAS NMR spectra of Poly(AcIm-2) and Poly(AcIm-6) are compared, substantial differences in the resolution of specific sites can be realized. From Figure 6.4 and Figure 6.6, the spectra of these samples can be seen. The resolution increase in the sample of Poly(AcIm-6) compared to Poly(AcIm-2) sample, is mainly because of the differences in the  $T_g$  values of the polymer systems, which is around  $60^\circ\text{C}$ . The  $T_g$  is usually decreased by the increase of the side chain length,  $n$ . As a result of lower  $T_g$  of Poly(AcIm-6) the molecular mobility at room temperature is increased and this leads to better resolved resonances in both the backbone region and side chain region.

$^1\text{H}$  MAS-NMR spectra give information about the different types of  $^1\text{H}$  sites in the samples. With this information in hand, one can understand many molecular properties of the system, for example, hydrogen-bonding arrangements. However, usually one-pulse experiments are not sufficient to gather information about dipolar coupling, especially in strongly coupled proton systems, because the detected signal has no information about the pair character of the dominant dipolar interaction. As a result, to improve the experimental aspect, we must also take into account two-spin correlations by using Double-Quantum Spectroscopy. With this method, it is rather easy to determine the interactions of protons in a pair wise manner. Additionally, by a comparison of  $^1\text{H}$  spectra with the double-quantum filtered BaBa spectra, the mobile and the rigid protons can be distinguished easily.

The BaBa homonuclear DQ recoupling pulse sequence was applied for 1 rotor period,  $t_R$ , (which corresponds to  $33.6 \mu\text{s}$  of excitation and reconversion period) at 30 kHz to excite and reconvert the  $^1\text{H}$ - $^1\text{H}$  DQ coherences (DQC). Only protons that become involved in a

DQC during the excitation period and remain involved in DQC until the end of the reconversion period can give rise to a signal in DQF spectra. More explicitly, signals from mobile protons are suppressed because their dipolar coupling is not sufficiently strong in the time period necessary to excite DQC. The liquid NMR spectra of polymeric ionic liquids are shown for the assignment of the related H peaks (Figure 7.3, 7.4).

When we compare the  $^1\text{H}$  MAS and  $^1\text{H}$  DQF spectra in Figures 7.5, it can easily be seen that there is nearly no change after the application of DQF. Only some very mobile backbone proton resonances disappeared. This result and the poor resolution of proton spectrum indicated the existing of a relatively rigid system at room temperature, appearing as very broad featureless peaks. When we moved to sample Poly(AcIm-6) which is shown in the Figure 7.5, there is one peak disappearing after the application of DQF around 5 ppm. This resonance is the  $-\text{OH}$  proton peak, and should be relatively mobile compared to other resonances. The other resonances again did not change as in Poly(AcIm-2) sample at room temperature.

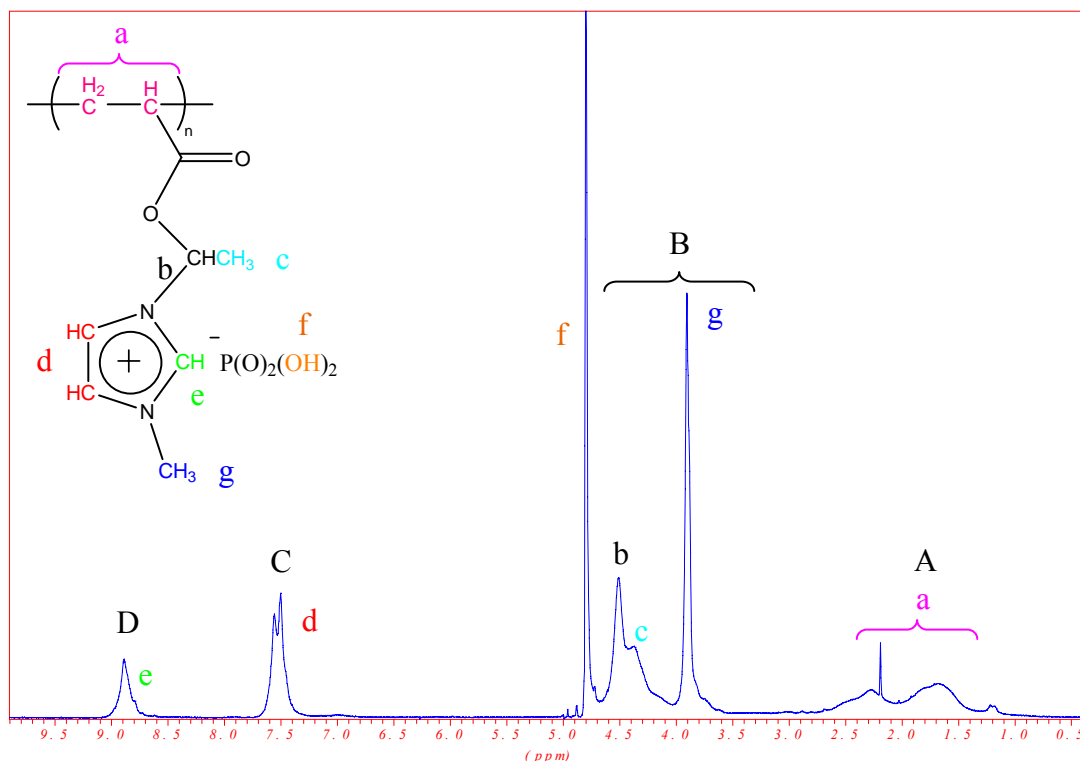


**Figure 7.3**  $^1\text{H}$ -NMR spectra of Poly(AcIm-2) in  $\text{D}_2\text{O}$ .



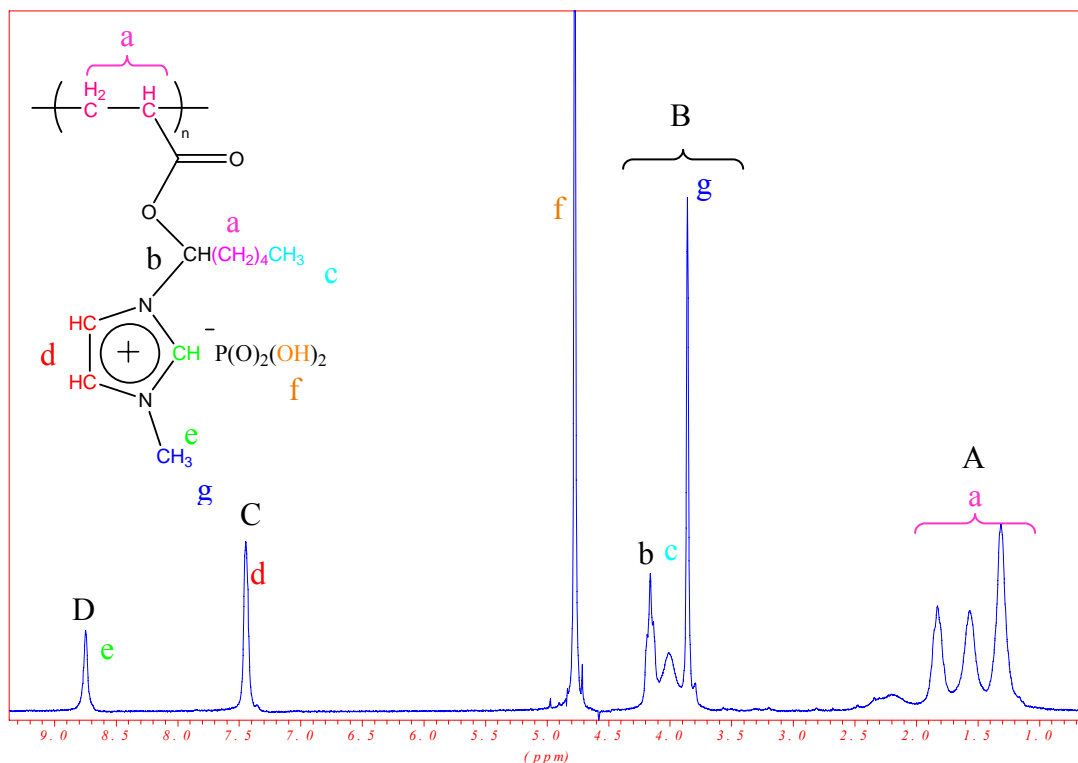


**Figure 7.4**  $^1\text{H}$ -NMR spectra of Poly(AcIm-6) in  $\text{D}_2\text{O}$ .

In Figure 7.5, different protons can be identified, and by the help of DQ filtered experiments mobile sites can be separated from the relatively rigid protons. In the one dimensional  $^1\text{H}$  DQ filtered MAS spectrum of Poly(AcIm-2) recorded at room temperature, all peaks observed in the  $^1\text{H}$ -MAS spectra are present, which means all protons have strong dipolar couplings on the timescale of one rotor period (66.6  $\mu\text{s}$ , 29762 kHz spinning frequency). Only peak around 1 ppm disappeared from the backbone region which was assigned to a mobile backbone species for Poly(AcIm-2).

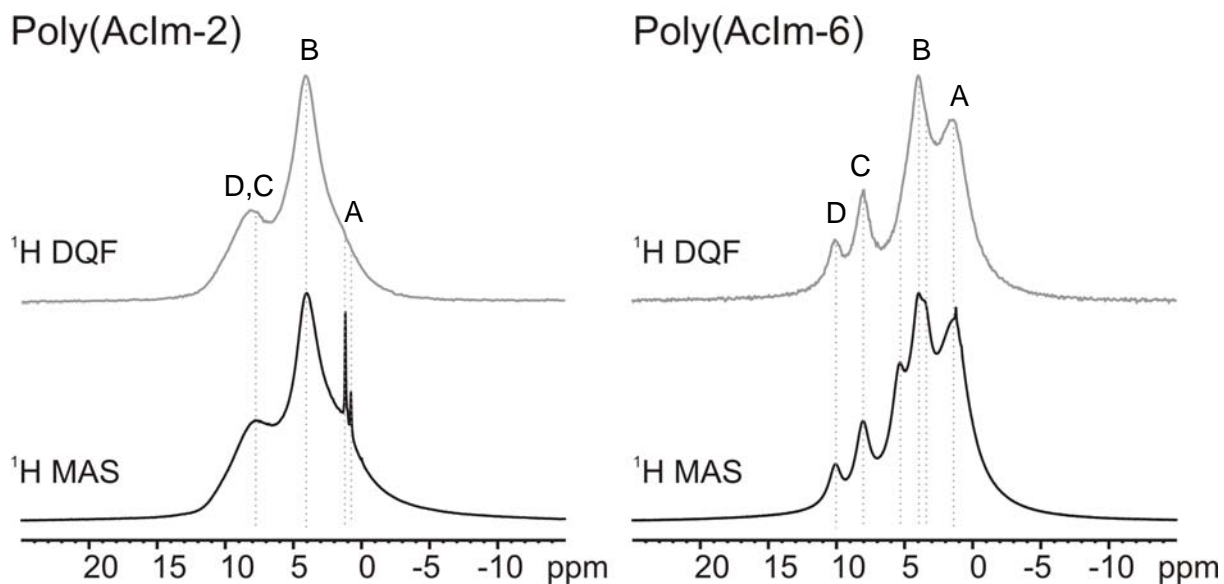


**Figure 7.5**  $^1\text{H}$  MAS and DQF MAS NMR spectra of Poly (AcIm-2) and Poly (AcIm-6) at room temperature and at 30 kHz MAS speed. The DQF spectra were recorded using BaBa dipolar recoupling pulse sequence with  $1 t_R$  excitation-reconversion time.

Although, the protons of the backbone of Poly(AcIm-6) are mobile, there is no change in this region. This might result from the overlapping of these protons with other  $-\text{CH}_2$  protons from the side chains (Figure 7.5). The disappeared peak around 6 ppm is due to the O-H protons from the  $\text{H}_2\text{PO}_4^-$  species. In addition to this, a shoulder disappeared around 4 ppm. This can be assigned to residual water since the sample is very hygroscopic. This is expected because the water molecule is highly mobile (Figure 7.6). In both cases, despite the mobility increase because of increased ring dynamics which provides spectral resolution between the two aromatic  $^1\text{H}$  sites, the dipolar coupling is still sufficient to give signal.

### 7.3.2 $^1\text{H}$ -MAS Variable Temperature Studies and Correlation to Conductivity

To investigate the effect of temperature has the current system and for having a deeper insight into the mobility of the proton species, variable temperature (VT) studies were carried out in the temperature range of 298K - 400K (In here the effect of frictional heating because of high spinning speeds around 30 kHz should also be considered, which normally corresponds to an up shift in temperature about  $\sim 20$  degrees compared to the temperatures values given). From the variable temperature  $^1\text{H}$ -MAS experiment, the mobility increase can be monitored by the obvious line narrowing. The VT  $^1\text{H}$  NMR spectra of Poly(AcIm-2) and Poly(AcIm-6) are shown in Figures 7.6-7.7. As expected, a continuous narrowing of the resonance lines is observed as the temperature is increased. The final width of the peaks in sample Poly(AcIm-6) is less than the peaks of Poly(AcIm-2), because of the  $T_g$  effect.

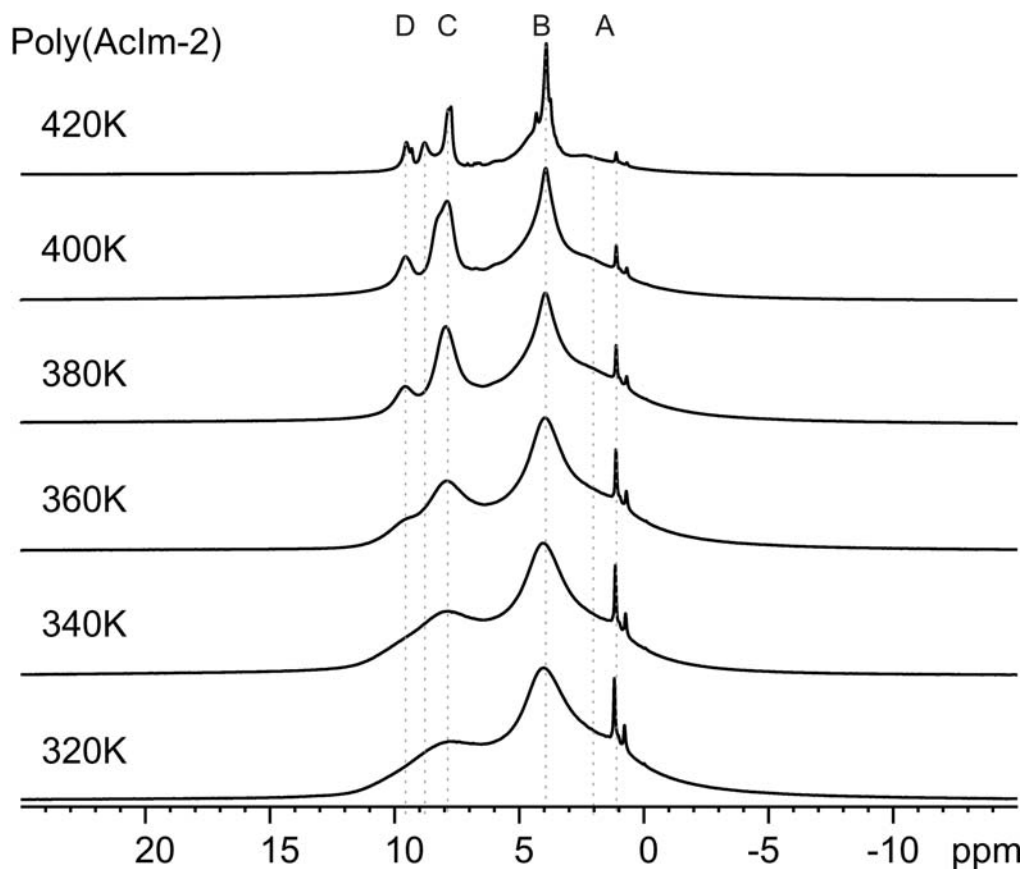


**Figure 7.6** Variable temperature  $^1\text{H}$  MAS NMR spectra of Poly (AcIm-2). The spectra recorded at 30 kHz MAS frequency and at 700 MHz  $^1\text{H}$  Larmor frequency.

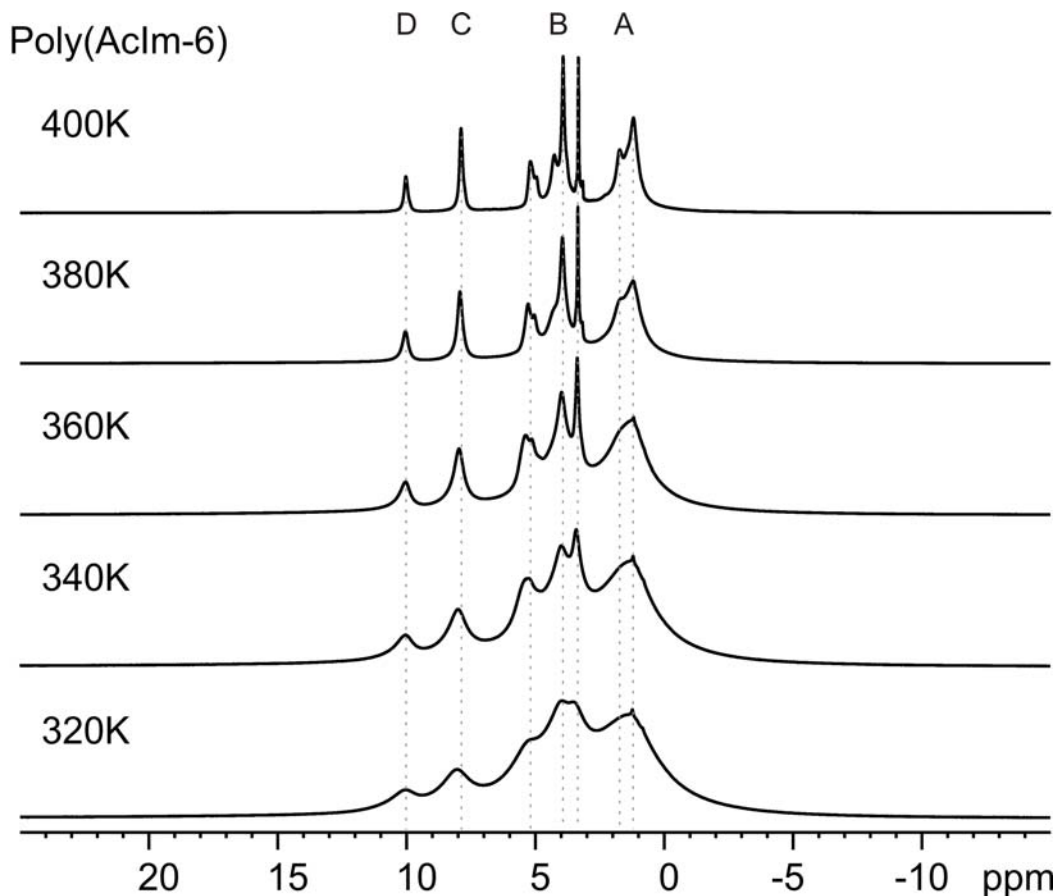


**Figure 7.7** Variable temperature  $^1\text{H}$  MAS NMR spectra of Poly (AcIm-6). The spectra recorded at 30 kHz MAS frequency and at 700 MHz  $^1\text{H}$  Larmor frequency.

The activation energy for the proton motion was determined from the variable temperature  $^1\text{H}$  MAS NMR spectra performed in the temperature range of 320-420 K. The line narrowing is a direct measure of proton mobility and by plotting linewidth against temperature one can obtain activation energy for that specific proton site in the fast exchange limit [Harris 83, Lee 07]. The change of linewidths with temperature is plotted in the proper way in Figure 7.8, to get the activation energy values 10 ppm (acidic  $-\text{OH}$  proton) and 8 ppm (ring  $-\text{CH}$  proton) resonances, respectively. These protons are from the positively charged ring which is attached to the  $\text{H}_2\text{PO}_4^-$  ion. The activation energy for the acidic  $-\text{OH}$  proton motion is smaller compared to the values reported for pure PVPA materials by Lee et. al. This represents the easiness of proton conduction in the current system.

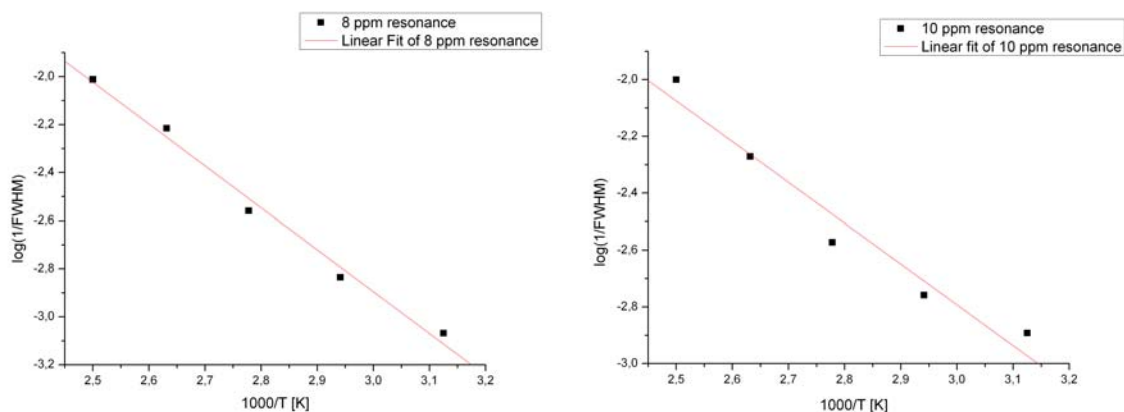


**Figure 7.8** Plots of  $1/\text{linewidths}$  ( $1/\text{FWHM}$ ), of the proton linewidths for two different proton sites (8 ppm and 10 ppm resonances) for Poly (AcIm-2) as a function of temperature. Experimental data were fitted to the Arrhenius equation.

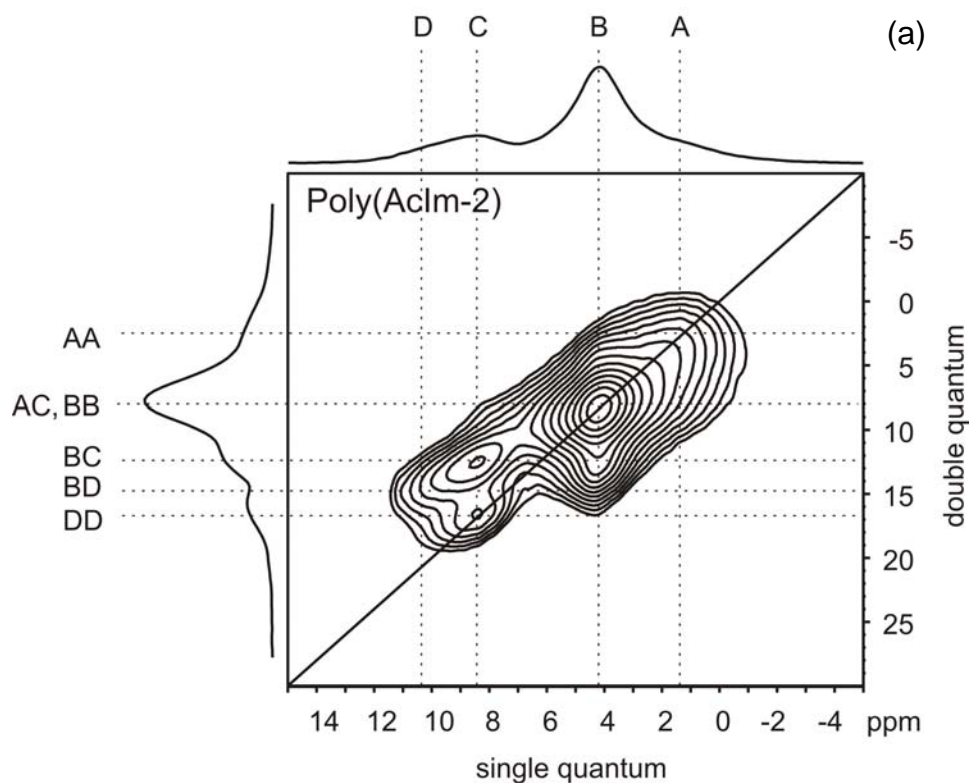
### 7. 3.3 2D $^1\text{H}$ - $^1\text{H}$ Double Quantum MAS Results

In order to determine the protons involved in the DQC, a 2D DQ spectrum is needed in which the  $^1\text{H}$  DQ dimension is correlated with the conventional  $^1\text{H}$  SQ dimension. The DQ frequency of a DQC is given by the sum of two  $^1\text{H}$  resonance frequencies involved. DQCs between similar spins give rise to the so called auto-peak located on the diagonal of the DQ spectra, while the DQCs between unlike spins give rise to pairs of cross-peaks symmetrically arranged on either side of the diagonal. The samples are examined at different temperatures and at different excitation times. In addition, one important point should be noted. An isolated  $^1\text{H}$  spin will not give a signal in 2D DQ NMR spectrum. The first point that must be clarified is the assignment of protons which are involved in DQC. The protons are assigned by the help of liquid NMR spectra as shown in previous Figures 7.3 and 7.4.

For Poly(AcIm-2) the proton signals of  $\text{CH}_2$ , CH (A), O-CH,  $\text{CH}_3$  (B), N-CH (C) and N-CH-N (D) can be distinguished (Figure 7.9a). Three auto peaks (A-A, A-B, B-B) are observed. The auto-peak A-A appears, because of the coupling of two aliphatic protons between these protons. The other peaks B-B which occurs because of the coupling of ring protons. Moreover the cross-peak show the interaction between these distinct protons (aliphatic and ring). These peaks must appear in the double-quantum dimension at a value

which is the sum of the single-quantum dimension values. A-type at 1 ppm, B-type at 4 ppm, C-type at 8.5 ppm and D-type at 10.5 ppm are the values in the single-quantum dimension. It is seen that there are three auto-peaks (A-A, B-B, D-D) and three cross-peaks (A-C, B-C, B-D). The cross-peaks are at 9, 12.5, 14.5 ppm which are assigned to A-C, B-C, B-D type interactions and they are at exactly double values in the double-quantum dimension.

For Poly(AcIm-6) four proton signals are observed which are assigned to CH<sub>2</sub> and CH (A), O-CH and CH<sub>3</sub> (B), N-CH (C) and N-CH-N (D) (Figure 7.9b). In this case, three auto-peaks and three cross-peaks appear in the DQ spectrum. The signals of A-B-C- and D-types protons located at around 1, 4, 8.5 and 10.5 ppm respectively. The cross-peaks are assigned to a DQC between the protons on the chain and on the ring. Double-quantum dimension values for cross-peaks are 9, 12.5 and 14.5 ppm which prove the A-C, B-C and B-D types of interactions, respectively.



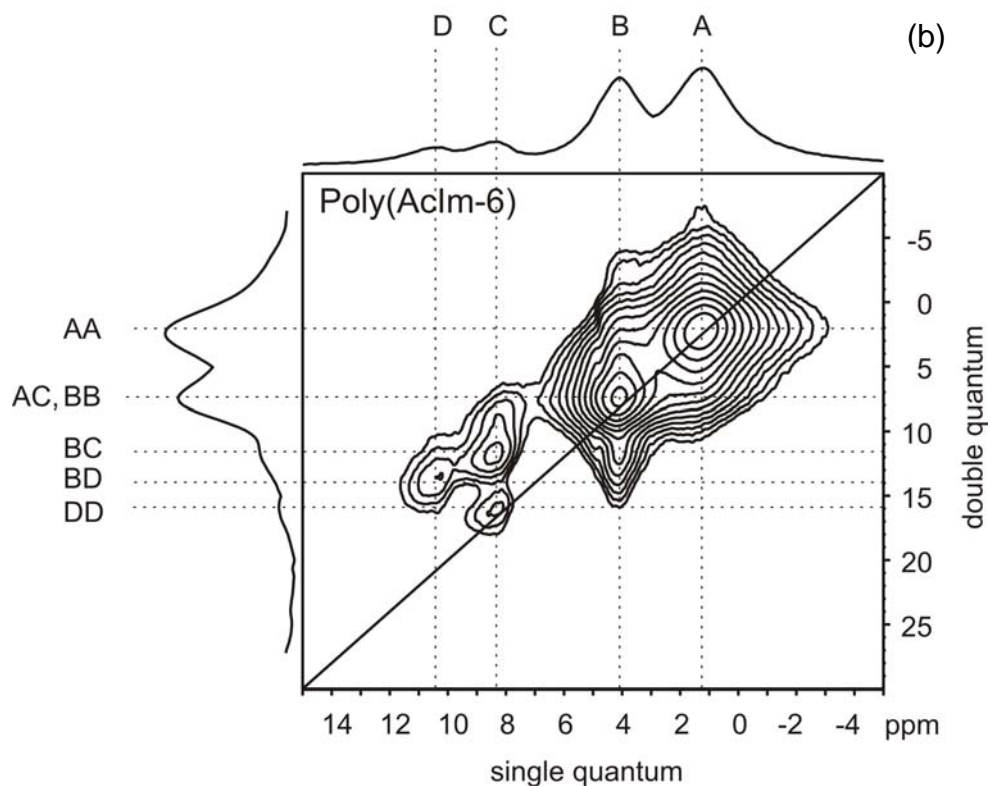


**Figure 7.9** 2D DQ  $^1\text{H}$ -MAS NMR spectra of (a) Poly (AcIm-2) and (b) Poly (AcIm-6) at room temperature and at 30 kHz MAS frequency.

The signal intensity and the resolution get worse for both samples by increasing excitation time, from  $1t_R$  ( $\sim 66 \mu\text{s}$ ) to  $4t_R$  ( $\sim 264 \mu\text{s}$ ). By increasing the excitation time the interference occurred between the timescales of polymer motion and the excitation, so the correlation time of polymer sites became less than the excitation time. As a result of this interference the spectral resolution drops.

### 7. 3.4 $^{31}\text{P}$ MAS NMR Results

The annealed samples are investigated with  $^{31}\text{P}$  CPMAS NMR methods to get an idea about the chemical structure of phosphorous groups in the system. To manage this CPMAS experiments done at 310K with 1ms contact time with a spinning speed of 15 kHz. The crosslinking ratio will be determined from the peak areas under phosphorous resonances corresponding to cross-linked and non-cross-linked P species.

From Figure 7.10, three different systems of Poly(AcIm-n) are shown. It can be realized that there are two resonances in each of three spectra. The non-crosslinked P species give resonance at 0 ppm, and crosslinked P species give a resonance at -11 ppm. The amount of crosslinked phosphoric acid is determined by integration of the resonance at -11 ppm. These amounts are shown in the Figure 7.10. There might be some error in these values because of the usage of CPMAS technique instead of more quantitative one-pulse approach. However, the very poor signal-to-noise ratio of the samples forced us to perform cross-polarization experiments, in which much more scans is possible because of delay time advantages. These values may give a general idea of the crosslinking ratio in the samples. One should keep in mind that, the crosslinking ratio might be more than these ratios, because of the usage of CPMAS method. After the crosslinking, the amount of proton around phosphorous decrease from two to one, which will cause a less efficient polarization transfer, and because of these effect the peak intensity at -11 ppm might be less than it actually is. One remarkable observation is that, from n=2 sample to n=6 sample, the ratio of crosslinking increased from %9 to %13. It is known that the side chain mobility increases with n resulting lower  $T_g$  in polymers. This might be reason of increase in crosslinking since the probability of meeting the groups causing condensation increases as well.



## Annealed Poly(AcIm-n) Samples

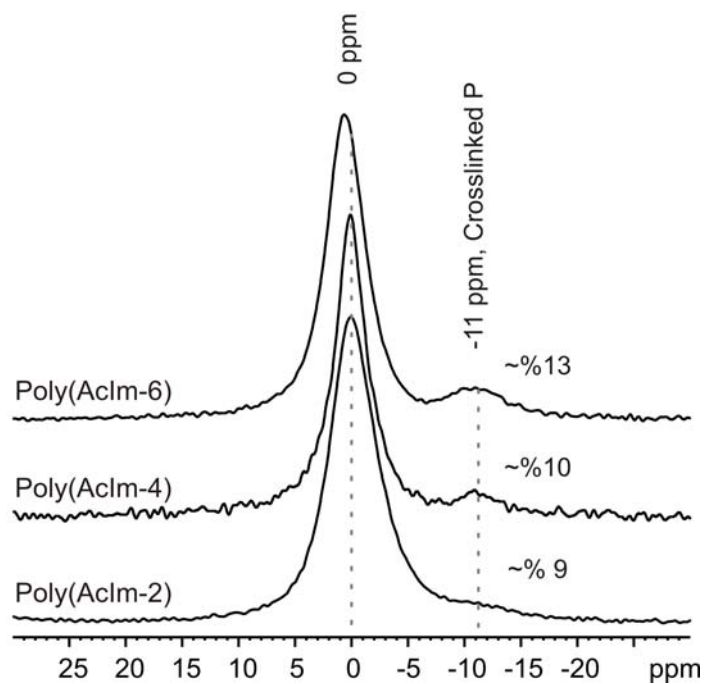


**Figure 7.10**  $^{31}\text{P}$  CPMAS spectra of Annealed Poly(AcIm-2), Poly(AcIm-4), and Poly(AcIm-6) recorded at 310 K with 1 ms contact time and at 15 kHz MAS spinning speed.

## 8. Conclusion

The main focus of this thesis is to synthesize and characterize anhydrous proton-conducting polymer electrolytes which composed of imidazolium moieties tethered to a polymer backbone and polymer electrolytes based on imidazolium ionenes for being used in fuel cells and lithium batteries.

The R-R'-Imidazolium type of ionic liquids with different counter ions were synthesized as model compounds. The water content in these samples was determined by the Karl-Fischer titration method. AcIm-n-X kinds of macromonomers were synthesized as precursor, where X is Cl<sup>-</sup> or Br<sup>-</sup>. These monomers were used to synthesize the materials based on imidazolium salt containing acrylic polymers. Free-radical polymerization was carried out using Azo(isobutyroic acid amidine)dihydrochloride (AIBA) as initiator.

Imidazolium salt containing acrylic polymers may present advanced properties for proton conduction. However, the condensation of H<sub>2</sub>PO<sub>4</sub><sup>-</sup> and H<sub>3</sub>PO<sub>4</sub> moieties restricts the use of these electrolytes at high temperatures. The chemical structure of the electrolytes obtained by the described synthetic routes was investigated by NMR-spectroscopy. The blends of the materials have been prepared by doping poly(AcIm-n) and poly(AcIm-n-Li) with various amounts of phosphoric acid (H<sub>3</sub>PO<sub>4</sub>) and lithium trifluoromethanesulfonimide (LiN(SO<sub>2</sub>CF<sub>3</sub>)<sub>2</sub>), to obtain poly(AcIm-n) x H<sub>3</sub>PO<sub>4</sub> and poly(AcIm-2-Li) x LiN(SO<sub>2</sub>CF<sub>3</sub>)<sub>2</sub>, where x is the number of moles of H<sub>3</sub>PO<sub>4</sub> and LiN(SO<sub>2</sub>CF<sub>3</sub>)<sub>2</sub> per polymer repeat unit.

The thermal properties of the electrolytes were investigated by TG. It illustrates that both electrolytes and their blends with H<sub>3</sub>PO<sub>4</sub> are thermally stable up to around 200 °C. DSC data reveal that the T<sub>g</sub>'s of the electrolytes decrease with increasing side chain length and blend ratio which results in the plasticization of the materials. The condensation of H<sub>2</sub>PO<sub>4</sub><sup>-</sup> moieties around 150 °C in the polymer electrolytes prevents the performance for high temperature applications above 200 °C.

The liquid like nature of the materials above T<sub>g</sub> was proved by Dynamic mechanical analysis (DMA) experiments. It can be also seen from the change in G' and η that the materials start to crosslink around 150 °C which may improve the mechanical properties to be used as membrane materials in fuel cells.

Furthermore, the properties related to the application of materials as membrane in fuel cells were investigated. The proton conductivity of the samples was studied in the temperature regime from -10 to 150 °C. Although, it was not examined above 150°C, it is known that condensation of the  $\text{H}_2\text{PO}_4^-$  and  $\text{H}_3\text{PO}_4$  moieties lead to cross-linking of the electrolytes which affects the proton conductivity.

The conductivities of poly(AcIm- $n$ )  $\times$   $\text{H}_3\text{PO}_4$  have been compared. The conductivity of the sample increases significantly with acid concentration reaching to about  $10^{-2} \text{ S}\cdot\text{cm}^{-1}$  at 120 °C for  $x=2$ . At the same temperature and the same acid concentration, the membrane composed of  $n=6$  has the higher conductivity. As the chain length ( $n$ ) increases  $T_g$  shifts to lower temperatures indicating an enhancement of the segmental motions. The proton conductivities of all electrolytes show VTF behavior with the glass transition temperature and blend amount of the amorphous materials being the dominant parameters. Accordingly, highest proton conductivities are observed for the structures with  $x=2$ .

The Li-ion conductivity of poly(AcIm-2-Li)  $\times$   $\text{LiN}(\text{SO}_2\text{CF}_3)_2$  was studied. It was observed that the ionic conductivity increases with blends up to certain composition and then leveled off independently from blend content.

Solid state  $^1\text{H}$  NMR measurements were carried out to obtain information about hydrogen bonding in solids. The hydrogen-bonding interactions play an important role in determining the properties of a range of materials particularly for the changes in glass transition temperatures and it is a crucial precondition for  $\text{H}^+$  transport in our membranes. Magic-angle spinning (MAS) and double-quantum (DQ)  $^1\text{H}$  NMR methods provide additional information on the hydrogen bonding. Comparison of  $^1\text{H}$  MAS NMR spectra of poly(AcIm-2) and poly(AcIm-6) demonstrates the significant differences in the resolution of specific sites which is mainly because of the differences in the  $T_g$  values of the polymer systems. The low  $T_g$  enhances molecular mobility and this leads to better resolved resonances in both the backbone region and side chain region. The mobile and immobile protons can be distinguished by comparing  $^1\text{H}$  MAS and  $^1\text{H}$ -DQF NMR spectra. The peaks of the mobile protons which are from backbones and from  $\text{H}_2\text{PO}_4^-$  disappeared in  $^1\text{H}$ -DQF NMR spectra. The interaction of the protons which may contribute to the conductivity is observed from the 2D double quantum correlation

(DQC) spectra. The cross-linking of poly(AcIm-n) are confirmed by  $^{31}\text{P}$  CPMAS NMR spectra. The cross-linking ratio was determined from the peak areas under phosphorous resonances corresponding to cross-linked and non-cross-linked P species.

The PFG-NMR diffusion measurements may be performed to obtain the proton self-diffusion coefficients in order to understand proton diffusion behavior of these electrolytes. The development of the proton conducting polymers is still in the state of basic research rather than close to application. In order to use these electrolytes as a proton exchange membrane in fuel cells, the conductivity of the polymer should be improved since  $10^{-2}$  S/cm is the minimum conductivity at room temperature that is required by the industry. Their thermal, mechanical and proton-conducting properties need to be improved for being used at higher temperatures. However, imidazolium based polymer-bound proton solvents seem still promising. The new ways of immobilizing these imidazolium salts as proton solvents remains challenging.

---

## 9. References

- [Acheson 76] Acheson R.M. *An introduction to the chemistry of heterocyclic compounds*. 3rd ed. Canada: Wiley (1976)
- [Aharoni 79] Aharoni S.M., Signorelli A.J., *J. Appl Polym. Sci.* 23(9) (1979) 2653–60
- [Almond 84] Almond D.P., Hunter C.C., West A.R., *J. Material Science* 19 (1984) 3236-3248
- [Angell 92] Angell, Annual. Rev. Phys. Chem. 43 (1992) 693-717
- [Angell 93] Angell C.A., Liu C., Sanchez E., *Nature* 362 (1993) 137.
- [Armand 78] Armand M.B., Chabagno J.M., Duclot M.J., Abstracts of Papers, “*Second International Meeting on Solid Electrolytes*”, St. Andrews, Scotland, 1978.
- [Armand 79] Armand M.B., Chabagno J.M., Duclot M.J., in: P. Vashishta, J.N. Mundy, G.K. Shenoy (Eds.), *Proc. Int. Conf. on Fast Ion Transport in Solids Electrodes and Electrolytes*, North-Holland, New York, 1979.
- [Armand 86] Armand M.B., *Ann. Rev. Mater. Sci.* 16 (1986) 245.
- [Bingöl 07] Bingöl B., thesis. (2007) Univ. Mainz, Germany, (<http://ubm.opus.hbz-nrw.de/volltexte/2007/1266/pdf/diss.pdf>)
- [Blythe 79] Blythe A.R; *Electrical Properties of Polymers*; Cambridge University Press, Cambridge 1979
- [Bonhôte 96] Bonhôte P., Dias A.-P., Papageorgiou N., Kalyanasundaram K., Grätzel M. *Inorg. Chem.* 35 (1996) 1168-1178
- [Bozkurt 99] Bozkurt A., Ise M., Kreuer K.D., Meyer W.H., Wegner G., *Solid State Ionics*, Vol. 125, (1999) 225-233
- [Bozkurt 03] Bozkurt A., Meyer W.H., Wegner G., *J. Power Sources* 123 (2003) 126-131
- [Brown 01] Brown S. P, Spiess H.W., *Chem. Rev.* 101 (2001) 4125-4155
- [Brunet 97] Brunet P., Simard M., Wuest J. D., *J. Am. Chem. Soc.* 1997, 119,2737

- [Castellan 83] Castellan G.W., *Physical Chemistry* Addison-Wesley Publishing Company London (1983)
- [Castellano 98] Castellano R. K., Rebek J., Jr., *J. Am. Chem. Soc.* 1998, 120, 3657
- [Chen 92] Chen R., Yang R., Durand B., Pradel A., Ribes M., *Solid State Ionics* 53-56 (1992)
- [Chowdari 87] Chowdari, Gopalakrishnan R., *Solid State Ionics* 23 (1987) 225-233
- [Cohen 59] Cohen, Turnbull D., *J.Chem. Phys.*, 31 (1959) 1164
- [Costa 07] Costa L. T., Lavall R. L., Borges R. S., Rieumont J., Silva G. G., Ribeiro M.C.C., *Electrochimica Acta* 53 (2007) 1568–1574
- [Craver 83] Craver, C. D., *Polymer Characterization*, Ch. 12, American Chemical Society, 1983.
- [DeCastro 00] DeCastro C., Sauvage E., Valkenberg M. H. and Hölderich W. F., *J. Catalysis* 196, (2000) 86-94
- [Dell 00] Dell R.M., *Solid State Ionics* 134 (2000) 139
- [Dias 00] Dias F.B., Plomp L., Veldhuis J.B.z., *J. Power Sources* 88 (2000) 169.
- [Dippel 91] Dippel Th. and Kreuer K.D. *Solid State Ionics* 46 (1991) 3.
- [Dippel 93] Dippel Th., Kreuer K.D., J.C. Lassègues, Rodriguez D., *Solid State Ionics* 61 (1993) 41-46
- [Doolittle 51] Doolittle, *J. Appl. Phys.* 22 (1951) 1471
- [Dominguez 88] Dominguez L., Meyer W.H., *Solid State Ionics* 28-30 (1988) 941-949
- [Donoso 98] Donoso P., Gorecki W., Berthier C., Defendini F., Poinignon C., Armand M.B., *Solid State Ionics* 28 (1998) 969-74
- [Doyle 00] Doyle M., Choi S. K. and Proulx G., *J. Electrochem. Soc.*, 147 (2000) 34

- [Dupont 02] Dupont J., de Souza R.F., Syarez P.A.Z, *Chem. Rev.* 102 (2002) 3667
- [Dygas 03] Dygas J.R., Mistal-Faraj B., Florjanczyk Z., Krok F., Marzantowicz M., Zygadlo-Monikowska E., *Solid State Ionis* 157 (2003) 249
- [Dyre 91] Dyre J., *J. Non-Cryst. Solids* 135(1991) 219
- [Dzyuba 01] Dzyuba S.V., Bartsch R.A., *Chem. Comm.* 16 (2001) 1466–1467.
- [Erdemi 04] Erdemi H., Bozkurt A., Meyer W.H., *Synthetic Metals* 143 (2004) 133-38
- [Every 00] Every H., Bishop A.G., Forsyth M., MacFarlane D.R., *Electrochimica Acta* 45 (2000) 1279-1284
- [Fenton 73] Fenton D.E., Parker J.M., Wright P.V., “Complexes of Alkali Aetal Ions with poly(ethylene oxide)”, *Polymer* 14 (1973) 589.
- [Fischer 58] Fischer L., Winkler G., Jander G., *Z. Elektrochem.* 62 (1958) 1
- [Frankfurter 03] Frankfurter Allgemeine Zeitung; Frankfurt; 19/8/2003
- [Fuller 99] Fuller J., and Carlin R. T., *Electrochem. Soc. Proc.*, 41 (1999) 27
- [Fung 93] Fung Y.S., Chau S.M., *J. Appl. Electrochem.* 23 (1993) 346
- [Garcia 04] Garcia B., Lavallee S., Perron G., Michot C., Armand M., *Electrochim. Acta* 49 (2004) 4583.
- [Gelus 68] Gelus M., Bonnier J.M., *J. Chim. Phys. Phys. Chim. Biol.* 65 (2) (1968) 253-259
- [Gieselman 92] Gieselman M.B., Reynolds J.R., *Macromolecules* 25 (1992) 4832.
- [Goward 02] Goward G.R., Schuster M.F.H., Sebastiani D., Schnell I., Spiess, H.W.J. *Phys. Chem. B*; 106(36) (2002) 9322-9334
- [Gray 91] Gray FM., *Solid Polymer Electrolytes-Fundamentals and Technological Applications*. VCH, New York, 1991.
- [Gray 97] Gray F.M., *Polymer electrolytes*, RSC materials monographs. Cambridge: The Royal Society of Chemistry; 1997.

- [Grondin 95] Grondin J., Rodriguez D., Lassegues J. C., *Solid State Ionics*, 77 (1995) 70-75
- [Guo 99] Guo Q., Pintauro P.N., Tang H., O'Connor S., *J. Membr. Sci.* 154 (1999) 175
- [Harris 83] Harris R. K., Nuclear Magnetic Resonance Spectroscopy, Pitman, London, 1983
- [Hartmann 62] Hartmann S.R., Hahn E.L., "Nuclear Double Resonance in the Rotating Frame" *Phys. Rev.* 128 (1962) 2042.
- [Havriliak 67] Havriliak S., Negami S., *Polymer* 8 (1967) 161-201
- [Havriliak 96] Havriliak S., Negami S., *J. Polymer Science Part C* 14 (1996) 99-103
- [Hayamizu 00] Hayamizu K., Aihara Y., *Electrochimica Acta* 49 (20) (2000) 3397-402
- [Herz 03] Herz H.G., Kreuer K.D., Maier J., Scharfenberger G., Schuster M.F.H. Meyer W.H., *Electrochim. Acta* 48 (2003) 2165-2171
- [Hirao 00] Hirao M., Ito-Akita K. and Ohno H., *Polym. Adv. Technol.* 11 (2000) 534 -538
- [Hirao 00] Hirao M., Ito K. and Ohno H., *Electrochimica Acta* 45 (2000) 1291-1294
- [Hogarth 01] Hogarth M., Glipa X., in *High Temperature Membranes for Solid Polymer Cells*, Johnson Matthey Technology Centre, (2001)
- [Holbrey 99] Holbrey J.D., Seddon K.R., *J. Chem. Soc., Dalton Trans.* (1999) 2133-2139
- [Honma 99] Honma I. , Hirakawa S., Yamada K., Bae J.M., *Solid State Ionics*, 118, (1999) 29-36
- [Hughes 04] Hughes C.E., Haufe S., Angerstein B., Kalim R., Ma1hr U., Reiche A., and Baldus M., *J. Phys. Chem. B*, 108 (2004) 13626-13631



- [Hussey 88] Hussey C.L., *Pure Appl. Chem.*, 60 (1988) 1763-1772.
- [Hussey 90] Hussey C.L., Sun I.W., Strunbinger S.K., Barnard P.A., *J. Electrochem. Soc.* 137 (1990) 2515
- [Ito 00] Ito K., Nishina N., Ohno H., *Electrochimica Acta* 45 (2000) 1295-1298
- [Jiang 99] Jiang D.D., Yao Q., McKinney M.A., Wilkie, C.A., *Polymer Degradation and Stability*, 63 (1999)423-434
- [Kerres 96] Kerres J., Cui W., Reichle S., *J. Polym. Sci. Part A Polym. Chem.* 34 (1996) 2421
- [Kerres 01] Kerres J.A., *J. Membrane Sci.* 185 (2001) 3
- [Kim 04] Kim D. W. And Chi D. Y., *Angew. Chem. Int. Ed.* 43 (2004) 483-485
- [Kirsche 94] Kirsche K. In *Methoden der organischen Chemie (Houben-Weyl)* ed. E. Schaumann E8b:401, Stuttgart/New York: Thieme (1994)
- [Kremer 02] Kremer F. and Schönhals, A. "*Broadband Dielectric Spectroscopy*" Springer, Berlin (2002).
- [Kremer 89] Kremer F., Dominguez L., Meyer W.H., Wegner G., *Polymer* 30 (1989) 2023.
- [Kreuer 82] Kreuer K.D., Rabenau A. and Wegner G., *Angew. Chem. Int. Edt. Engl.*, 21 (1982) 208
- [Kreuer 96] Kreuer K. D., *Chem. Mater.* 8 (3) (1996) 610-41
- [Kreuer 98] Kreuer K. D., Fuchs A., Ise M., Spaeth M. and Maier J., *Electrochimica Acta*, Vol. 43, Iss. 10-11, (1998) 1288
- [Kreuer 99] Kreuer K.D., In *Solid State Ionics: Science&Technology*, ed.BVRChowdari, Singapore: World Scientific, (1999) 263–74
- [Kreuer 01] Kreuer K.D., *J. Membrane Sci.*185 (2001) 29–39
- [Kreuer 02] Kreuer K.D., *Chem. Phys. Chem.* 3 (2002) 771

- [Ku 87] Ku, C.C. and Liepins, R. “*Electrical Properties of Polymers*” Hanser, München (1987)
- [Lee 07] Lee Y. J., Bingöl B., Murakhtina T., Sebastiani D., Meyer W. M., Wegner G., Spiess H. W., *J. Phys. Chem. B* 111 (2007) 9711.
- [Li 03] Li Q., He R., Jensen J.O., Bjerrum N.J., *Chem. Mater.* 15 (2003) 4896
- [MacCallum 87<sup>1</sup>] MacCallum J.R., Vincent C.A., *Polymer Electrolytes Reviews—I*, Elsevier. London, 1987.
- [MacCallum 87<sup>2</sup>] MacCallum J.R., Vincent C.A., *Polymer Electrolytes Reviews—II*, Elsevier. London, 1987.
- [MacDonald 74] MacDonald J.R., *The Journal of Chemical Physics*, 61 (1974) 3977-3996
- [MacFarlane 99] MacFarlane D.R., Huang J., Forsyth M., *Nature* 402 (1999) 792.
- [Marcilla 04] Marcilla R., Blazquez J. A., Rodriguez J., Pomposo J. A., Mecerreyes D., *J. Polym. Sci.: Part A: Polym. Chem.*, 42 (2004) 208–212
- [McCrum 91] McCrum, N.G., Read, B.E., Williams, G., *Anelastic and Dielectric Effects in Polymeric Solids*, Dover, New York, 1991.
- [Mehnert 02] Mehnert C. P., R. Cook A., Dispenziere N. C., and Afeworki M., *J. Am. Chem. Soc.* 124 (2002) 12932 – 12933.
- [Mehring 83] Mehring M., *Principles of High-Resolution NMR in Solids*; Springer: Berlin, 1983.
- [Meyer 98] Meyer W. H., *Adv. Mater.* 10 (1998) 439- 448
- [Ngo 00] Ngo H. L, LeCompte K., Hargens L. and McEwen A. B., *Thermochim. Acta*, 357 (2000) 97-102
- [Noda 03] Noda A., Susan Md.A.B.H., Kudo K. Mitsushima S., Hayamizu K. Watanabe M., *J. Phys. Chemistry B* 107 (2003) 4024-4033
- [Noda 01] Noda A., Hayamizu K., Watanabe M., *J. Phys. Chem. B* 105 (2001) 4603

- [Ogawa 01] Ogawa K., Wang B., and Kokufuta E., *Langmuir* 17 (2001) 4704-4707
- [Ohno 04] Ohno H., Yoshizawa M., Ogihara W., *Electrochim. Acta* 50 (2004) 255
- [Ohno 02] Ohno H., Yoshizawa M., *Solid State Ionics* 154-155 (2002) 303-309
- [Papageorgiou 96] Papageorgiou N., Athanassov Y., Armand M., Bonhote P., Petterson H., A. Azam, Gratzel M., *J. Electrochem. Soc.* 143 (1996) 3009.
- [Pettersson 06] Pettersson J., Ramsey B., Harrison D., *J. Power Sources* 157 (2006) 28–34
- [Petty-Week 88] Petty-Week S., Zupancic J.J., Swedo J.R., *Solid State Ionics* 31 (1988) 117-125
- [Pines 73] Pines A., Gibby M.G., Waugh J.S., *J. Chem. Phys.* 59 (1973) 569-90
- [Pohl 64] Pohl H.A., Chartoff R.P., *J. Polym. Sci. Polym. Chem.* 2(6) (1964) 2787–806
- [Polak 86] Polak A.J., Petty-Weeks S., Beuhler A.J., *Sensors and Actuators* 9 (1986) 1-7
- [Przyluski 93] Przyluski J., Dabrowska A., Stys S., Wieczorec W., *Solid State Ionics*, 60 (1993) 141-46.
- [Pu 01] Pu H.T., Meyer W.H., Wegner G., *Macromol Chem. Phys.* 202(9) (2001) 1478–82
- [Pu 02] Pu H.T., Meyer W.H., Wegner G., *J. Polym. Sci.: Part B: Polym. Phys.* 40 (2002) 663-69
- [Ratner 87] Ratner M A., in *Polymer Electrolyte Reviews* (Ed.: J.R. Mac Cullum), Elsevier, New York **1987**.
- [Ratner 88] Ratner M.A., Shriver D.F., *Chem. Rev.* 88 (1988) 109
- [Ratner 92] Ratner M.A., Nitzan A., *Faraday Discuss. Chm. Soc.* 88 (1992) 693-717

- [Reicha 91] Reicha F.M., El-Hiti M., El-Sonabati A.Z., Diab M.A., *J. Phys. D: Appl. Phys.* 24, (1991) 369
- [Reisinger <sup>1</sup>] Reisinger T., Meyer W.H., Wegner G., Haase T., Schultes K. and Wolf B.A., *Acta Polym.* 49 (1998) 710 – 714
- [Reisinger <sup>2</sup>] Reisinger T.J.G., Scholl H.U., Meyer W.H., Wegner G., *Chem.Phys. Letter* 283 (1-2) (1998) 15-20
- [Ren 96] Ren X., Wilson M.S., Gottesfeld S., *J. Electrochem. Soc.* 143, L12 (1996).
- [Rietz 93] Rietz Ralf-R., Meyer W.H., *Polymer for Advanced Technologies* 4 (1993) 164-171
- [Rietz 94] Rietz Ralf-R., Rohr K.S., Meyer W.H., Spiss H.W., Wegner G., *Solid State Ionics* 68 (1994)
- [Rodriguez 93] Rodriguez D., Jegat C., Trinquet O., Grondin J., Lassegues J.C., *Solid State Ionics*, 61 (1193) 195-202
- [Schaefer 76] Schaefer J. and Stejskal E. O., *J. Am. Chem. Soc.* 98 (1976) 1031.
- [Scherer 90] Scherer G. G., Bunsenges Ber., *Phy. Chem.* 94 (1990) 1008-1014
- [Sharma 00] Sharma S. K., Tandon M., Lown J. W., *J. Org. Chem.* 65 (2000) 1102.
- [Schlick 96] Schlick S., *Ionomers: Characterization, Theory and Applications*; CRC Press: Boca Raton, FL, 1996.
- [Schnell 98] Schnell I, Brown S. P, Lee H. L, Ishida H, Spiess H. W, *JACS* 120 (1998) 11784-11795
- [Schuster 01] Schuster M., Meyer W.H., Wegner G., Herz H.G., Ise M., Schuster M., Kreuer K.D., Maier J., *Solid State Ionics* 145 (2001) 85–92
- [Schuster 02] Schuster M.F.H., PhD thesis. (2002) Univ. Mainz, Germany. 127 pp. (<http://ubm.opus.hbz-nrw.de/volltexte/2002/257/pdf/diss.pdf>)
- [Schuster 03] Schuster M.F.H., Meyer W.H., *Annu. Rev. Mater. Res.* 33 (2003) 233-61

- [Schuster 04] Schuster M.F.H., Meyer W.H., Schuster M., Kreuer K.D., *Chem. of Mater.* 16 (2) (2004) 329-337
- [Scrosati 93] Scrosati B., *JEC Battery Newsletters*, 6, 44 (1993) 53.
- [Scrosati 93] Scrosati B., *Applications of Electroactive Polymers*, Chapman&Hall, London,1993.
- [Shobukawa 04] Shobukawa H., Tokuda H., Tabata S., Watanabe M., *Electrochim. Acta* 50 (2004)305.
- [Shobukawa 05] Shobukawa H., Tokuda H., Susan M.A.H., Watanabe M., *Electrochim. Acta* 50 (19) (2005) 3872-3877.
- [Soczka-Guth 99] Soczka-Guth T., Baurmeister J., Frank G., Knauf R., International Patent WO 99/29763 (1999).
- [Souza 03] Souza R. F., Padilha J.C., Goncalves R.S., Dupont J., *Electrochemistry Communications* 5 (2003) 728-31
- [Stenger-Smith 02] Stenger-Smith J.D., Webber C.K., Anderson N., Chafin A.P., Zong K., Reynolds J.R., *J. Electrochem. Soc.* 149 (2002) A973.
- [Sugden 29] Sugden S., Wilkins H., *J. Chem. Soc.* (1929) 1291
- [Sun 01] Sun J., Jordan L.R., Forsyth M., MacFarlane D.R., *Electrochim. Acta* 46 (2001) 1703-08
- [Susan<sup>1</sup>] Susan Md.A.B.H., Yoo M., Nakamoto H., Watanabe M., *Chemistry Letters* 32 (9) (2003)
- [Susan<sup>2</sup>] Susan Md.A.B.H., Noda A., Mitsushima S., Watanabe M., *Chem. Commun.* 8 (2003) 938.
- [Tanaka 00] Tanaka R., Yamamoto H., Shono A., Kubo K., Sakurai M., *Electrochim. Acta* 45 (8-9) (2000) 1385-1389
- [Tang 05] Tang J., Tang H., Sun W., Radosz M., Shen Y., *J. Polym. Sci.: Part A: Polym. Chem.*, Vol. 43 (2005) 5477-5489
- [Tarascon 01] Tarascon J.-M., Armand M., *Nature* 414 (2001) 359

- [Tokuda 04] Tokuda H., Hayamizu K., Ishii K., Susan M.A.B.H., Watanabe M., *J. Phys. Chem. B* 108 (2004) 16593.
- [Vincent 87] Vincent C.A., *Prog. Solid State Chem.* 17 (1987) 145.
- [Vincent 00] Vincent C.A., *Solid State Ionics* 134 (2000) 159.
- [Visser 01] Visser A.E., Holbrey J.D., Rogers R.D., *Chem. Comm.* 23 (2001) 2484–2485
- [Vogel 26] Vogel, *Phy. Z.*, 22 (1921) 645, Tamman G., Hesse G., *Z. Anorg. Allgem. Chem.*, (1926) 245
- [Wainright 95] Wainright J.S., Wang J-T., Weng D., Savinell R.F., Litt M., *J. Electrochem Soc.* L121 (1995) 142
- [Wasssercheid 00] Wasssercheid P., Keim W., *Angew. Chem. Int. Ed.* 39 (2000) 3772-789
- [Wieczorec 95] Wieczorec W., Florjanczyk Z., Stevens J.R., *Electrochim. Acta* 40 (1995) 2327-2330
- [Walden 14] Walden P., *Bull. Acad. Imper. Sci. (St. Petersburg)* (1914) 1800.
- [Walker 99] Walker M., Baumgärtner K.M., Kaiser M., Kerres J., Ullrich A., Rächle E., *J. Appl. Polym. Sci.* 74, 67 (1999).
- [Wang 96] Wang J.-T., Savinell R.F., Wainright J.S., Litt M., Yu H., *Electrochimica Acta*, Vol. 41, (1996) 193-197
- [Wang 03] Wang P., Zakeeruddin S.M., Comte P., Exnar I., Gratzel M., *J. Am. Chem. Soc.* 125 (2003) 1166.
- [Washiro 04] Washiro S., Yoshizawa M, Nakajima H. and Ohno H., *Polymer* 45 (2004) 1577–1582
- [Wasserscheid 00] Wasserscheid P., Keim W., *Angew. Chem. Int. Ed.* 39 (2000) 3772.
- [Watanabe 88] Watanabe M., Ogata N., *Br. Polym. J.* 20 (1988) 181.
- [Watanabe 93] Watanabe M., Yamada S., Sanui K., Ogata N., *J. Chem. Soc. Chem. Commun.* (1993) 929.

- [Welton 99] Welton T., Chem. Rev. 99 (1999) 2071-2083
- [Wilkes 82] Wilkes J. S., Levisky J. A., Wilson R. A., Hussey C. L., *Inorg. Chem.* 21 (1982) 1263-1264.
- [Williams] Williams G., Thomas D.K., *Application Note Dielectrics 3*, Novocontrol
- [Williams 55] Williams J. Phys. Chem. 59 (1955) 95
- [Williams 79] Williams G., *Advance Polymer Science*,33 (1979) 60
- [Williams 94] Williams G., *Polymer*, 35 (1994) 1915
- [Wirasate 98] Wirasate S., Dhumrongvaraporn S., Allen D. J., Ishida H., *J. Appl. Polym. Sci.* (70) 7 (1998) 1299-1306
- [Wright 75] Wright P.V., *Br. Polymer J.* 7 (1975) 319
- [Wundlich 90] Wundlich B., *Thermal Analysis*, Ch.7, Academic Press, Inc., 1990.
- [Yang 01] Yang C., Costamagna, P., Srinivason S., Benziger J., and Bocarsly A. B., *J. Power Source* 103 (2001) 1
- [Yoshizawa 01] Yoshizawa M., Ohno H., *Electrochimica Acta* 46 (2001) 1723-1728
- [Yoshizawa 03] Yoshizawa M., Xu W. and Angell C. A., *J. Amer. Chem. Soc.* (125) 50 (2003) 15411-15419

## 10. Experimental

### Chemicals

All used chemicals were obtained from Aldrich, Fluka, Merck, Acros and Riedel de Haen with high purity. Acryloylchloride, N-Methylimidazole, 2-Bromethanol, 4-Chlorbutanol and 6-Chlorhexanol were distilled before use. Methylenechloride was dried over  $\text{CaH}_2$ . Tetrahydrofuran was dried over sodium metal. Anhydrous phosphoric acid (99.7 %) in crystalline form was obtained from Aldrich.

### Instrumentation and Procedure

Bruker 250 MHz spectrometer or Bruker AC 300 FT- spectrometer were used to performe Nuclear Magnetic Resonance (**NMR**) experiments. Small amounts (10 mg) of the purified samples were dissolved in suitable amounts (0.5-1.0 ml) of the solvent.

**TGA** Thermal stabilities of polymers and polymer blends were investigated by TGA Mettler TG 50. The measurements were done with a heat rate of  $10^\circ\text{C}/\text{min}$  under  $\text{N}_2$ .

**DSC** thermograms of polymers and polymer blends were obtained using Mettler DSC TA 3000 Scanning Calorimeters under dry nitrogen atmosphere. The samples were weighted (10-15 mg) and loaded into aluminum pans and cooled down to starting temperature. Then, temperature was increased to the desired temperature with a scan rate of  $10^\circ\text{C}/\text{min}$ . The second heating curves were evaluated for  $T_g$  investigations. Empty aluminum pans were used as a reference.

**Elemental analysis** have been performed by Analytical Laboratory of the Prof. Dr. H. Malissa & G.Reuter GmbH /Lindlar. Samples were dried prior to analysis.



Impedance measurements were obtained using the **dielectric spectrometry**. The AC measurements were carried out with SI1260 Analyser from Novocontrol dielectric spectrometer within the frequency range of  $10^{-2}$  Hz to  $10^7$  Hz and in the temperature regime from -30 to 150°C. The samples were placed between two Pt-coated steel plates and their conductivities were measured in the cooling cycle of 10°C intervals. The thickness of samples was determined with micrometer screw for films and with Teflon stripes, which have standard thickness, for viscous materials. The temperature change was controlled with a Novocontrol cryosystem with a precision of 0,01°C. The DC conductivities were obtained by linear fitting of the AC conductivities .

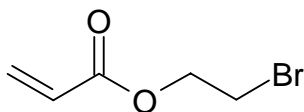
**Solid State NMR** experiments were done by Bruker Avance 500 and 700 spectrometers. Magic Angle Spinning (MAS) and Double Quantum (DQ) filtered experiments were done at different temperatures and frequencies.

**Dynamic mechanical studies** of Poly(AcIm-2) x H<sub>3</sub>PO<sub>4</sub> and Poly(AcIm-6) x H<sub>3</sub>PO<sub>4</sub> were studied with parallel plate rheometer RMS-800 with a cooling rate 2K/min and frequency 10rad/sec. The samples were hot pressed above their T<sub>g</sub> with the thickness ~1mm.

## Synthesis

Same procedure was used for all of the following 3 products : A mixture of bromoalcohol and triethylamine was dissolved in methylen chloride. 2,6-di-tert.butyl-4-methylphenol was used as inhibitor. Then acryloyl chloride was added slowly under dry N<sub>2</sub> atmosphere at 0°C. The mixture was refluxed for 12 h. CH<sub>2</sub>Cl<sub>2</sub> was then removed by rotavap. The remaining product was dissolved in diethylether and extracted firstly with saturated NaHCO<sub>3</sub> solution to neutralize the solution and then 3 times with water. Ether phase was collected and dried over MgSO<sub>4</sub>. Finally, the reaming organic solvent was removed by rotavap at 40°C to obtain orange liquid.

### 2-bromoethyl acrylate



30 g (240 mmol) bromoethanol

27.14 g (300 mmol) acryloyl chloride

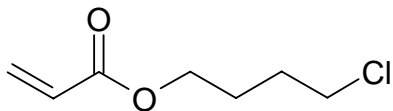
30.36 g (300 mmol) triethylamine

0.66 g (3 mmol) 2,6-di-tert.butyl-4-methylphenol

Yield : 81 % (34.68 g)

<sup>1</sup>H-NMR (CDCl<sub>3</sub>, 250 MHz) : δ = 6.12 (d of t, 3H, CH<sub>2</sub>=CH-), 4.43 (t, 2H,O-CH<sub>2</sub>-), 3.51(t, -CH<sub>2</sub>-Br) ppm

### 4-chlorobutyl acrylate



13.6 g (125 mmol) 4-chloro-1-butanol

17.02 g (188 mmol) acryloyl chloride

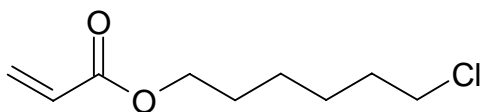
19.02 g (188 mmol) triethylamine

0.5 g (2.3 mmol) 2,6-di-tert.butyl-4-methylphenol

Yield : 71 % ( 14.43 g)

$^1\text{H-NMR}$  ( $\text{CDCl}_3$ , 250 MHz) :  $\delta$  = 6.09 (d of t, 3H,  $\text{CH}_2=\text{CH-}$ ), 4.15 (t, 2H,  $\text{O-CH}_2-$ ), 3.54 (t,  $-\text{CH}_2-\text{Cl}$ ), 1.80 (m, 4H,  $-\text{CH}_2\text{CH}_2-$ ) ppm

6-chlorohexyl acrylate



40 g (293 mmol) 6-chlor-1-hexanol

33.13 g (366 mmol) acryloylchloride

37.03 g (366 mmol) triethylamine

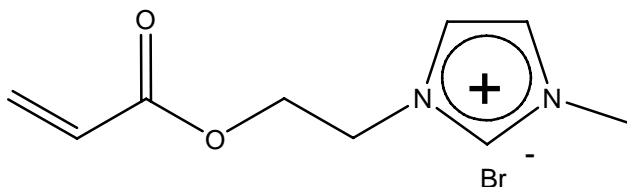
0.88 g (4 mmol) 2,6-di-tert.butyl-4-methylphenol

Yield : 85 % (17.9 g)

$^1\text{H-NMR}$  ( $\text{CDCl}_3$ , 250 MHz) :  $\delta$  = 6.08(d of t, 3H,  $\text{CH}_2=\text{CH-}$ ), 4.10 (t, 2H,  $\text{O-CH}_2-$ ), 3.48 (t,  $-\text{CH}_2-\text{Cl}$ ), 1.74-1.39 (3 m, 8H,  $-(\text{CH}_2)_4-$ ) ppm

The obtained liquid acrylates were mixed with N-Methyl imidazole, and the mixture was stirred for 3 days at 45°C. The mixtures were precipitated in diethyl ether to obtained a yellow viscous pure products.

## 1-methyl 3-(2-acryloyloxy ethyl) imidazolium bromide



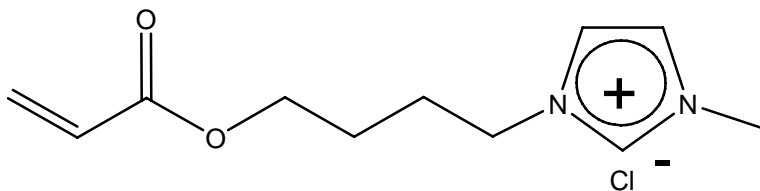
20 g (112 mmol) 2-Bromo-ethyl-acryl ester

9.2 g (112 mmol) N-Methylimidazole

Yield : 72 % (20.91 g)

$^1\text{H-NMR}$  ( $\text{CD}_3\text{CN}$ , 250 MHz) :  $\delta$  = 9.31 (s, 1H, Im-H), 7.59 (s, 1H, Im-H), 7.46 (s, 1H, Im-H), 6.18 (d of t, 3H,  $\text{CH}_2=\text{CH-}$ ), 4.56 (t, 2H, O- $\text{CH}_2-$ ), 4.44 (t, - $\text{CH}_2$ -N), 3.89 (s, 3H, N- $\text{CH}_3$ ) ppm

## 1-methyl 3-(4-acryloyloxy butyl) imidazolium chloride



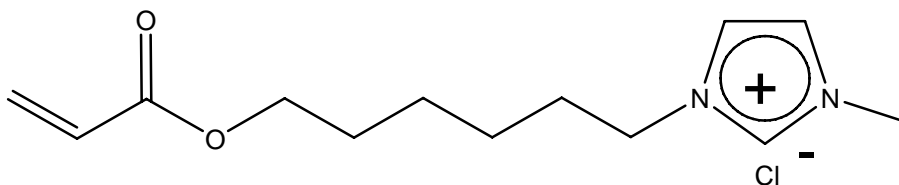
14.43 g (88.8 mmol) 4-Chloro-butyl-acryl ester

7.3 g (88.8 mmol) N-Methylimidazole

Yield : 75 % ( 16.22 g)

$^1\text{H-NMR}$  (Methanol-  $d_4$ , 250 MHz) :  $\delta$  = 7.64-7.57-7.56 (s, 3H, Im-H), 6.15 (d of t, 3H,  $\text{CH}_2=\text{CH-}$ ), 4.25 (t, 2H, O- $\text{CH}_2-$ ), 4.18 (t, - $\text{CH}_2$ -N), 3.91 (s, 3H, N- $\text{CH}_3$ ), 1.94-1.70 (m, 4H, - $(\text{CH}_2)_2-$ ) ppm

## 1-methyl 3-(6-acryloyloxy hexyl) imidazolium chloride



17.93 g ( 94.1 mmol) 6-Chlor-hexyl-acryl ester

7.75 g (94 mmol) N-Methylimidazole

Yield : 61 % (15.67 g)

$^1\text{H-NMR}$  ( $\text{CD}_2\text{Cl}_2$ , 250 MHz) :  $\delta = 10.14(\text{s}, 1\text{H}, \text{Im-H}), 7.49(\text{s}, 1\text{H}, \text{Im-H}), 7.39(\text{s}, 1\text{H}, \text{Im-H})$  6.1(d of t, 3H,  $\text{CH}_2=\text{CH-}$ ), 4.3 (t, 2H, $\text{O-CH}_2-$ ), 4.09 (t,  $-\text{CH}_2-\text{N}$ ), 4.03 (s, 3H, N- $\text{CH}_3$ ), 1.88-1.37 (m, 8H,  $-(\text{CH}_2)_4-$ ) ppm

*N-N'-bis(imidazolyl) alkane*

The alkane linkers C2, C5 and C6 were introduced by the alkylation of imidazole with 1,2-dibromoethane, 1,5-dibromopentane and 1,6-dibromohexane, respectively, and this process was successfully achieved by dropwise addition of the alkyl halides to the sodium salt of imidazole generated in situ from sodium and imidazole in refluxing tetrahydrofuran for 12 h. Mixture was then cooled to room temperature and filtered. After removal of THF by rotavap the obtained liquid was dissolved in water and extracted with diethyl ether 3 times. The crude product was obtained from aqueous solution after drying by freeze-drier.

***l=2*** : *N,N'*-bis(imidazolyl) ethane

10 g (147 mmol) imidazole

13.81 g (73.5 mmol) *l*,2-dibromoethane

3.38 g (147 mmol) Na-metal

Yield : 64 % (7,66 g)

***l=5*** : *N,N'*-bis(imidazolyl) pentane

15 g (220 mmol) imidazole

25.3 g (110 mmol) *l*,2-dibromopentane

8.58 g (220 mmol) Na-metal

Yield : 65 % (14.61 g)

 $^1\text{H-NMR}$  ( $\text{D}_2\text{O}$ , 250 MHz) :  $\delta$  = 7.45 (s, 2H, Im-H), 6.94 (s, 2H, Im-H), 6.85 (s, 2H, Im-H), 3.78 (t, 4H, N- $\text{CH}_2$ ), 1.55 (m, 4H, - $\text{CH}_2$ -), 0.97 (m, 2H, - $\text{CH}_2$ -) ppm***l=6*** : *N,N'*-bis(imidazolyl) hexane

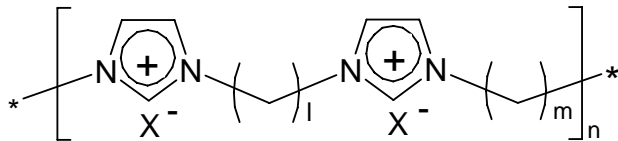
15 g (220 mmol) imidazole

26.87 g ( 110 mmol) *l*,6-dibromhexan

5.07 g ( 220 mmol) Na-metal

 $^1\text{H-NMR}$  ( $\text{D}_2\text{O}$ , 250 MHz) :  $\delta$  = 7.48 (s, 2H, Im-H), 6.96 (s, 2H, Im-H), 6.89 (s, 2H, Im-H), 3.81 (t, 4H, N- $\text{CH}_2$ ), 1.53 (m, 2H, - $\text{CH}_2$ -), 1.02 (m, 2H, - $\text{CH}_2$ -) ppm

Yield : 58 % (14 g)

*ionenes*

Equimolar mixture of  $N,N'$ -bis(imidazolyl) alkane and  $l,m$ -diiodoalkane were prepared. The mixture was heated at  $80^{\circ}\text{C}$  overnight under  $\text{N}_2$  atmosphere to accelerate the condensation reaction. The mixture was then cooled to room temperature. It was precipitated in acetone for  $m = 2$ . For  $m = 6$ , it was first precipitated in diethylether and then was washed several times with excess amount of acetone. The products were obtained in powder.

 **$l=5, m=2$** 

4.72 g (23.1 mmol)  $N,N'$ -bis(imidazolyl) pentane

6.85 g (23.1 mmol)  $1,2$ -diiodoethane

Yield : 42 % (4.91 g)

$^1\text{H-NMR}$  (DMF- $d_6$ , 250 MHz) :  $\delta = 8.51$  (s, 2H, Im-H), 7.59 (s, 2H, Im-H), 7.42 (s, 2H, Im-H), 4.24 (t, 4H, N- $\text{CH}_2$ ), 1.92 (m, 4H, - $\text{CH}_2$ -), 1.32 (m, 4H, - $\text{CH}_2$ -) ppm

 **$l=5, m=6$** 

9 g (44.1 mmol)  $N,N'$ -bis(imidazolyl) pentane

14.9 g (44.1 mmol)  $1,6$ -diiodohexane

Yield : 32 % (7.7 g)

$^1\text{H-NMR}$  (DMF- $d_6$ , 250 MHz) :  $\delta = 9.66$  (s, 2H, Im-H), 8.07 (s, 2H, Im-H), 4.44 (m *br*, 8H, N- $\text{CH}_2$ ), 2.00 (m *br*, 8H, - $\text{CH}_2$ -), 1.42 (s *br*, 6H, - $\text{CH}_2$ -) ppm

$l=6, m=6$

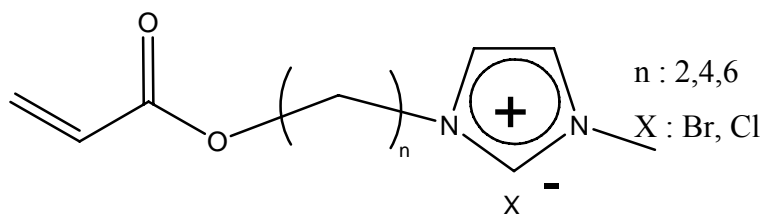
5 g (23 mmol)  $N,N'$ -bis(imidazolyl) hexane

7.77 (23 mmol) 1,6-diiodohexane

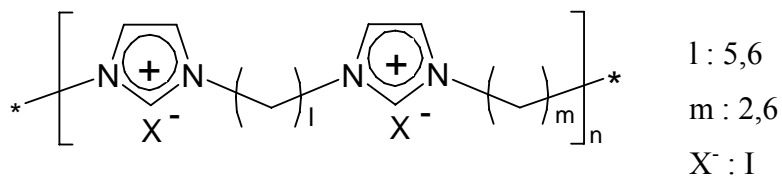
Yield : 30 % (3.83 g)

$^1\text{H-NMR}$  (Methanol- $d_4$ , 250 MHz) :  $\delta = 9.24$  (s, 2H, Im-H) , 7.72(s, 4H, Im-H) , 4.30 (t br, 8H, N- $\text{CH}_2$ ), 1.97 (br, 8H,  $-\text{CH}_2-$ ), 1.45 (br, 8H,  $-\text{CH}_2-$ ) ppm

**Counter Ion-Exchange with  $\text{H}_2\text{PO}_4^-$**



The monomers were dissolved in methylenchloride and stoichiometric amount (1:1 mol ratio) of crystalline  $\text{H}_3\text{PO}_4$  was added. The mixture was stirred overnight at RT. The desired compounds became insoluble in  $\text{CH}_2\text{Cl}_2$ . They were isolated from reaction medium and washed several times with excess amount of  $\text{CH}_2\text{Cl}_2$ .



These ionenes and required amount of  $\text{H}_3\text{PO}_4$  were mixed in DMF. The mixture was stirred overnight at RT. DMF was removed by rotavap. The substances were dissolved in water and put in dializ to get rid of low molecular weight compounds.



### Polymerizations

Polymerization was initiated with Azo(isobutyroic acid amidine)dihydrochloride (AIBA) (1 mol %) in water at 70°C. After polymerization the water solution of the polymer was put in 2000 MWCO dializ membrane to remove oligomers and low molecular weight chains. The product was obtained after removing solvent by freeze-drier.

